이학박사학위논문

스티릴 염료와 보디피 스티릴 염료로 이뤄진 집중된 라이브러리를 통한 형광 프로브의 개발

Development of fluorescent probes based on styryl dye and styryl BODIPY from focused libraries

2018년 2월

서울대학교 대학원
화학부 유기화학전공
이 상 욱

Abstract

Development of fluorescent probes based on styryl dye and styryl BODIPY from focused libraries

Sang Wook Lee

Department of Chemistry

The Graduate School

Seoul National University

Fluorescent probes based on small molecules are versatile tools for optical imaging and analytical sensing owing to their high sensitivity levels, fast response times, and simplicity. In addition, the development of a new probe is as important as its usefulness. Although many researchers have developed numerous fluorescent molecular probes, systematic probe development approaches are still lacking.

An early conventional strategy for probe development is the target-oriented approach. Probes have been designed based on available empirical knowledge of molecular recognition mechanisms for individual targets. However, this strategy has serious limitations when studying unknown targets. Meanwhile, diversity-oriented fluorescent probe libraries with broad chemical diversity can be an alternative means of discovering new probes for targets that may not be accessible with known sensing moieties. Nevertheless, this strategy has a very low success rate despite the great investments in labor and time.

As an alternative to both strategies, we considered focused fluorescent probe libraries that were designed to aid in the development of fluorescent probes based on an understanding of the target or target family. Sensing moieties of our probes were focused on the target family.

Herein, we demonstrate the effectiveness of a focused library consisting of sensing

moieties and styryl-based fluorescent dyes to provide selective probes for the detection of various targets. First, we prepared a focused fluorescent probe library for metal cations that was developed by combining metal cation ligand moieties and picolinium/quinolinium moieties as combinatorial blocks, which were connected through a styryl group. Selective probes for Hg^{2+}, Ag^{+}, and Zn^{2+} can be found in this library. Secondly, we constructed a focused probe library for phosphorylated biomolecules using metal complexes obtained from the previous library having a high binding affinity levels for metal cations. From the metal complexes, a selective probe for dTTP was developed. Thirdly, several of our styryl dyes from the previous library showed enhanced fluorescence in cells, and we found fluorescent nucleic acid probes. The feasibility of these probes was confirmed by cellular nucleic acid digestion experiments. Fourth, we developed a ratiometric fluorescent hydrogen peroxide probe, **1A**. This probe was used to quantify glucose in diluted urine with enzyme-assisted glucose oxidation. Furthermore, we demonstrated that probe **1A** could detect the activities of various oxidases as well as the presence and quantity of specific biomolecules by means of enzyme-assisted metabolism. Lastly, we developed a fluorescent imaging probe based on styryl BODIPY, **v-BDP**, for a mitochondria-targeting cancer therapy study. This was developed to deliver anticancer drugs to the mitochondria through triggering with intracellular esterase.

Keyword: Fluorescent probe, Focused library, Styryl dye, Styryl BODIPY, Hydrogen peroxide, Thymidine triphosphate, Drug delivery

Contents

Part 1. General introduction

Science is a systematic method that organizes knowledge attained through in the form of demonstrable explanations and predictions about the universe. Chemistry is a field of natural science that studies the change of matter in molecular level. A chemist focuses change on understanding about a matter of interest and asks oneself about what is cause and effect. Determination of reliable origin and demonstration of the rational result of the event are not only a mission but also a pleasure for the chemist. Notably, for the chemist, particular elucidation on electron behavior of a molecule is the main method for investigating the change.

Chemosensors are objects, that convert the particular property of a matter into an observable signal. The chemosensor transduces chemical properties into a signal in molecular level. Commonly, fluorescence is used in the life sciences as a non-destructive way of tracking or analyzing biological molecules. Fluorescence is the light emitted by an atom or molecule after a finite duration subsequent to the absorption of electromagnetic energy. Fluorescence property of a molecule is easily manipulated by molecular functionalization. Many fluorescent chemosensors and probes have been designed by utilizing this fluorescence character. Fluorophores have been modified and functionalized variously to improve their photostability, solubility, and biocompatibility. Since their small size, these can be crosslinked to macromolecules including antibodies, biotin or avidin, nucleic acid, and enzyme without interfering biological function. So, academia respectably expended on developing better quality probes. In this part, basic concepts of molecular fluorescent probe and whose fundamental development strategies were described below.

1.1 Fluorescence and fluorophores

Luminescence is emission of light by any substance, and occurs from electronically excited state. This energy relaxation is not resulting from heat and therefore the emission is a form of cold-body radiation. There are many types of luminescence. Types of luminescence are divided into categories depending on excitation energy sources. The followings are several forms of luminescence:

Chemiluminescence, from a chemical reaction

Crystalloluminescence, produced during crystallization

Electroluminescence, from an electric current passed through any substance

Electrochemiluminescence, from electrochemical reaction

Photoluminescence (PL), from absorption of photons, is split into three components: fluorescence, phosphorescence, and Raman emission.

1.1.1 Fluorophores fluoresce

Fluorescence, a result of singlet-singlet electronic relaxation, is a form of photoluminescence. Before fluorescence emission, an organic fluorescent molecule, a fluorophore, absorbed UV-Vis light or other electromagnetic radiation. Absorption of electromagnetic radiation is photon energy transmission to matter, typically the electrons of the fluorophore. In other words, the light is transformed `into excitation energy of the electrons that of the fluorophore.

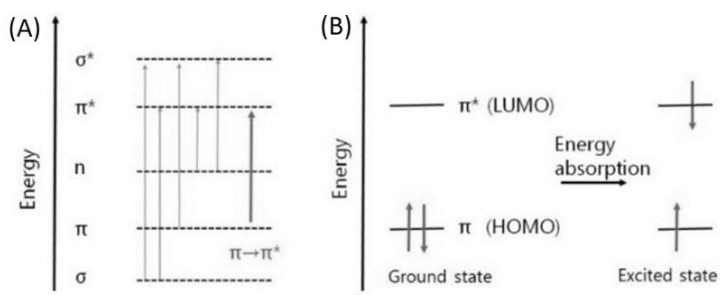

Figure 1.1. (A) Theoretically possible electronic transitions in organic compound. (B) Diagram of the HOMO and LUMO of a molecule.

By ultraviolet-visible light spectroscopy, these electronic transitions of organic fluorophores can be verified. Excitation of an electron from a π- bonding orbital (highest occupied molecular orbital (HOMO)) to an antibonding π orbital (lowest occupied molecular orbital (LUMO)) is denoted as a $\pi \rightarrow \pi^*$ transition (**Figure 1.1**). The $\sigma \rightarrow \sigma^*$, $\sigma \rightarrow \pi^*$, $n \rightarrow \sigma^*$, $n \rightarrow \pi^*$ and $\pi \rightarrow \sigma^*$ *transitions in organic fluorophore usually have slight transition probabilities* in the UV-vis range, therefore, the $\pi \rightarrow \pi^*$ transition is considered mainly. At this time, electrons are quantized and have discrete energy level. For this reason, not all the light that reaches fluorophore is absorbed, but specific wavelength light is absorbed selectively by electrons. Most organic fluorophores contain several combined aromatic groups or inflexible planar cyclic molecules with several π-bonds. In this conjugated system, the excited π electron is easily converted to a different state of motion. Thus, the π electrons in larger conjugated system are readily excited by lower-energy photons, commonly. Thus, organic compounds, which have longer π-electron conjugated system, show longer wavelength light absorption. On this principle, each fluorophore has its distinct color and fluorescence wavelength.

1.1.2 Fluorophore brightness

The brightness of a fluorophore is calculated as the product of molar extinction coefficient (ε) and quantum yield (Φ), both of which are distinct characteristics for each fluorophore. The ε is defined as the quantity of light that can be absorbed by a fluorophore at a given wavelength. Since the absorbance is unitless, the units for ε must cancel with units of measure in concentration and light path, hence, ε have units of M-1 cm-1. The Φ is calculated as the number of emitted photons divided by the number of absorbed photons of the fluorophore, so, this fluorescence efficiency of a fluorophore has a maximum of 1. Conversely, computing fluorescence efficiency is possible by utilizing brightness and ε value.

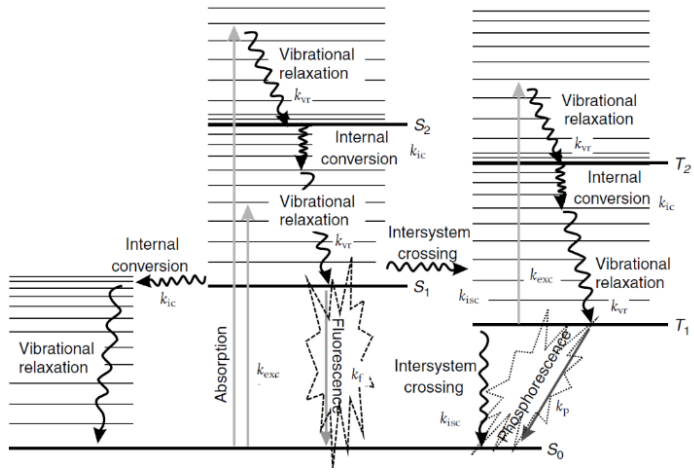

Figure 1.2. A Jablonski diagram showing the excitation of molecule to its singlet excited state that relaxes to the ground state by fluorescence.

1.1.3 Fluorescence and Competing Processes

On the other hand, there are many other non-radiative processes that can compete with fluorescence and thus reduce the fluorescence quantum yield. The electronic states of most organic luminophores (fluorescence or phosphorescence emitters) can be divided into singlet states and triplet states, and all electrons in the luminophore are spin paired or one set of electron spins is unpaired, respectively. With light of suitable wavelength, electrons are excited to one of the vibrational levels (see **Figure 1.2**). The occupying of singlet states is regulated by the interaction of the electron, which involved in the transition with the electric field of the excitation light. By collision with other molecules, electrons in higher vibrational levels will fall to the lowest vibrational level, vibrational relaxation. Through internal conversion, excited electrons are relaxed to vibrational levels of the first excited singlet state, S_1. In the same way, the fluorophore lose energy via internal conversion followed by vibrational relaxation from the lowest lying vibrational level of the first excited singlet state that result low fluorescence quantum yield. Alternatively, the fluorescence quantum yield of a fluorophore can be determined via measurement of the solvent temperature of related parameters (for example, the refractive index),

since both vibrational relaxation and internal conversion cause heating of the solvent.

In most organic fluorophores, intersystem crossing is not efficient as a spin forbidden process, although energy level of the triplet state is of lower than that of the excited singlet state. The intersystem crossing efficiency fairly depends on properties of the fluorophore. Several study reported that the presence of heavy atoms could increase the intersystem crossing efficiency. The fluorophore in a high vibrational level of the triplet state undergo vibrational relaxation (through collisions with other molecules including solvent) and intersystem crossing to singlet ground state, where the lowest vibrational level through vibrational relaxation. These processes also result fluorescence quenching.

By absorption of a second photon, the fluorophore can possibly excited to higher singlet states. Subsequent ionization of the fluorophore is a possible photobleaching pathway. As in the case of singlet states, triplet states can be excited into higher excited triplet states. Because the triplet/singlet transition is also spin forbidden, triplet state lifetimes can last up to 100 s. In most organic fluorophore, triplet states are most probably involved in photobleaching pathways since overlap of the $T_1 \rightarrow T_n$ and the $S_0 \rightarrow S_1$ absorption wavelength. However, the photobleaching can be avoided by: 1) exposing the fluorophore to minimum level of excitation light intensity and length of time that still yields good signal detection to analyze, 2) using photostable fluorophores and/or using anti-fade reagents.

Minimization of non-radiative decay is difficult on the molecular structure of the fluorophore. Although flawless design of the fluorescence quantum efficiency of a certain fluorophore is impracticable. Several requirements can be carried out for high fluorescent fluorophore: (1) rigid structure to reduce non-radiative deactivation due to rotation or vibration of fluorophore, generally loose and floppy molecules exhibiting several rotational and vibrational degrees of freedom will seriously exhibit lower fluorescence intensity, (2) to decrease intersystem crossing rate constant, strong spin–orbit coupling should be avoided, and (3) conjugated electron donor and acceptor groups for charge transfer transitions.

Table 1.1 Radiative and nonradiative reaction pathways in common organic fluorophore and corresponding time scales

Internal Conversion	$S_n \rightarrow S_1$, $T_n \rightarrow T_1$	k_{ic}	10^{10}-10^{14}/s
Internal Conversion	$S_1 \rightarrow S_0$	k_{ic}	10^{6}-10^{7}/s
Vibrational relaxation	$S_{1,v=n} \rightarrow S_{1,\ v=o}$	K_{vr}	10^{10}-10^{12}/s
Singlet-singlet absorption	$S_1 \rightarrow S_n$	k_{exc}	10^{15}/s
Fluorescence	$S_1 \rightarrow S_o$,	k_f	10^{7}-10^{9}/s
Intersystem crossing	$S_1 \rightarrow T_1$, $S_n \rightarrow T_n$, $T_n \rightarrow S_n$	k_{isc}	10^{5}-10^{8}/s
Phosphorescence	$T_1 \rightarrow S_{=o}$	K_p	10^{-2}-10^{3}/s
Triplet-triplet absorption	$T_1 \rightarrow T_n$	K_{exc}	10^{15}/s

1.1.4 Effect of solvent on fluorophores

As mentioned above, each fluorophore have distinct photophysical properties both the excitation and emission wavelengths. A typical spectra for a fluorophore depicted on x,y plots, that indicate the wavelengths correspond to the absorption and emission signal intensity of the fluorophore (**Figure 1.3**). The distance between positions of the band maxima of the absorption and emission spectra, in other words, shift of the fluorescence emission band compared with the absorption band due to non-radiative relaxation processes, is called the Stokes Shift.

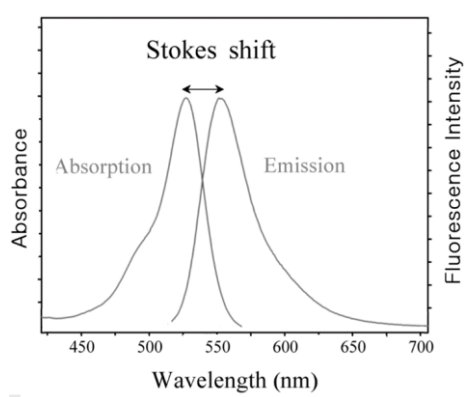

Figure 1.3. Representative absorption and fluorescence emission spectra of a fluorophore.

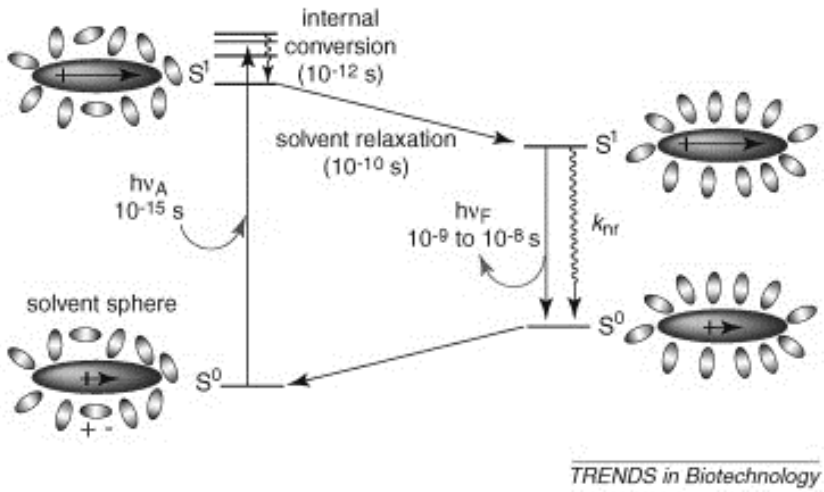

Figure 1.4. Origin of solvatochromic effects on fluorescence. Reprinted from ref X. Copyright (2009) with permission from Elsevier.

Upon excitation, the electron distribution of the fluorophore altered that generate different bonding forces and dipole moments. The solvent molecules undergo a new equilibrium configuration, which they change to within several picoseconds at room temperature. In more polar solvent, the electronic polarization of the solvent molecule changes immediately to the new electron distribution in the molecule. However, the solvent molecules' orientational polarization does not change immediately with the excitation. As a result, the excited dipole does not match the solvent configuration. By dielectric relaxation, the solvent molecules have to respond until the equilibrium configuration agreement. Typically, dielectric relaxation is completed in 10 ps. The different properties of the ground and excited states which are dependent on solvent polarity, is called solvatochromism. Also, the similar event happens upon subsequent fluorescence emission. The Stokes shift can be expressed as a function of solvent properties and the dipole moments of the fluorophore in the ground and excited states. In biological research, this is an important factor in the detection of fluorescence, which must be easy to distinguish signal from noise since a fluorophore with shorter Stokes shift exhibits larger background signal.

1.1.5 Fluorescence in Actual samples

The important matter should be noted in experiments with fluorophore is that fluorophore does not exist alone. As mentioned above, fluorescence contains information about the environment of the fluorophore and its interactions with other molecules including solvent. Therefore, the fluorescence lifetime and fluorescence quantum yield directly reveal interactions of the fluorophore with other molecules. Moreover, large quantity of fluorescent molecules are exist in cells. In short, fluorescent signal contains noise and followings should be considered, especially in cellular imaging experiment.

Autofluorescence

By high background fluorescence, fluorescent of target fluorophore detection in a given sample is indistinguishable from noise. Mostly, autofluorescence in biological samples emits when using short wavelength excitation light (< 500 nm). Thus, autofluorescence can be avoided by using fluorophores that do not excite in the short wavelength or filter sets that narrow the excitation light specifically to that of the target fluorophores.

Low/quenched fluorescence

Low fluorescence intensity can limit the detection of the target fluorophore, especially when background fluorescence is high. Intense fluorescence can be obtained by increasing the quantity of fluorophore at the target site. However, increasing the concentration of the fluorophore could cause cellular distortions or self-quenching by aggregation or even induce cell death. Low fluorescence intensity can be increased by raising the excitation light power, but this approach must be controlled with avoiding photobleaching the fluorophore.

Fluorescent signal quantitation in cells

With the advent of microscopy, fluorescent signal quantitation has become familiar in any fluorescent applications (requires specialized software). This provides the capability to measure a broad range of parameters, including:

Flow cytometer

- amount of fluorophore localized to cells or even discrete cellular compartments
- rate of cell motility or movement of intracellular components
- viability

Measuring amount of DNA, RNA or protein in a sample

-nucleic acid or protein sequence

Enzyme activity

-rate of gene expression and protein synthesis

1.1.6 Biocompatibility

Perhaps, the most important aspect of fluorophore in cellular experiment is biocompatibility. Then, what is the biocompatibility of the fluorophore? The definition of biocompatibility is vague, since it related to the behavior of biomaterials (fluorophore) in various contexts. Here are some definitions of biocompatibility.

"The ability of a material to perform with an appropriate host response in a specific application"[1]

"Comparison of the tissue response produced through the close association of the implanted candidate material to its implant site within the host animal to that tissue response recognized and established as suitable with control materials"[2]

"Refers to the ability of a biomaterial to perform its desired function with respect to a medical therapy, without eliciting any undesirable local or systemic effects in the recipient or beneficiary of that therapy, but generating the most appropriate beneficial cellular or tissue response in that specific situation, and optimizing the clinically relevant performance of that therapy".[3]

In short, the term refers to the ability of biomaterial (fluorophore) to perform with an appropriate response in a specific condition. *Cells* are composed of *water*, inorganic ions, and organic molecules. *Water* is the most abundant molecule in *cells*, accounting for 70%. Thus, the biocompatible fluorophore must be soluble in

aqueous solution. Also, the water soluble fluorophore must not interact with macro molecules including nucleic acid, protein, and lipid bilayers, which is hydrophobic organic molecules composed of carbohydrate chain that leading to misleading fluorescent signals.[4] However, the biocompatibility of the fluorophore in cell, which is a complex and different condition to test tube of it, is unknown until we try to cellular experiment. As a result, fluorescent cellular imaging of specific event is not a simple work but a complex task, which requires systematic strategy.

1.1.7. Fluorescent labeling and conjugates

The small size of molecular fluorophore is a benefit over biological fluorophore for bioconjugation strategies, since it could be attached to macromolecules, such as antibodies, proteins, enzymes, and nucleic acid without interfering biological function of that. Generally, by using reactive derivatives of the fluorophore, the crosslinking is performed that selectively binds to the target molecule. Fluorescent labeling is widely employed to detect the specific target and allows quantitative measurement.

Fluorophore conjugation

A chemically reactive derivative of a fluorophore is essential for labeling molecules. The fluorophore must be linked to detect the fluorescent signal with biocompatibility (not interfering with the biological characteristics) and various reactive functional groups for labeling have been utilized (**Figure 1.5**).[5]

In summary, the fluorophore is a useful tool for biological research and development of fluorophore for specific target is integral part of the biological study. In next section, strategies of modulating fluorescence of the fluorophore were presented.

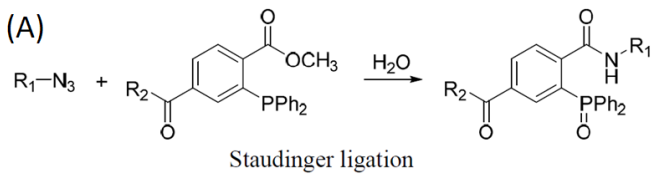

Staudinger ligation

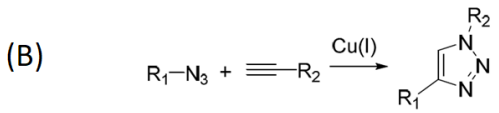

Copper-catalyzed alkyne-azide cycloaddition (CuAAC)

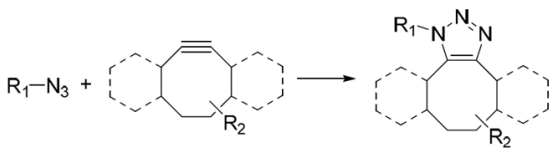

Strain-promoted alkyne-azide cycloaddition (SPAAC)

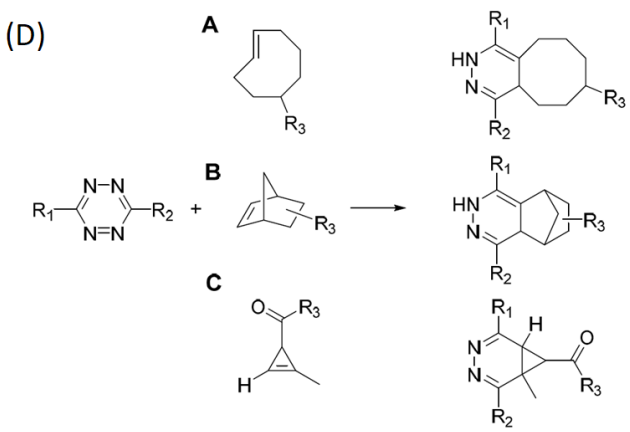

Tetrazine ligations between tetrazine and trans-cyclooctene (**A**), norbornene (**B**), cyclopropene (**C**).

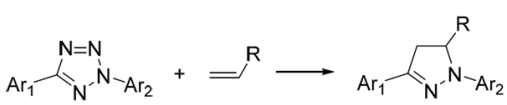

Photo-click reaction

R_1, R_2, R_3, R, Ar_1, Ar_2 = biomolecules, bioactive molecules, fluorophores, affinity tags, etc.

Figure 1.5. Bioorthogonal Reactions. (A) Staudinger ligation, (B) Copper-catalyzed alkyne-azide cycloaddition, (C) Strain-promoted alkyne-azide cycloaddition, (D) Tetrazine ligations between tetrazine and trans-cyclooctene, norbornene, cyclopropene, (E) Photo-click reaction.

1.2 Fluorescence modulation of the fluorophore

In previous section, characteristics of fluorescence and the usefulness of the fluorescent probe in biological research were examined. Now we know that when the fluorophore absorbs photons of suitable wavelength, excited electronic state is developed. However, not all organic fluorophores fluoresced strongly, since these subsequent following processes can occur:

1) heat: The absorbed energy is delivered to the environment as heat by collisions
2) intersystem crossing: Before emission of the photon the fluorophore undergoes a radiationless transition to a triplet state
3) energy transfer: The excited electron (energy) is directly transferred to other molecule (not only the fluorophore but also solvent) or other part of itself

If we can understand and utilize these phenomenon that will be useful for development of fluorescent probes. Then, is it possible a rational probe design, which based on general fluorescence modulation mechanisms, would enable biological researcher to develop fluorescent probes for target molecules rapidly? Herein, we present general principles for modulating the fluorescence properties of fluorophores.

- Förster Resonance Energy Transfer (FRET)
- Photoinduced electron Transfer (PeT)

Let us learn more about the mechanism of these energy transfers.

1.2.1 Radiative energy transfer

Excited energy of donor molecule can be transferred to the acceptor molecule by a light form. Emitted photon from the donor D can be absorbed by the acceptor A. This process denoted as:

1) $D^* \rightarrow D + h\nu$ 2) $h\nu + A \rightarrow A^*$

The efficiency of it depends on the following parameters:

1) the quantum yield (Φ_e) of acceptor and donor

2) the number density of ground state A molecule, which can absorb the emitted photon from donor

3) the absorption cross section (or extinction coefficient) of A

4) the overlap of the fluorescence emission spectrum of donor and the absorption (or excitation) spectrum of A.

However, this phenomenon is rarely used in fluorescent probe development because of low signal (fluorescence) efficiency.

1.2.2 Non-radiative energy transfer

In addition to the radiative energy transfer from a donor molecule to an acceptor molecule, the energy can also be transferred in a non-radiative pathway. This can occur in two ways:

1) by collision (Dexter energy transfer)

2) by Coulomb interaction (Förster energy transfer, in detail, it is discussed below)

3) by through bond energy transfer

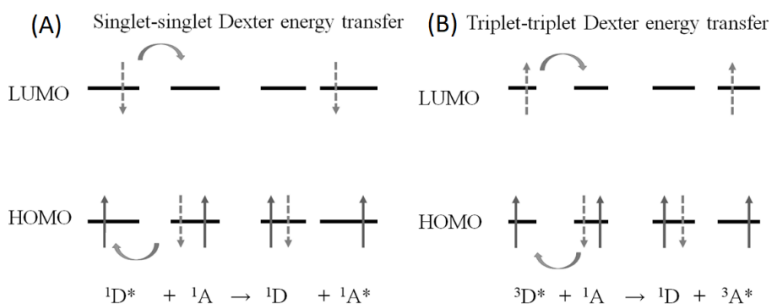

Figure 1.6. Schematic mechanism of Dexter energy transfer

1.2.2.1 Dexter energy transfer

Dexter energy transfer involved collision of electronic orbitals which causes exchanging of the excited donor electron and an acceptor electron of ground state. This energy transfer occurs in short distances between donor/acceptor with an

interpenetration of their orbitals. Since this interaction decreases exponentially with the distance *r* between donor and acceptor, it occurs efficiently only for distances *r* < 1 nm.

1.2.2.2 Förster energy transfer

Förster energy transfer (fluorescence resonance energy transfer (FRET), resonance energy transfer or electronic energy transfer) is a mechanism, which describes electronic energy transfer between light-sensitive molecules. This is being used increasingly in biological and biochemical research today. FRET is a physical phenomenon first described in 1948.[6] FRET occurs when a molecule(donor) is excited by light absorption and the excited energy transferred to other molecule(acceptor) through non-radiative dipole–dipole coupling by Coulomb interaction (**Figure 1.7**). FRET is in the radius of interaction that is much smaller than the wavelength of the light. In the near-field region, the excited molecule emits a virtual photon that is instantly absorbed by a receiving molecule. To detect these virtual photons are not possible in current technology, since their existence disobeys the conservation of energy and momentum. Thus, FRET is known as a radiation-less mechanism.

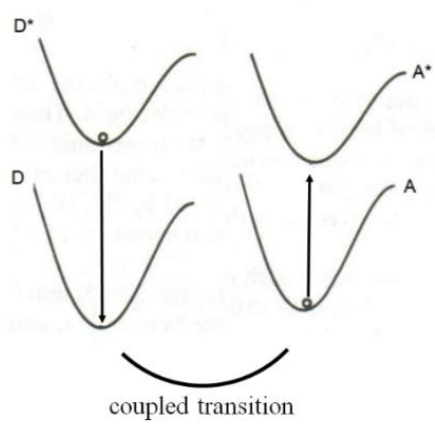

Figure 1.7. Schematic illustration of the Förster mechanism. The deactivation of D* and the excitation of A are coupled to each other by Coulombic dipole-dipole interaction.

FRET is not sensitive to the surrounding solvent shell of the molecule. Thus, FRET relies upon the distance-dependent energy transfer between the donor and the acceptor. Since this distance-dependent property, FRET has been used to investigate molecular interactions.[7-8] A pair of molecules that FRET occurs is referred to as a donor/acceptor pair. Here are examples (**Figure 1.8** and **Table 1.2**).

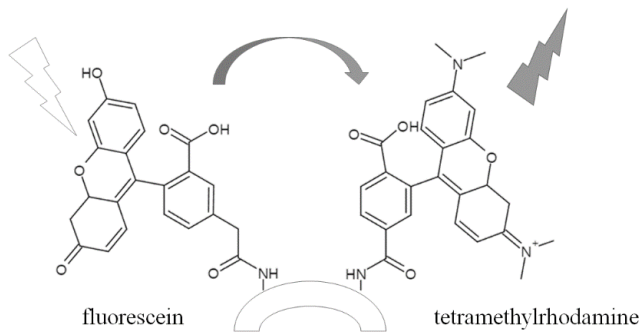

Figure 1.8. Schematic representation of FRET pair between two fluorescent molecules, fluorescein and tetramethylrhodamine.

Table 1.2. Overview several organic dye and fluorescent proteins FRET pairs, and some relevant photophysical properties.[9]

Donor	Acceptor	Donor Excitation λ_{max} (nm)	Acceptor Emission λ_{max} (nm)	Donor QY (–)	Acceptor ε ($M^{-1}cm^{-1}$)	Förster Distance (nm)
Fluorescent protein FRET pairs						
BFP	DsRFP	380	586	0.18	72,500	3.1–3.3
EBFP2	mEGFP	383	507	0.56	57,500	4.8
CFP	GFP	433	509	0.40	21,000	4.7–4.9
CFP	YFP	433	526	0.40	77,000	~ 5.0
Cerulean	YFP	440	526	0.62	77,000	–
ECFP	EYFP	440	527	0.40	83,400	4.9
Cerulean	Venus	440	528	0.62	92,200	5.4
MiCy	mKO	472	559	0.90	51,600	5.3
GFP	YFP	475	526	0.77	77,000	5.5–5.7
GFP	mRFP	475	579	0.77	50,000	~ 4.7
CyPet	YPet	477	530	0.51	104,000	5.1
TFP1	mVenus	492	528	0.85	92,200	5.1
EGFP	mCherry	507	510	0.60	72,000	5.1
Venus	mCherry	528	610	0.57	72,000	5.7
Venus	tdTomato	528	581	0.57	138,000	5.9
Venus	mPlum	528	649	0.57	41,000	5.2
Fluorescent protein-dye FRET pairs						
EGFP	Alexa Fluor 555	484	568	0.6	155,000	6.3
EGFP	Alexa Fluor 546	484	573	0.6	112,000	5.7
EGFP	Alexa Fluor 594	484	618	0.6	92,000	5.3
EGFP	Alexa Fluor 568	484	603	0.6	88,000	5.4
Dye and dye-biofluorochrome FRET pairs						
Cy2	Cy3	489	570	> 0.12	150,000	5.0–6.0
Cy3	Cy5	550	670	> 0.15	250,000	>5.0
Cy5	Cy5.5	649	694	> 0.28	250,000	>8.0
Fluorescein	Tetramethylrhodamine	487 [1]	574	0.93 [2]	~ 87,000	4.9–5.5
FITC	TRITC	494	572	0.92	100,000	5.4
Phycoerythrin	APC [3]	(546), 565	660	0.98	700,000	4.0–11.0
Europium	APC	340	660	–	700,000	9.0
Tryptophan	Dansyl	280	525	0.01–0.35 [4]	4050	2.1
Dansyl	FITC	335	519	< 0.035 [5]	77,000	3.3–4.1
Dansyl	Octadecylrhodamine	335	625	< 0.035	106,000	4.3
Europium	Cy5	340	670	–	250,000	7.0
Atto 488	Atto 647N	501	670	0.8	150,000	5.1
Atto 488	Atto 590	501	621	0.8	120,000	6.0
Atto 550	Atto 647N	554	670	0.8	150,000	6.5
Atto 550	Atto 655	554	684	0.8	125,000	6.4
Atto 590	Atto 655	594	684	0.8	125,000	7.3
Alexa 405	Alexa 430	401	541	–	16,000	–
Alexa 488	Alexa 514	495	542	0.92	80,000	–
Alexa 488	Alexa 532	495	554	0.92	81,000	–
Alexa 488	Alexa 546	495	573	0.92	104,000	6.4
Alexa 488	Alexa 610	495	628	0.92	138,000	–
Alexa 647	Alexa 680	650	702	0.33	184,000	–
Alexa 647	Alexa 700	650	723	0.33	192,000	–
Alexa 647	Alexa 750	650	780	0.33	240,000	–
Non-fluorescent acceptor pairs						
Rhodamine 6G	Malachite Green (Abs 628 nm)	526		0.95	76,000	6.1
Alexa 488	QSY 35 (Abs 475 nm)	495		0.92	23,000	4.4
Alexa 488	Dabcyl (Abs 453 nm)	495		0.92	32,000	4.9
Alexa 647	QSY 21 (Abs 661 nm)	650		0.33	90,000	6.9

Although many factors influence FRET, the key requirement for efficient FRET are as follows:

1) Donor and acceptor molecules must be in close proximity (typically 1-10 nm). Due to the dipole-dipole coupling mechanism, FRET efficiency (*E*) depends on the separation distance *r* between donor and acceptor with an inverse 6th-power law. $E = \frac{1}{1+(\frac{r}{Ro})^2}$ (Ro: Förster distance of this pair of donor and acceptor)

2) The absorption spectrum of the acceptor must overlap the fluorescence emission spectrum of the donor (consider quantum yield) (see **Figure 1.9**).

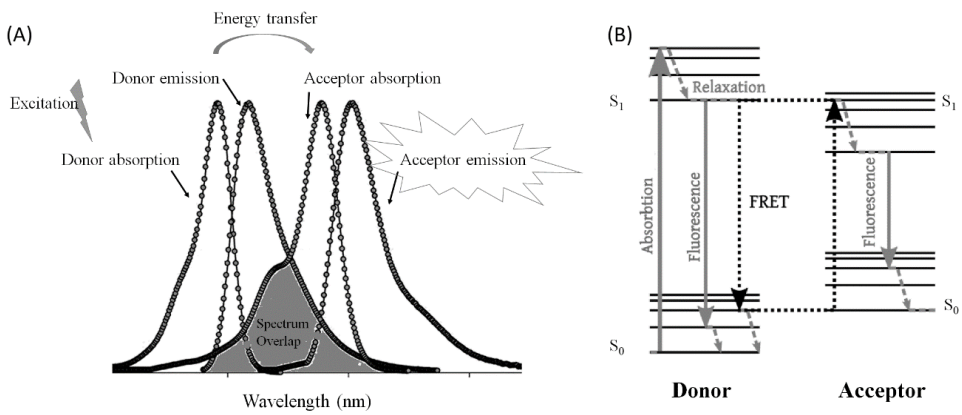

Figure 1.9. (A) The normalized absorption and fluorescence emission spectra of a FRET pair. The shaded area represents the overlap integral. (B) Schematic Jablonski diagram of FRET.

3) Donor and acceptor transition dipole orientations must be approximately parallel (FRET occurs through non-radiative dipole–dipole coupling by Coulomb interaction and FRET correlates with the interaction energy between two dipoles which is given by: $E_{dipole-dipole} = (\kappa / 4\pi\epsilon_0) \cdot (\mu_D \mu_A / r_{DA}^3)$. κ is a geometric factor.) (see **Figure 1.10**)

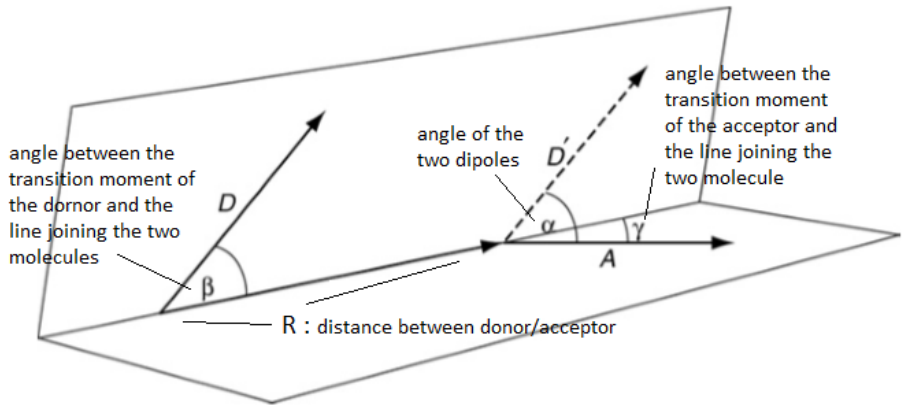

Figure 1.10. The orientation of the emission dipole of the donor (D) and the absorption dipole of the acceptor (A).

1.2.2.3 Photoinduced Electron Transfer (PeT)

Electron transfer reaction involves the transfer of an electron from a donor to an acceptor. This can occur both thermally and photochemically. The latter reactions are referred to as **P**hotoinduced **e**lectron **T**ransfer (PET) reactions. Unlike Dexter or Förster electron transfer, a charge separation is generated due to PeT, thus, redox reaction can occur in excited state. A general reaction involving the excitation of A is given in equations:

$^*A + B \rightarrow A^+ + B^-$ oxidative electron transfer (**Figure 1.11A**)

$^*A + B \rightarrow A^- + B^+$ reductive electron transfer (**Figure 1.11B**)

$^*A + B \rightarrow A + B^*$ energy transfer (not PeT)

The molecule, which absorbs light and gets excited, is generally referred to as the sensitizer (fluorescence reporter). When the electron transferred, fluorescence process is blocked. So, the other part is referred to as the quencher (modulator) (see **Figure 1.11**).

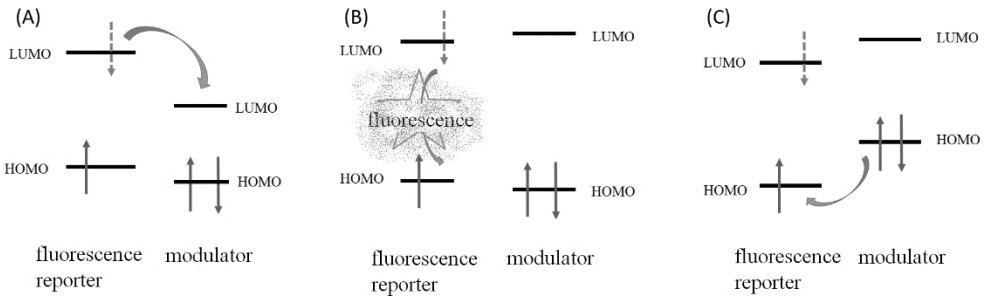

Figure 1.11. Schematic illustration of the modulation of fluorescence properties of a fluorophore (fluorescent probe) by PeT. The fluorophore can be regarded as conjugates of two independent moieties, the fluorescence reporter and the modulator. (A) the donor-excited PeT (d-PeT) mechanism (for this to occur, the LUMO (lowest occupied molecular orbital) energy level of the modulator must be lower than that of the fluorophore), (B) PeT fail (successful fluorescence), (C) acceptor-excited PeT (a-PeT) mechanism (for this to occur, the HOMO (highest occupied molecular orbital) energy level of the modulator must be higher than that of the fluorophore). Although the fluorescent reporter is highly fluorescent, the derivatives have almost no fluorescence owing to PeT by the modulator.

1.2.3 Through Bond Energy Transfer (TBET)

Energy transfer can occur through bonds. Most energy (~99%) are transferred from a donor to an acceptor via twisted π-electron systems. The fluorophore based on TBET (through-bond energy transfer) fluorophore, which have a donor linked to an acceptor via electronically conjugated bonds. However, theories describing through bond energy transfer (TBET) are not clear, but there are distinct characteristics of through-bond energy transfer. Firstly, there is no known restriction in TBET that corresponds to the spectrum overlap integral. Secondly, the donor and acceptor parts are more intimately connected but π-orbitals of them are not overlapped.[10-14]

For high efficiency of through bond energy transfer, requirements for the fluorophore for labeling biological systems include:

(1) donor components with high extinction coefficient

(2) acceptor components with high quantum yield

(3) functional groups that allow attachment linkers

The linker must prevent the donor and acceptor fragments from becoming planar (in other words, through- twisted bond energy transfer).

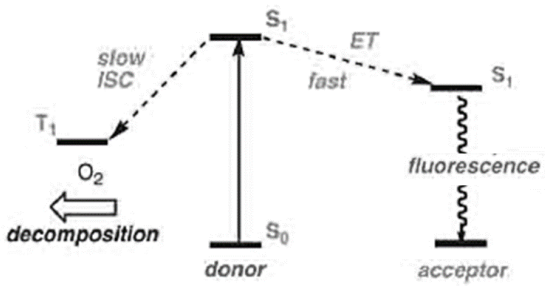

Figure 1.12. Schematic excitation and emission energy level of a typical TBET fluorophore.

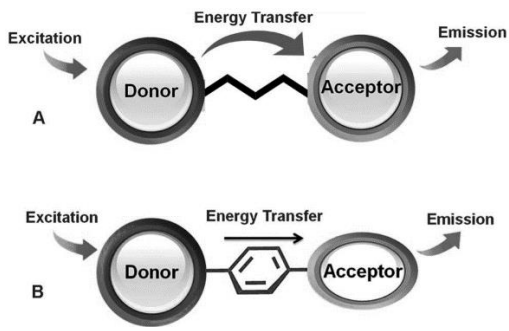

Figure 1.13 Schematic representation of through-space (A) and through bond energy transfers (B). Adapted from reference 14 with permission from Royal Society of Chemistry.

If donor-to-acceptor energy transfer in a TBET fluorophore is faster than the intersystem crossing process, then the energy is preferentially transferred to the acceptor part. The acceptor tend to fluoresce quicker than they undergo singlet-to-triplet crossover, thus, the photostability of the fluorophore overall is better than the donor alone. There are several advantages of TBET fluorophore in biological study.

(1) large pseudo-Stokes shift

(2) low photobleaching (see **Figure 1.12**)

1.3 Development of chemosensor and fluorescent molecular probe

Although most people are not aware, innumerable applications of sensors are used in everyday. Purposes of sensors are detecting changes of environment, particular events or specific object through construable signal. Chemosensors, which are developed to detect a certain molecule or microscopic environment, are widely used for molecular probes as a tool to examine chemical phenomena in molecular level. Fluorescent probes, that are small molecules absorb and emit light of a specific wavelength, are widely used to study biological samples. The molecules interact with a target molecule and act as a marker for analysis with fluorescence microscopy. Since their usefulness and simplicity, numerous fluorescent probes have been developed and utilized. Certainly, a remption of fluorescent probes are available, then why should we develop new ones? Things that we know are from with known tools but how can we see a thing that cannot detect with the existing tools? Researchers can settle the requirements by creating or improving probes. Then, how can we develop a fluorescent probe, which is biocompatible and shows specific signal with strong fluorescence? Although molecular sensing studies have advanced for the design of probe, systematic approaches for developing fluorescent probes are still lacking. So let's look at how researchers have developed fluorescent probes.

1.3.1 Development of new sensing motif is not easy

Any scientist has recognized a necessity for a new or improved probe, a development of probe is starting to shape up. However, a developing a new probe is formidable task. Theoretically, development of the new one is possible that accurately recognizes specific targets by flawless calculations or reacted with a particular molecule. However, the result, that from the new thing in experiment with a real sample, is not predictable. Since we use the ‘unknown’ probe to find out what we don't know at unknown biological environment. In other words, the probe is developed serendipitously by half rational design and half luck. Therefore, harmony

of the reasonable design of the probe and increase finding probability is a shortcut to the development of new probe.

1.3.2 Molecular recognition is a sensor development strategy

Every bimolecular reaction begins with recognition events. Molecular recognition plays an important role especially in biological system, and many biological macromolecules, including between antigens and antibodies, nucleic acids and nucleic acids, nucleic acid and proteins, proteins and proteins, enzymes and substrates, are related to that. The molecular recognition is the specific interaction between guest molecule and host molecule to form a host-quest complex. The complex is maintained through complementary noncovalent bonding, including hydrogen bond, metal co-ordination, van der Waals forces, π−π interaction, hydrophobic interaction, and electrostatic interactions. The molecules identify each other through organizing these noncovalent interactions.

Small molecules can be designed to recognize into complex structures with the target. The molecular recognition process is reversible and dynamic, thus the complex is formed and dissipated constantly. In this process, electrons in frontier molecular orbital are involved with molecular recognition which directly influence on electronic structure of whose molecule. In short, a fluorescent sensor can be developed by this principle, which is the molecular recognition. At first, if an analyte of interest is known that it docks into an active site, we can utilize this fact. Synthesis of a fluorescent 'active site' is a preparation of candidate for the probe. Next, determine which the fluorescent molecule shown a sensing property and improve the sensing performance. Or we can design a new fluorescent active site from the beginning. However, designing novel and robust chemical active site is not easy.

1.3.3 Chemodosimeter

Transformation of one set of chemical reactants and reagents to other substances is chemical reaction. This process involves forming and breaking of chemical

bonds between atoms. In consequence, the changes of electronic states of substances are accompanied and photophysical properties of that matters are also altered. Here what we need to focus on is the condition of a particular chemical reaction of the substance. The specific condition stated here implies that the chemical reaction occurred selectively. A fluorescent chemodosimeter utilize this selective chemical reaction with the specific target that result fluorescent signal. This can be described as chemical equation, which symbolically presents starting materials and products, if necessary, intermediate products and reaction conditions are written together.

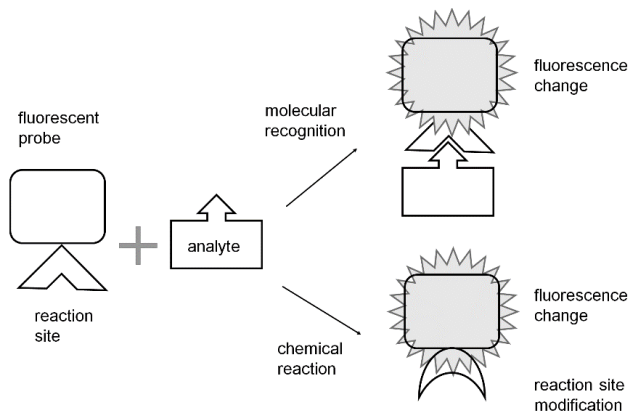

Figure 1.14. Schematic illustration of molecular sensing of fluorescent probe.

1.3.4 Hypothesis-driven fluorescent probe development approach is a limited strategy

The early development of fluorescent sensors was approached by hypothesis-driven synthesis or target-oriented synthesis. Fluorescent sensors have been designed by using fluorophores containing sensing groups (**Figure 1.14**). Most case in this approach, the target sensing groups of the sensor is designed on the basis of empirical knowledge, which has shown selectivity and sensitivity toward to a target of interest. Then the fluorophore is simply used as a signal reporter. However, it is difficult to find new aspect of the sensor by putting on existing ideas of the sensor development, so the opportunity of sensor discovery is hard to be expanded.

1.3.5 Diversity oriented fluorescent probe development approach

In the case where the target analyte was not analyzed before, the development of fluorescent probes by the traditional strategy is not appropriate, as there have been not available working hypothesis for the unknown analyte. The diversity oriented fluorescent probe development approach can be an alternative in this problem, although we don't have any information about the target.[15-16] When any candidate probe was discovered, then an improvement of the candidate leads to the fluorescent probe development. This is a similar way to how species were created by evolution. A life was born and over-produced offspring exposed to a new environment. Through selection, a few suitable entities survive. And its properties are strengthened. The biggest advantage of this operation is that can discover a wholly new type of fluorescent probe (**Figure 1.15).** When the target was analyzed, the binding mode of the probe to the target must be investigated. However, both target identification and binding mode study are complicated in a complex environment where numerous factors exist.

1.3.6 Focused library is an alternative strategy for new fluorescent probe development

So, what is the next alternative? Although it cannot be the best way, we decided to adopt a compromise instead of presenting a completely new method. Reduce size of the library and enhance discovering chance that is what we think is a simple but better way. To reduce size of the library, rather than considering all the unknown subjects, focusing on specific targets and similar classes. To enhance new probe discovering chance, use a slightly modified alternate method for the particular target. As a result, the amount of data that needs to be analyzed are condensed and require less labor. In the next section, the approaches will be described how fluorescent probes were developed from focused libraries.

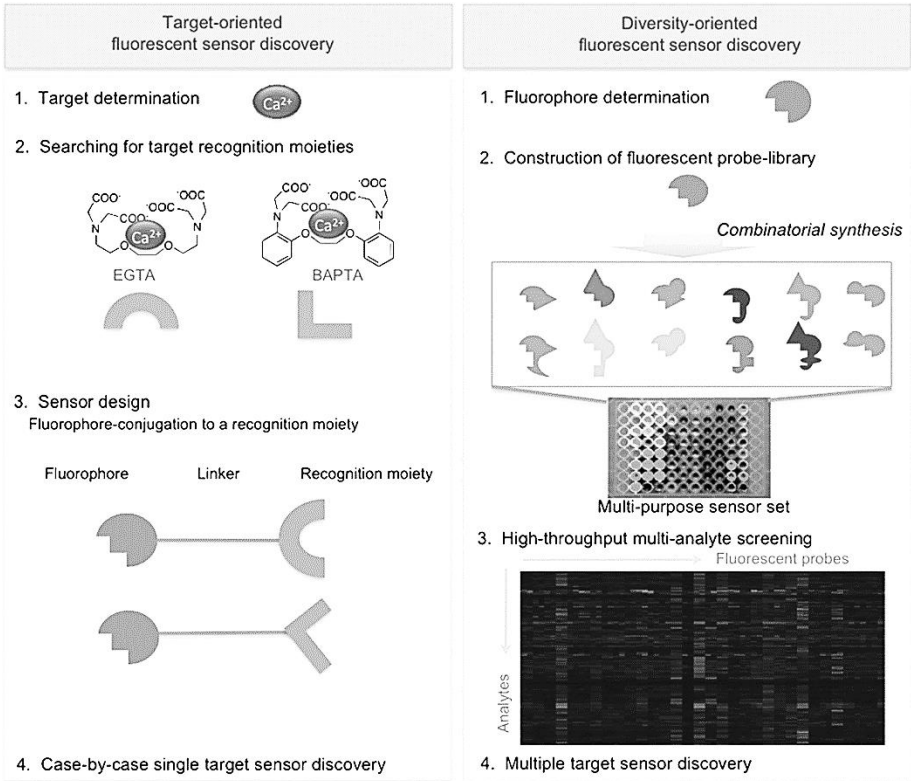

Figure 1.15. Target-oriented approach vs. diversity-oriented approach for fluorescent probe development. Adapted from reference 16 with permission from Royal Society of Chemistry.

1.4 References

1. Williams, D. F., *The Williams dictionary of biomaterials*. Liverpool University Press: Liverpool, 1999; p xvii, 343 p.

2. Morais, J. M.; Papadimitrakopoulos, F.; Burgess, D. J., Biomaterials/Tissue Interactions: Possible Solutions to Overcome Foreign Body Response. *Aaps J* **2010,** *12* (2), 188-196.

3. Williams, D. F., On the mechanisms of biocompatibility. *Biomaterials* **2008,** *29* (20), 2941-2953.

4. Hughes, L. D.; Rawle, R. J.; Boxer, S. G., Choose Your Label Wisely: Water-Soluble Fluorophores Often Interact with Lipid Bilayers. *Plos One* **2014,** *9* (2).

5. Zheng, M. M.; Zheng, L.; Zhang, P. Y.; Li, J. B.; Zhang, Y., Development of Bioorthogonal Reactions and Their Applications in Bioconjugation. *Molecules* **2015,** *20* (2),

3190-3205.

6. Förster, T., Zwischenmolekulare Energiewanderung und Fluoreszenz. *Annalen der Physik* **1948,** *437* (1-2), 55-75.

7. Sekar, R. B.; Periasamy, A., Fluorescence resonance energy transfer (FRET) microscopy imaging of live cell protein localizations. *The Journal of Cell Biology* **2003,** *160* (5), 629-633.

8. Jares-Erijman, E. A.; Jovin, T. M., Imaging molecular interactions in living cells by FRET microscopy. *Current Opinion in Chemical Biology* **2006,** *10* (5), 409-416.

9. Ishikawa-Ankerhold, H. C.; Ankerhold, R.; Drummen, G. P. C., Advanced Fluorescence Microscopy Techniques—FRAP, FLIP, FLAP, FRET and FLIM. *Molecules* **2012,** *17* (4), 4047.

10. Jiao, G.-S.; Thoresen, L. H.; Burgess, K., Fluorescent, Through-Bond Energy Transfer Cassettes for Labeling Multiple Biological Molecules in One Experiment. *Journal of the American Chemical Society* **2003,** *125* (48), 14668-14669.

11. Bandichhor, R.; Petrescu, A. D.; Vespa, A.; Kier, A. B.; Schroeder, F.; Burgess, K., Water-Soluble Through-Bond Energy Transfer Cassettes for Intracellular Imaging. *Journal of the American Chemical Society* **2006,** *128* (33), 10688-10689.

12. Lin, W.; Yuan, L.; Cao, Z.; Feng, Y.; Song, J., Through-Bond Energy Transfer Cassettes with Minimal Spectral Overlap between the Donor Emission and Acceptor Absorption: Coumarin–Rhodamine Dyads with Large Pseudo-Stokes Shifts and Emission Shifts. *Angewandte Chemie International Edition* **2010,** *49* (2), 375-379.

13. Fan, J.; Hu, M.; Zhan, P.; Peng, X., Energy transfer cassettes based on organic fluorophores: construction and applications in ratiometric sensing. *Chemical Society Reviews* **2013,** *42* (1), 29-43.

14. Kumar, N.; Bhalla, V.; Kumar, M., Resonance energy transfer-based fluorescent probes for Hg2+, Cu2+ and Fe2+/Fe3+ ions. *Analyst* **2014,** *139* (3), 543-558.

15. Yun, S.-W.; Kang, N.-Y.; Park, S.-J.; Ha, H.-H.; Kim, Y. K.; Lee, J.-S.; Chang, Y.-T., Diversity Oriented Fluorescence Library Approach (DOFLA) for Live Cell Imaging Probe Development. *Accounts of Chemical Research* **2014,** *47* (4), 1277-1286.

16. Lee, J.-S.; Kim, Y. K.; Vendrell, M.; Chang, Y.-T., Diversity-oriented fluorescence library approach for the discovery of sensors and probes. *Molecular BioSystems* **2009,** *5* (5), 411-421.

Part 2. Fluorescent probes based on picolinium/quinolinium styryl dye from focused libraries

2.1 Introduction to syryl dye

The latter half of the 19th century, the numerous synthetic dyestuffs, that hit world markets, were manufactured from abundant and cheap waste product of coal-gas. The manufacture of synthetic dyestuffs was one of the major growth engine for the industrial revolution. Since then, the use of the 'organic' dyes have expanded to the field of functional dyes. The most important role of the organic dyes is not confined their color, but the photophysical, biological, and chemical properties of the dyes themselves.

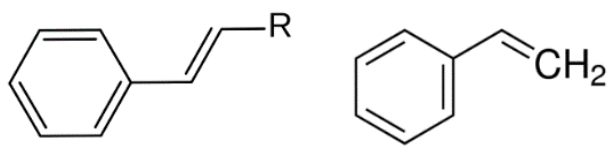

Figure 2.1.1. General structure of styryl group (left) and styene (right).

Styryl is the univalent radical C_6H_5–CH=CH– that is derived from styrene. Dyes containing this fragment are named styryl dyes and these can be modified with charged N-fused heterocycle aromatic ring (for example: picolinium, quinolinium, indolinium). Since the discovery of styryl dyes in 1920[1], many styryl dyes have been synthesized and have been applied as sensitizers in the photographic film industry mainly. Now, styryl dye is a widely used functional group for chromogenic or fluorogenic molecule synthesis in various fields. Above all, the most important applications for the styryl dyes are in bio-labelling and in medicinal analysis. Here, a few examples of fluorescent probes based on styryl dyes and their applications.

1. Organelle-Targeted Fluorescent Library Based on styryl Scaffold

Chang's group developed the first fluorescent styryl dye library with a broad color range. Each styryl dye was synthesized by combinatorial condensation of 41

aldehydes and 14 picolinium derivative compounds. Organelle specific staining experiments were conducted with the styryl dyes. [2]

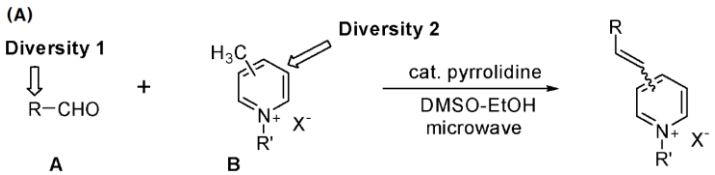

(B)

	A	B	C	D	E	F	G	H	I	J	K	L	M	N
1	•	•						♦	♦	♦				
3								♦	♦	♦				
4									▲					
7							♦							
8							♦							
9							♦	♦		♦	♦			
10								♦	■ •	♦	♦	♦		
11		♦												
12	♦	x	♦ x		x ■		♦ *	■	■	■	x	x	x	
14	♦	x					♦	■	■		♦	♦ x	♦	
15								♦		■				
16		♦						*	■*	■				
17								■ *	■		x	x	x	
18							♦	♦ *	*					
19	♦ *	♦ x	♦		♦		♦	*	*	♦	♦	♦	♦	*
20							♦	*	*	■				*
21							♦	♦ *	■*					
22		♦												
23	♦ •	•	•	•	•		■	■*			•	•	•	
24	•	♦				■	♦	•			♦			•
25		•												
27	•	♦ x					♦	♦	*		♦		♦	
28								#	*					
30									♦					
31		♦					♦ *	♦#	♦#•	♦				
32	♦•■	♦					♦	♦ *	♦#*	♦	♦	♦	♦	
33	♦•■						♦ •	♦#•■	♦#■	♦	♦	♦	♦	
34														
35									•	•		♦		
36		♦												
37		♦		♦	♦ *				•	x	■			♦ *
38		♦#					■•#		•	♦				
39		♦						•		♦	♦		♦	
41		▲												

Figure 2.1.2. (A) Synthesis of styryl dyes. (B) Localization distribution of the organelle specific styryl dyes [(#) Nuclear, (*) Nucleolar, (◆) Mitochondria, (●) Cytosolic, (x) Endoplasmic Reticular (ER), (■) Vesicular, (▲) Granular. Reprinted with permission from ref 2. Copyright (2003) American Chemical Society.

2. Fluorescence of styryl dyes-DNA complexes

The series of monomer and homodimer styryl dyes based on (*p*-dimethylaminostyryl) benzothiazolium residues were synthesized and studied as possible fluorescent probes for nucleic acids detection. Fluorescence emission induced by two-photon excitation of dye-DNA complexes in aqueous buffer solution was registered. Two-photon absorption cross section values of the studied dyes in DNA presence were evaluated.[3]

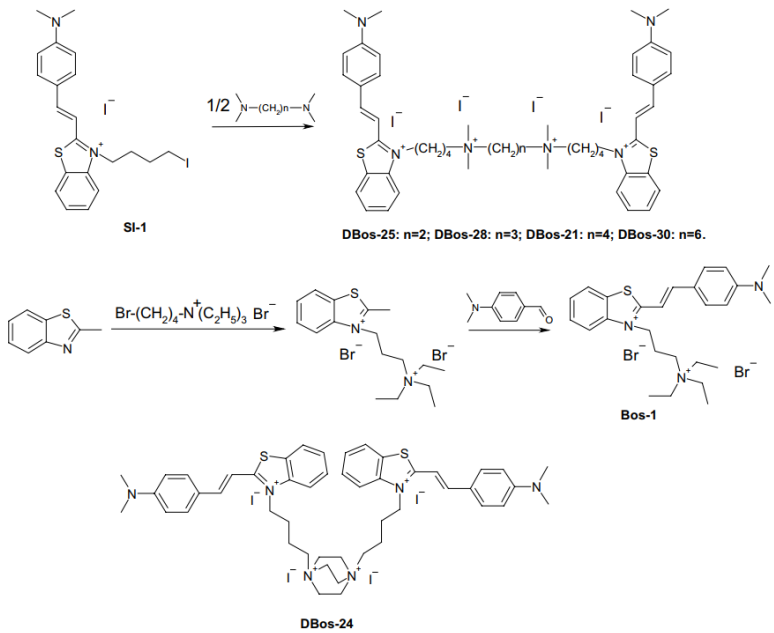

Figure 2.1.3. Synthesis and chemical structures of homodimer and monomer styryl dyes. Reprinted with permission from ref 3. Copyright © 2006, Springer Science+ Business Media, LLC.

3. Imaging exocytosis and endocytosis

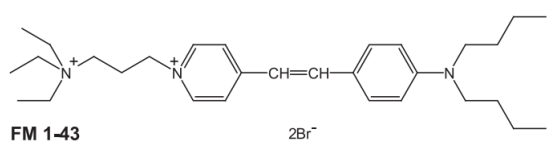

Figure 2.1.4. Structure of FM 1-43.

Styryl dye FM 1-43 become highly fluorescent upon binding to membranes which have been used to follow exocytic and endocytic events in many cell types.[4-5]

The commonality of the above mentioned styryl dyes is biocompatibility. Based on the strategy described in the previous section, we sought to develop fluorescent probes based on picolinium styryl dyes. In this part, fluorescent probes based on picolinium/ quinolinium styryl dyes from focused libraries were presented.

References

1. F Hammer, Cyanine Dyes and Related Compounds (London / New York: Interscience Publisher, 1964) p 398.

2. Rosania, G. R.; Lee, J. W.; Ding, L.; Yoon, H.-S.; Chang, Y.-T., Combinatorial Approach to Organelle-Targeted Fluorescent Library Based on the Styryl Scaffold. *Journal of the American Chemical Society* **2003,** *125* (5), 1130-1131.

3. Tokar, V.P., Losytskyy, M.Y., Kovalska, V.B. et al. J Fluoresc (2006) 16: 783. https://doi.org/10.1007/s10895-006-0127-3

4. Wu, Y.; Yeh, F. L.; Mao, F.; Chapman, E. R., Biophysical Characterization of Styryl Dye-Membrane Interactions. *Biophysical Journal 97* (1), 101-109.

5. Betz, W. J.; Mao, F.; Smith, C. B., Imaging exocytosis and endocytosis. *Current Opinion in Neurobiology* **1996,** *6* (3), 365-371.

2.2 Fluorescent metal cation probes

2.2.1 Introduction

Selectivity of a fluorescent probe is the most important factor in the detection of a specific target among a myriad of analytes for scientific research including molecular biology, disease diagnosis, environmental protection.[1-4] Designing selective probe, which shows precise signal for specific analyte is challenging since it is too complicated to describe the structure of a probe-analyte complex and the signal change upon analyte sensing is not predictable accurately. Actually, many reported selective probes were developed serendipitously in the course of screening various analytes.

Diversity-oriented fluorescence library approach has shown potential for detecting of diverse analytes for recent years.[5-8] We thought a focused library would reduce the size of the library and increasing the chance of success, rather synthesizing hundreds of fluorescent molecules and screening thousands of analytes. Therefore, we sought to development of fluorescent metal cation probes thorough a focused fluorescent styryl dye based ligand library, which is simpler and more effective operation than a big library. Thirty-five styryl dye based ligands (**Figure 2.2.1**) were synthesized by combining two groups of molecules through the Knoevenagel condensation reaction (**Scheme 2.2.1**), five pico-/quinolinium blocks (**A**–**E,** Group **1**)[9] and seven aldehyde functionalized receptor blocks (**1**–**7,** Group **2**). The products were purified by silica gel column chromatography and prep-HPLC, and their characteristics including ^{1}H, ^{13}C NMR, and high-resolution mass data are listed Experimental Section.

Our supramolecular chemistry approach for target metal cation involves the use of synthetic molecular receptors as building blocks that have a N,N,N′,N′-Tetrakis(2-pyridylmethyl) ethylenediamine (TPEN) moiety (**1**,[10] **2**,[11] **3**, **4**) or an aza-thia crown ether moiety unit (**5**,[12] **6**,[13] **7**[14]). Since following points, we chose styryl conjugated Group **1** molecules for signaling unit. Firstly, through a single condensation reaction

between pico-/quinolinium blocks and aniline-benzaldehyde receptor blocks yields the desired π-conjugated styryl dyes that have electron push-pull structure. Secondly, fluorescence of styryl dye, since their fully conjugated structure, is directly affected by proper binding with a specific metal cation through intramolecular charge transfer (ICT) mechanism.[15-16] Thirdly, each fluorophore has a positive net charge, which enhances its solubility in water. Herein, the effectiveness of the focused library for the detection of metal ions was demonstrated with selected metal cation sensor titration and cellular imaging experiments.

Scheme 2.2.1. Schematic strategy of combinatorial synthesis for fluorescent metal cation probes based on styryl dye ligand.

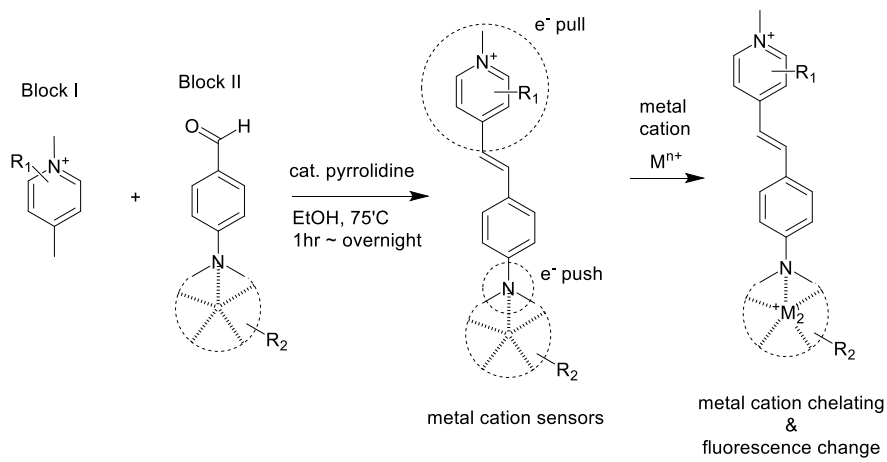

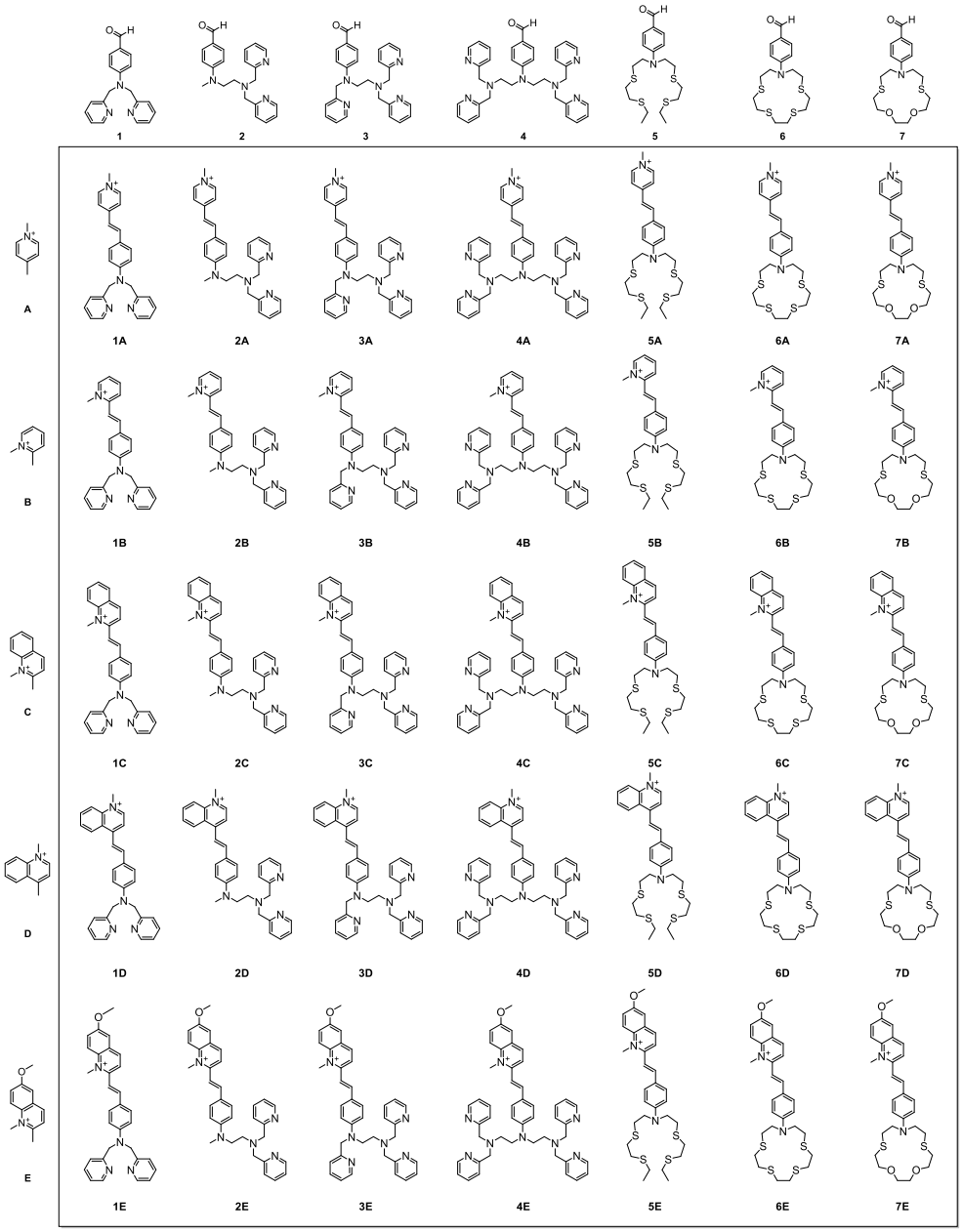

Figure 2.2.1. Building blocks for synthesis of styryl based ligands and structures of synthesized 35 fluorescent ligands.

2.2 Data & results

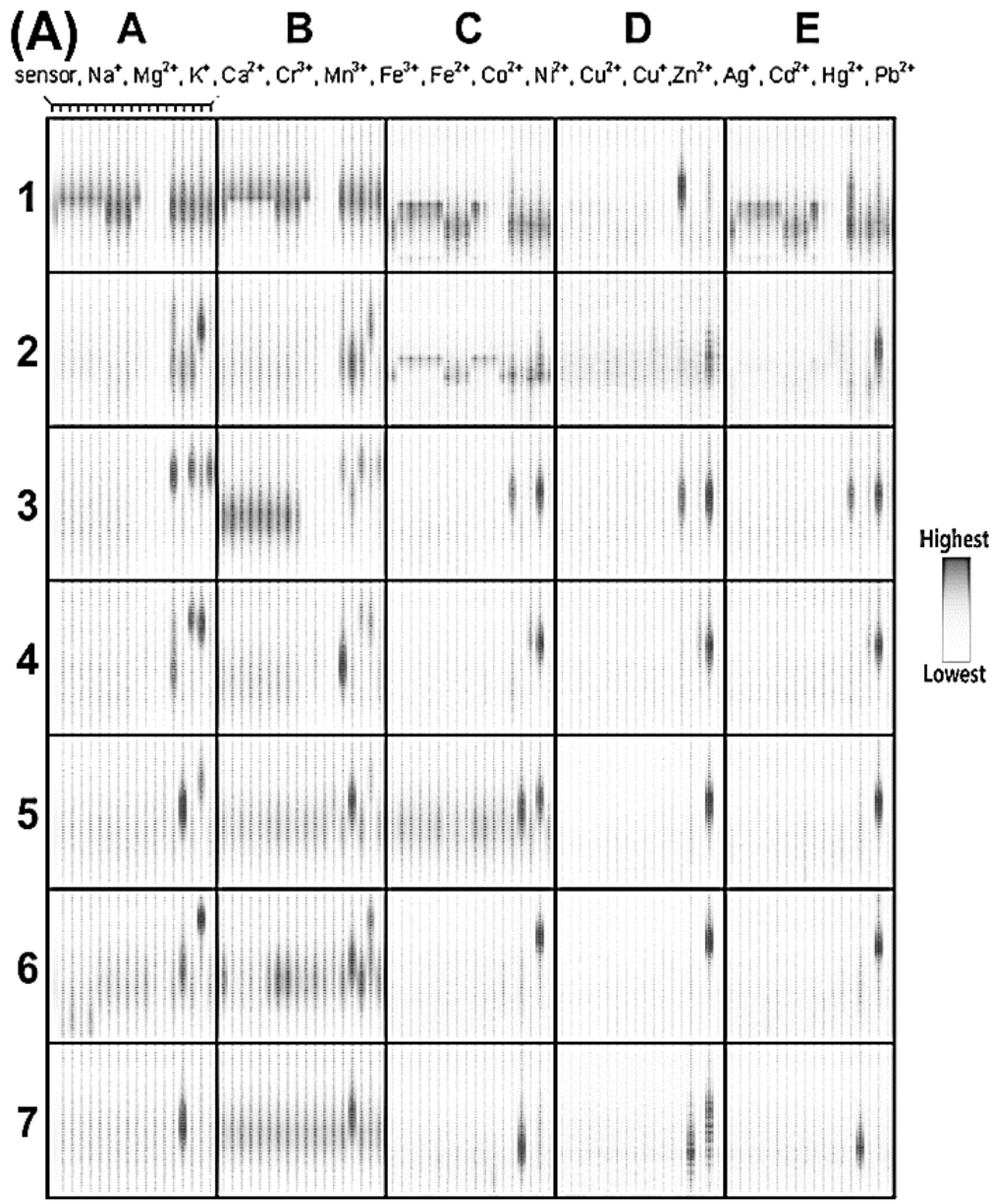

Figure 2.2.2. Primary screening of metal cations (from left column to right: no metal cation, Na^{+}, Mg^{2+}, K^{+}, Ca^{2+}; each 100 mM. Cr^{3+}, Mn^{3+}, Fe^{3+}, Fe^{2+}, Co^{2+}, Ni^{2+}, Cu^{2+}, Cu^{+}, Zn^{2+}, Ag^{+}, Cd^{2+}, Hg^{2+}, Pb^{2+}; each 50 μM.) against metal ion probes (each 5 μM). (A) Metal cation-induced excitation spectra change of 35 fluorescent probes: 300–550 nm. λ_{em}: 580 nm.

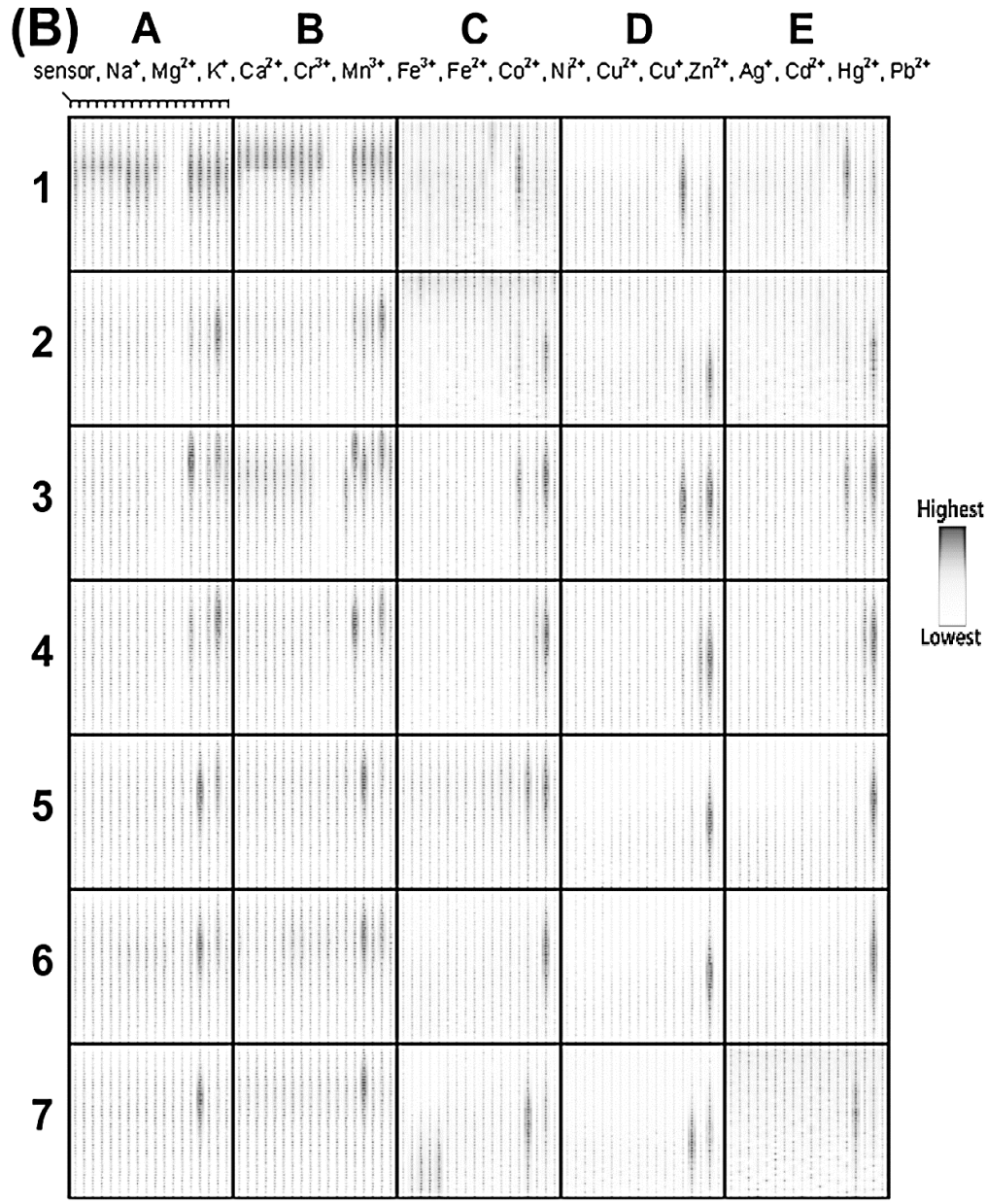

(B) Metal cation-induced emission spectra change of 35 fluorescent probes: 500–750 nm. λ_{ex}: 400 nm. The intensity of fluorescence spectrum is converted to false-color intensity. The highest and lowest values of the fluorescence intensity were determined from the total titration values for each probe. (see false-color intensity map producing protocol in Experimental section)

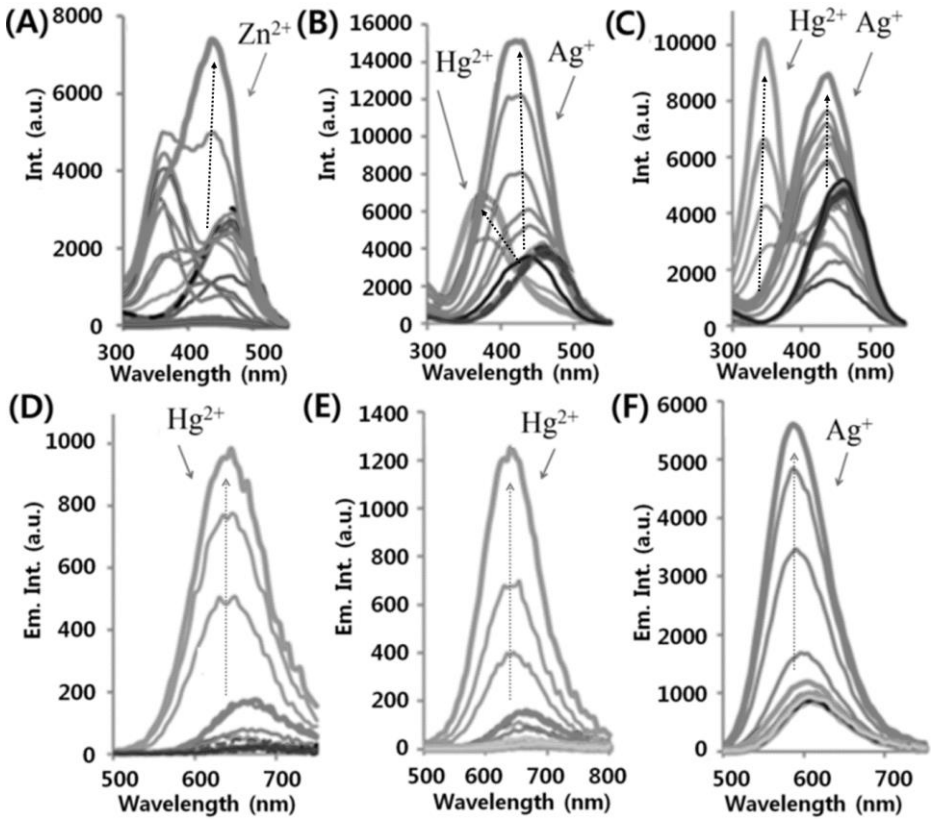

Figure 2.2.3. Fluorescence titration spectra of the selected probes (each 5 μM) for metal cations: excitation spectra (ex. spec.) changes (A, B and C. x-axis: wavelength, y-axis: emission intensity) and emission spectra (em. spec.) changes (D, E and F. x-axis: wavelength, y-axis: emission intensity) for each probe. Spectra changes of the probe upon addition of metal ions (depicted in figure) and without metal cation (balck colored line). (A) **4B**, Zn^{2+} (1, 2, 5, 10, 20 μM), other metal cations (each 50 μM); (B) **5A**, Hg^{2+} or Ag^{+} (each 1, 2, 5, 7, 10 μM), other metal cations (each 50 μM); (C) **6A**, Hg^{2+} or Ag^{+} (each 5, 7, 10, 20, 50 μM), other metal cations (each 50 μM); (D) **5D**, Hg^{2+} or Ag^{+} (each 2, 5, 10, 20 μM), other metal cations (each 50 μM); (E) **6D**, Hg^{2+} or Ag^{+} (each 5, 10, 20, 50 μM), other metal cations (each 50 μM); and (F) **7A**, Hg^{2+} or Ag^{+} (each 5, 7, 10, 20 μM), other metal cations (each 50 μM). These spectra were recorded in HEPES buffer solution (10 mM, pH 7.4, 25°C). Emission and excitation spectra were collected at fixed excitation and emission wavelengths, 400 and 580 nm, respectively.

As seen in the primary screening false-color intensity map, most of the styryl dyes showed fluorescent changes (turn-on, turn-off, or fluorescence shift) when the metal cation was added. Those showed varied fluorescence emission wavelengths, ranging from 540 to 675 nm (λ_{ex} = 400 nm). More conjugated and para-*N*-methyl substituted styryl dye showed fluorescence at the longer wavelengths. Several styryl dyes, probes, showed selectivity to certain metal cations.

To verify the performance of the probes, titration experiments of selected probes **(4B**, **5A**, **6A**, **5D**, **6D**, and **7A**) were carried out for the metal cations with various concentrations (0, 2, 5, 10, 20, 50 μM). The excitation spectra of **4B** showed gradually shifted wavelength of maximum emission with an increase in the concentration of Zn^{2+} ions (**Figure 2.2.3A**). Similarly, blue-shifted excitation and enhanced emission fluorescence spectra of **5A** and **6A** were obtained upon the increasing addition of Ag^{+} or Hg^{2+} ions (**Figure 2.2.3B** and **C**). Interestingly, **5D** and **6D**, that had same metal cation ligand as **5A** and **6A**, displayed gradually enhanced fluorescence emission with the concentration of Hg^{2+} ions, but significant fluorescence emission change was not detected with Ag^{+} (**Figure 2.2.3D** and **E**). Meanwhile, **7A** revealed a selective response to Ag^{+} ions with an increase in the emission intensity (**Figure 2.2.3F**). Also, the binding affinities of styryl dyes to specific metal cations were calculated, in some cases, the binding affinities of probes to specific metal cations are very strong (see **Table 2.2.1** in Experimental section). These metal ion probes did not show significant fluorescence response to pH changes in a physiological condition (pH 6–8) due to low pK_a values of the aniline-based receptors (see **Figure 2.2.4**).

Selective probe **6A** was utilized successfully for selective cellular imaging of Hg^{2+}. As seen in **Figure 2.2.5**, **6A** showed significant fluorescence response with Hg^{2+} only. However, negligible fluorescence showed **6A** itself in cells and quenched fluorescence response with Hg^{2+} when treated with TPEN which is known for a strong metal cation chelator.

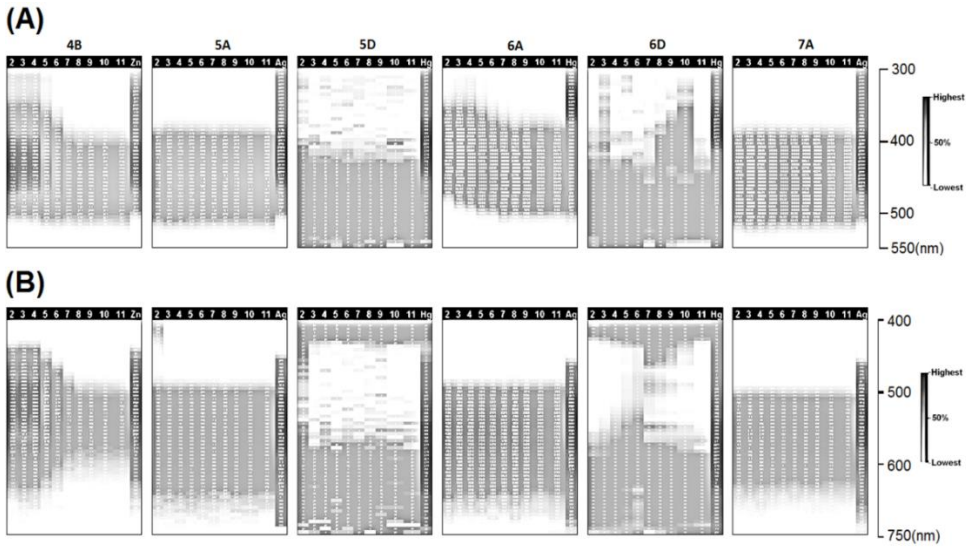

Figure 2.2.4. Fluorescence changes in the excitation and emission spectra of selected metal ion probes (each 5 μM) in phosphate buffer solution (10 mM, pH 2, 3, 4, 5, 6, 7, 8, 9, 10, 11, left to right on the graph) are compared with fluorescence response upon the addition of a specific metal cation (50 μM) to each selected metal ion probe. (A) For the excitation spectrum: 300–550 nm. (B) For the emission spectrum: 450 (500 for 7 series)–750 nm. The highest and lowest values of the fluorescence intensity were determined from the total values for each probe.

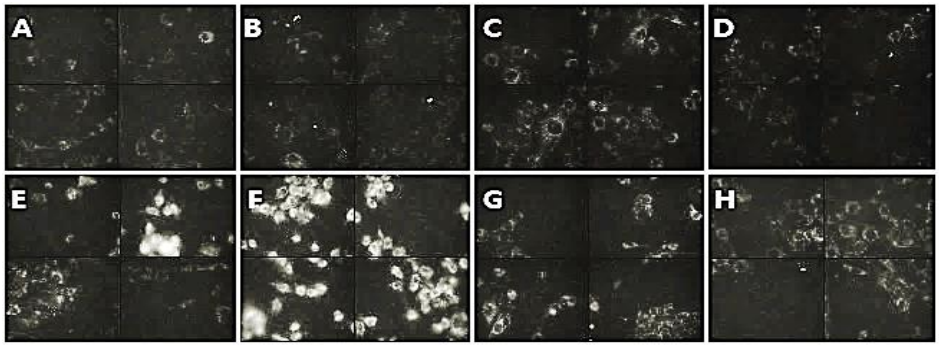

Figure 2.2.5. Fluorescence cellular imaging of **6A** (5 μM) in NIH3T3 cells incubated with (A) Zn^{2+} (B) Cd^{2+} (C) Pb^{2+} (D) Ag^{+} (E) Hg^{2+} (50 μM) (F) Hg^{2+} (100 μM) (G) TPEN (50 μM) after incubation of Hg^{2+} (100 μM), (H) is control picture of 6**A** (5 μM) in the cell. All the incubated metal concentration is 100 μM except Hg^{2+}.

In summary, from the focused styryl ligand dye library, selective metal cation probes were developed. These probes showed strong binding affinity for certain metal cation and negligible response with pH change. Mercury(II) cation selective probe **6A** showed relevance for cellular imaging study.

2.2.3 Experimental section

Materials and Methods

Materials and solvents were purchased from commercial suppliers and were used without further purification. The plate reader was Biotek SYNERGY Microplate Reader. Synthesized compounds were characterized by ^{1}H-NMR, ^{13}C-NMR (Bruker 300 MHz, 500 MHz NMR spectroscopy) and high-resolution mass spectrometry (Gas Chromatography-Mass Spectrometer, Mass System: JEOL, JMS-600W – GC System Agilent, 6890 Series).

General Procedure for Synthesis of the Library

Stock solutions of building blocks I and II were prepared in absolute ethanol (40 mM), respectively. In a 20 mL glass vial, 80 μmol of each reactant (each 2.0 mL) and 10 μL pyrrolidine were added at room temperature and stirred at 65°C for overnight. Quinolinium blocks (**C**, **D**, **E**) reacted faster with blocks II compared to picolinium blocks (**A**, **B**). Building block **3** and **4** needed to take more time (overnight incubation) to complete the condensation reaction with blocks Group **1** than other blocks (**1, 2, 5, 6, 7**). Each reaction was monitored by TLC and LC-MS. LC-MS characterization was performed on a LC-MS-IT-TOF Prominence Shimadzu Technology, using a DAD (SPD-M20A) detector, and a C18 column (20 mm × 4.0 mm, 100 Å, Phenomenex Inc.), with 7 min elution using a gradient solution of CH_3CN-H_2O (containing 0.1% TFA) and an electrospray ionization source. When the reaction was completed, the organic solvent was evaporated under a low pressured rotary evaporator, and the resulting mixture was completely dried *in vacuo*. Then, the reaction mixture was purified by flash column chromatography (Merck Silica Gel 60, particle size: 0.040−0.063 mm, 230−400 mesh ASTM) and was further

purified by reverse phase semi-prep HPLC (Gilson RP-HPLC with a C18 column, 100 mm × 21.2 mm, Axia column from Phenomenex Inc.) using water and acetonitrile as eluents. NMR spectra (^{1}H-NMR, ^{13}C-NMR) of the products were recorded on a Bruker 300 MHz or a 500 MHz NMR spectroscopy. High-resolution mass spectra were recorded by Gas Chromatography—Mass Spectrometer (Mass System: JEOL, JMS-600W, GC System Agilent, 6890 Series).

Synthesis and Preparation of combinatorial building blocks

Building blocks **A** and **B** were purchased and **C**, **D**, **E** blocks were prepared by following the reported procedure.[9] Building blocks **1**, **2**, **5**, **6**, and **7** blocks were prepared by following the published reports.[10-14] Prepared and purchased building block and synthesized probes are listed in **Figure 2.2.1**.

Synthesis of building block 3

Scheme 2.2.2. Synthesis of building block 3

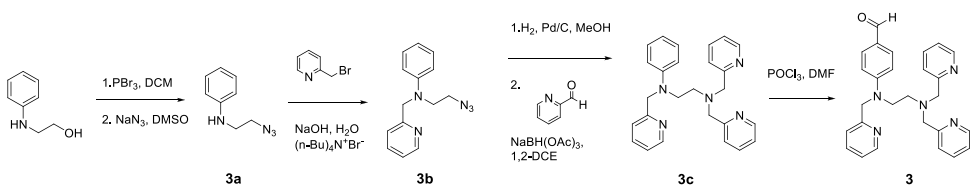

*Synthesis of compound **3a*** To a solution of N-(2-hydroxyethyl)aniline (3.0 g, 21.8 mmol) in 10 mL of MC was added dropwise phosphorous tribromide (22.0 mmol) at 0°C. The reaction mixture was stirred for 3hr at room temperature. Checked by TLC, if N-(2-hydroxyethyl)aniline was totally consumed, the reaction mixture was added 20 mL of water and stirred 5 min more. Decanted the organic layer carefully and dried over sodium sulfate (Na_2SO_4). Removed organic solvent in low pressure and remained residue was directly used in the next step without further purification. The residue was solvated in dimethyl sulfoxide (DMSO) (2 mL) and which was stirred at room temperature. Sodium azide (5.2 g, 80 mmol) in DMSO (2 mL) was added to the solution, the reaction mixture was heated up to 80°C and stirred for 1

hr. The reaction mixture was poured into ethyl acetate (EA) (20 mL) and water (20 mL). Organic layer was washed with water three times. Decanted organic layer carefully and dried over Na_2SO_4. Filtrated organic solvent was condensed in low pressure. Remained crude compounds were purified by silica-gel column chromatography (hexane: EA = 10:1) to afford light brown solid, **3a** (3.21 g, 19.8 mmol, 91% yield^{1}H NMR (300 MHz, $CDCl_3$): δ 3.38 (2H, t, *J* = 5.4 Hz), 3.55 (2H, t, *J* = 5.4 Hz), 3.90 (1H, s), 6.68-6.71 (2H, m), 6.80 (1H, m), 7.25 (2H, m). ^{13}C NMR (75 MHz, $CDCl_3$): δ 43.134, 50.596, 76.786, 77.209, 77.633, 113.144, 118.168, 129.464, 147.349.

*Synthesis of compound **3b*** 2-bromomethylprydine hydrobromide (3.18 g, 12.6 mmol) was solvated in H_2O (0.5 mL), then **3a** (1.70 g, 10.5 mmol), 5 N NaOH (3 mL) and tetrabutylammonium bromide (15 mg) were added under N_2. Reaction mixture was stirred for 24 h at room temperature. Resulting solution was extracted with 10 mL of CH_2Cl_2, and the extract was washed with H_2O. Decanted organic solvent and dried over Na_2SO_4. Filtrated organic solvent was condensed in low pressure. Remained residue was purified by silica-gel column chromatography (CH_2Cl_2: EA = 4:1) yielded brown compound **3b** (1.57 g, 6.19 mmol, 59% yield). ^{1}H NMR (300 MHz, $CDCl_3$): δ 3.50 (2H, t, *J* = 6.4 Hz), 3.66 (2H, t, *J* = 6.2 Hz), 4.73 (2H, s), 6.72-6.76 (3H, m), 7.11-7.23 (4H, m), 7.51-7.56 (1H, m), 8.59-8.60 (1H, m). ^{13}C NMR (75 MHz, $CDCl_3$): δ 49.018, 50.864, 57.118, 112.608, 117.458, 120.837, 122.060, 129.476, 136.728, 147.490, 149.661, 158.861.

*Synthesis of compound **3c*** The azide of **3b** (1.0 g, 3.9 mmol) was hydrogenated using MeOH as solvent and Pd/C (10%, 0.2 g) as catalyst with hydrogen gas bubbling. The mixture was stirred at room temperature for 24 h which was qualitatively monitored by TLC (n-hexane: EtOAc = 2: 1). When **3b** was consumed totally, Pd/C was removed by filtration and the solvent was evaporated *in vacuo*. The product (N^1-phenyl-N^1-(pyridin-2-ylmethyl) ethane-1,2-diamine) was directly used in the next step. N^1-phenyl-N^1-(pyridin-2-ylmethyl) ethane-1, 2-diamine (0.89 g, 3.9 mmol) was added to a stirred solution of 2-pyridinecarboxaldehyde (0.88 g, 8.22

mmol) in 1, 2-dicholroethane (60 mL). After 30 min, sodium triacetoxyborohydride (2.5 g, 12 mmol) was added to the mixture. The reaction mixture was stirred for overnight. After then, the solution was extracted with EA which was washed with water three times. Decanted organic layer carefully and dried over Na_2SO_4. Filtrated organic solvent was condensed in low pressure. Remained crude compounds were purified by silica-gel column chromatography (CH_2Cl_2 to 5% MeOH in CH_2Cl_2) to give sticky brown compound **3c** (0.80 g, 1.95 mmol, 50% yield). ^{1}H NMR (300 MHz, $CDCl_3$): δ 2.88 (2H, t, *J* = 7.2 Hz), 3.64 (2H, t, *J* = 7.6 Hz), 3.92 (4H, s), 4.59 (2H, s), 6.52 (2H, d, *J* = 8.0 Hz), 6.69 (1H, t, *J* =5.6 Hz), 7.06-7.16 (6H, m), 7.50-7.52 (3H, m), 7.62-7.64 (2H, m), 8.53-8.55 (3H, m). ^{13}C NMR (75 MHz, $CDCl_3$): δ 49.664, 50.807, 56.845, 60.820, 111.856, 116.233, 120.561, 121.718, 121.988, 122.937, 129.073, 136.311, 136.513, 147.661, 148.904, 149.312, 159.100, 159.168.

*Synthesis of compound **3*** $POCl_3$ (1 mL, 17 mmol) was added dropwise to a stirring solution of DMF (2 mL, 26mmol) at 0 °C. Stirred for 30 min, then **3c** (0.50 g, 1.22 mmol) in dimethyl formamide (DMF) (1 mL) was slowly added dropwise. The reaction mixture was warmed to room temperature and stirred overnight. The reaction mixture was poured into ice cool water (15 mL), and the pH was adjusted to pH 7-8 with saturated $K_2CO_{3(aq)}$ solution. The mixture was extracted with CH_2Cl_2 for three times. Combined organic extracts were dried over Na_2SO_4. Filtrated organic solvent was condensed in low pressure. Remained crude reaction mixture was purified by silica-gel column chromatography (CH_2Cl_2 to 7% MeOH in CH_2Cl_2) to give the product **3**(sticky brown compound) (0.28 g, 0.64 mmol, 52 % yield). ^{1}H NMR (300 MHz, $CDCl_3$): δ 2.88 (2H, t, *J* = 7.0 Hz), 3.69 (2H, t, *J* = 7.6 Hz), 3.93 (4H, s), 4.67 (2H, s), 6.56 (2H, d, *J* = 8.9 Hz), 7.05 (1H, d, *J* =5.6 Hz), 7.17-7.19 (3H, m), 7.46 (2H, d, *J* =7.8 Hz), 7.58-7.65 (5H, m), 8.55-8.56 (3H, m), 9.70 (1H, s). ^{13}C NMR (75 MHz, $CDCl_3$): δ 49.779, 50.285, 56.723, 60.918, 111.302, 120.360, 122.212, 123.137, 125.562, 131.912, 136.449, 136.818, 149.098, 149.738, 152.634, 157.504, 158.777, 189.996 HRMS (FAB): m/e calcd. for $C_{27}H_{28}N_5O$ $[M+H]^+$ 438.2294, found 438.2290.

Synthesis of building block 4

Scheme 2.2.3. Synthesis of building block 4

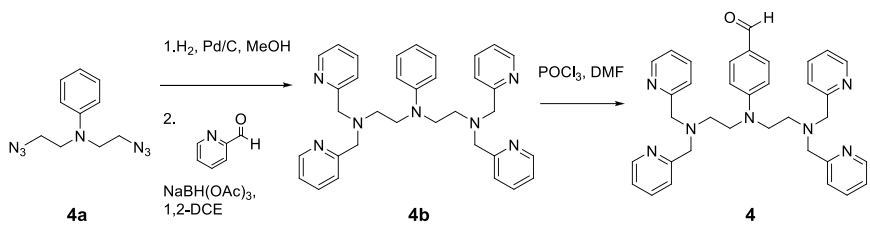

*Synthesis of compound **4b*** With compound **4a**,[2(f),(g)] the synthesis procedure is similar to that of **3C**. The crude product was purified by column chromatography (silica gel, CH2Cl2 to 5% MeOH in CH2Cl2) to obtain sticky brown compound. (48% yield) ^{1}H NMR (300 MHz, $CDCl_3$): δ 2.65 (4H, t, *J* = 7.1 Hz), 3.35 (4H, t, *J* = 7.7 Hz), 3.85 (8H, s), 6.36 (2H, d, *J* = 8.1 Hz), 6.52 (1H, t, *J* = 7.3 Hz), 6.99 (2H, t, *J* = 7.4 Hz), 7.11-7.16 (4H, m), 7.45-7.47 (4H, m), 7.58-7.64 (4H, m), 8.52 (4H, q, J_1 = 4.1 Hz). ^{13}C NMR (75 MHz, $CDCl_3$): δ 49.110, 50.832, 60.865, 111.268, 115.310, 121.970, 122.843, 129.008, 136.302, 147.377, 148.941, 159.301.

*Synthesis of compound **4*** The synthesis procedure is similar to that of **3**. The crude product was purified by column chromatography (silica gel, CH_2Cl_2 to 7% MeOH in CH_2Cl_2) to obtain sticky brown compound. (45% yield) ^{1}H NMR (300 MHz, $CDCl_3$):). ^{1}H NMR (300 MHz, $CDCl_3$): δ 2.65 (4H, t, *J* = 7.2 Hz), 3.41 (4H, t, *J* = 7.6 Hz), 3.85 (8H, s), 6.33 (2H, d, *J* = 8.9 Hz), 7.11-7.15 (4H, m), 7.40-7.47 (6H, m), 7.56-7.62 (4H, m), 8.50 (4H, d, *J* = 4.7 Hz), 9.62 (1H, s). ^{13}C NMR (75 MHz, $CDCl_3$): δ 49.837, 50.181, 60.700, 110.528, 122.199, 123.012, 124.533, 131.847, 136.513, 148.876, 152.223, 158.773, 189.871. HRMS (FAB): m/e calcd. for $C_{35}H_{38}N_7O$ $[M+H]^+$ 572.3138, found 572.3141.

Characteristics of Styryl dyes

Characteristics of **1A** ^{1}H NMR (500 MHz, DMSO-d_6) δ 4.17 (3H, s), 4.93 (4H, s), 6.76 (2H, d, *J* = 9 Hz), 7.11 (1H, d, *J* = 16 Hz), 7.27-7.32 (4H, m), 7.49 (2H, d, *J*

= 15.2 Hz), 7.74-7.75 (2H, m), 7.82 (1H, d, *J* = 15.8 Hz), 8.01 (2H, d, *J* = 6.5 Hz), 8.55 (2H, d, *J* = 4.5 Hz), 8.67 (2H, d, *J* = 6.3 Hz). ^{13}C NMR (125 MHz, DMSO-d_6) δ 46.396, 56.635, 112.508, 117.700, 121.191, 122.244, 122.315, 123.245, 129.985, 136.851, 141.461, 144.387, 149.371, 150.162, 153.186, 158.119. HRMS (FAB): m/e calcd. For $C_{26}H_{25}N_4$ [M^+] 393.2079, found 393.2086.

Characteristics of **1B** ^{1}H NMR (500 MHz, DMSO-d_6) δ 4.26(3H, s), 4.95(4H, s), 6.77(2H, d, *J* = 8.7 Hz), 7.18 (1H, d, *J* = 15.6 Hz), 7.28(2H, m), 7.32(2H, d, *J* = 7.7 Hz), 7.61 (2H, d, *J* = 8.7 Hz), 7.71(1H, t, *J* = 7.5 Hz), 7.74(2H, t, *J* = 7.7 Hz), 7.83(1H, d, *J* = 15.6 Hz), 8.33(1H, t, *J* = 7.7 Hz), 8.40(1H, d, *J* = 7.7 Hz), 8.56(2H, d, *J* = 4.8 Hz), 8.76(1H, d, *J* = 4.7 Hz). ^{13}C NMR (125 MHz, DMSO-d_6) δ 45.704, 56.753, 111.327, 112.421, 121.244, 122.335, 123.090, 123.269, 123.701, 130.525, 136.864, 143.225, 143.702, 145.352, 149.371, 150.405, 153.033, 158.107. HRMS (FAB): m/e calcd. For $C_{26}H_{25}N_4$ [M^+] 393.2079, found 393.2073.

Characteristics of **1C** ^{1}H NMR (500 MHz, DMSO-d_6): δ 4.42(3H, s), 4.99(4H, s), 6.83(2H, d, *J* = 8.96 Hz), 7.29-7.31(2H, m), 7.34(2H, d, *J* = 7.9 Hz), 7.51(1H, d, *J* = 15.5 Hz), 7.75-7.78(4H, m), 7.85(1H, t, *J* = 7.7 Hz), 8.08(1H, t, *J* = 7.7 Hz), 8.19(1H, d, *J* = 15.6 Hz), 8.26(1H, d, *J* = 7.8 Hz), 8.48-8.52(2H, m), 8.57-8.58(2H, m), 8.81(1H, d, *J* = 8.0 Hz). ^{13}C NMR (125 MHz, DMSO-d_6): δ 41.646, 56.715, 112.624, 118.878, 120.251, 121.309, 121.902, 122.399, 123.249, 126.935, 128.153, 128.699, 129.808, 130.771, 134.234, 136.892, 139.195, 148.376, 149.411, 151.422, 156.284, 157.885. HRMS (FAB): m/e calcd. For $C_{30}H_{27}N_4$ [M^+] 443.2236, found 443.2236.

Characteristics of **1D** ^{1}H NMR (500 MHz, DMSO-d_6): δ 4.44(3H, s), 4.98(4H, s), 6.81(2H, d, *J* = 8.89 Hz), 7.28-7.31(2H, m), 7.34(2H, d, *J* = 7.75 Hz), 7.75-7.78(4H, m), 7.95-7.98(2H, m), 8.07(1H, d, *J* = 15.5 Hz), 8.19(1H, t, *J* = 7.7 Hz), 8.32-8.34(2H, m), 8.57(2H, d, *J* = 3.87 Hz), 8.97(1H, d, *J* = 8.45 Hz), 9.12-9.13(1H, m). ^{13}C NMR (125 MHz, DMSO-d_6): δ 44.080, 56.767, 112.574, 113.877, 114.222, 119.044, 121.269, 122.357, 123.848, 125.800, 126.223, 128.635, 131.031, 134.633, 136.878,

138.750, 144.101, 146.966, 149.390, 150.644, 153.012, 158.080. HRMS (FAB): m/e calcd. For $C_{30}H_{27}N_4$ [M^+] 443.2236, found 443.2233.

Characteristics of **1E** ^{1}H NMR (500 MHz, DMSO-d_6): δ 3.95(3H, s), 4.40(3H, s), 4.97(4H, s), 6.80(2H, d, J = 8.96 Hz), 7.28-7.31(2H, q, J_1 = 4.85 Hz, J_2 = 1.9 Hz), 7.33(2H, d, J = 7.76 Hz), 7.49(1H, d, J = 15 Hz), 7.71-7.72(4H, m), 7.75-7.78(2H, m), 8.03(1H, d, J = 15 Hz), 8.35-8.42(2H, m), 8.56-8.57(2H, m), 8.70(1H, d, J = 8.4 Hz). ^{13}C NMR (125 MHz, DMSO-d_6): δ 40.102, 56.134, 56.766, 108.729, 112.574, 112.890, 120.707, 120.751, 121.316, 122.415, 123.319, 125.094, 128.825, 131.267, 134.437, 136.923, 141.238, 146.799, 149.168, 149.422, 151.037, 153.888, 158.252. HRMS (FAB): m/e calcd. For $C_{31}H_{29}N_4O$ [M^+] 473.2341, found 473.2349.

Characterization of **2A** ^{1}H NMR (500 MHz, DMSO-d_6): δ 2.62 (2H, t, J = 6.7 Hz), 2.92 (3H, s), 3.55 (2H, t, J = 6.7 Hz), 3.81 (4H, s), 4.17 (3H, s), 6.62 (2H, d, J = 8.6 Hz), 7.11 (1H, d, J = 16.0 Hz), 7.22-7.25 (2H, m), 7.45-7.50 (4H, m), 7.69 (2H, t, J = 7.6 Hz), 7.85 (1H, d, J = 16.1 Hz), 8.02 (2H, d, J = 6.4 Hz), 8.48 (2H, d, J = 4.7 Hz), 8.65 (2H, d, J = 6.4 Hz). ^{13}C NMR (125 MHz, DMSO-d_6): δ 38.368, 46.333, 49.436, 49.882, 59.987, 111.560, 116.789, 122.032, 122.142, 122.655, 130.165, 136.452, 141.864, 144.217, 148.719, 150.686, 153.366, 159.024. HRMS (FAB): m/e calcd. For $C_{29}H_{32}N_5$ [M^+] 450.2658, found 450.2661.

Characterization of **2B** ^{1}H NMR (500 MHz, DMSO-d_6): δ 2.65 (2H, t, J = 6.7 Hz), 2.95 (3H, s), 3.57 (2H, t, J = 6.8 Hz), 3.83 (4H, s), 4.28 (3H, s), 6.67 (2H, d, J = 8.8 Hz), 7.17 (1H, d, J = 15.7 Hz), 7.23-7.25 (2H, m), 7.45 (2H, d, J = 7.6 Hz), 7.60 (2H, d, J = 8.7 Hz), 7.69-7.71 (3H, m), 7.86 (1H, d, J = 15.7 Hz), 8.33 (1H, m), 8.42 (1H, d, J = 7.6 Hz), 8.49 (2H, d, J = 4.1 Hz), 8.73 (1H, d, J = 6.4 Hz). ^{13}C NMR (125 MHz, DMSO-d_6): δ 38.369, 45.581, 49.407, 49.965, 59.955, 110.242, 111.446, 121.954, 122.112, 122.616, 122.872, 123.476, 130.719, 136.411, 142.986, 144.138, 145.229, 148.727, 151.000, 153.239, 159.025. HRMS (FAB): m/e calcd. For $C_{29}H_{32}N_5$ [M^+] 450.2658, found 450.2663.

Characterization of **2C** ^{1}H NMR (500 MHz, DMSO-d_6): δ 2.68 (2H, t, *J* = 6.6 Hz), 3.00 (3H, s), 3.61-3.65 (2H, m), 3.84 (4H, s), 4.43 (3H, s), 6.72 (2H, d, *J* = 8.7 Hz), 7.23-7.26 (2H, m), 7.45 (2H, d, *J* = 7.7 Hz), 7.50 (1H, d, *J* = 15.5 Hz), 7.70-7.77 (4H, m), 7.84 (1H, m), 8.21 (1H, t, *J* = 8.5 Hz), 8.41 (1H, d, *J* = 8.9 Hz), 8.48-8.50 (3H, m), 8.78 (1H, d, *J* = 6.7 Hz). ^{13}C NMR (125 MHz, DMSO-d_6): δ 38.535, 49.473, 50.068, 59.941, 111.574, 111.679, 118.769, 120.167, 122.143, 122.223, 122.658, 126.749, 127.958, 129.765, 132.014, 134.098, 136.436, 139.225, 141.796, 148.756, 148.887, 151.957, 156.332, 158.998 HRMS (FAB): m/e calcd. For $C_{33}H_{34}N_5$ [M^+] 500.2814, found 500.2818.

Characterization of **2D** ^{1}H NMR (500 MHz, DMSO-d_6): δ 2.67 (2H, t, *J* = 6.7 Hz), 2.98 (3H, s), 3.60 (2H, t, *J* = 6.7 Hz), 3.84 (4H, s), 4.43 (3H, s), 6.70 (2H, d, *J* = 8.7 Hz), 7.23 (2H, d, *J* = 6.3 Hz), 7.46 (2H, d, *J* = 7.7 Hz), 7.71-7.74 (4H,m), 7.76 (2H, d, *J* = 8.6 Hz), 7.95-7.98 (2H, m), 8.12-8.20 (2H, m), 8.31-8.34 (2H, m), 8.49 (2H, d, *J* = 4.5 Hz), 9.00 (1H, d, *J* = 8.6 Hz) 9.11 (1H, d, *J* = 6.4 Hz). ^{13}C NMR (125 MHz, DMSO-d_6) δ 38.505, 43.985, 49.471, 50.053, 59.980, 111.650, 112.840, 113.836, 119.016, 122.194, 122.684, 122.813, 125.734, 126.319, 128.539, 131.412, 134.606, 136.498, 138.802, 144.704, 146.713, 148.787, 151.278, 153.172, 159.041. HRMS (FAB): m/e calcd. For $C_{33}H_{34}N_5$ [M^+] 500.2814, found 500.2817.

Characterization of **2E** ^{1}H NMR (500 MHz, DMSO-d_6): δ 2.66 (2H, t, *J* = 6.7 Hz), 2.97 (3H, s), 3.59 (2H, t, *J* = 6.7 Hz), 3.83 (4H, s), 3.96 (3H, s), 4.42 (3H, s), 6.68 (2H, d, *J* = 8.7 Hz), 7.23 (2H, q, J_1 = 5.21 Hz), 7.45 (3H, m), 7.69-7.74 (6H, m), 8.07 (1H, d, *J* = 15 Hz), 8.35 (1H, d, *J* = 9.3 Hz), 8.45 (1H, d, *J* = 7.5 Hz), 8.49 (2H, d, *J* = 4.4 Hz), 8.68 (1H, d, *J* = 9.3 Hz). ^{13}C NMR (125 MHz, DMSO-d_6): δ 38.484, 49.458, 50.034, 56.098, 59.962, 108.808, 111.589, 111.726, 120.598, 120.656, 122.166, 122.236, 122.672, 124.827, 128.612, 131.562, 134.408, 136.469, 140.858, 147.305, 148.764, 151.574, 154.010, 158.143, 159.016. HRMS (FAB): m/e calcd. for $C_{34}H_{36}N_5O$ [M^+] 530.2920, found 530.2911.

Characterization of **3A** ^{1}H NMR (500 MHz, DMSO-d_6): δ 2.73 (2H, t, *J* = 7.0 Hz), 3.70 (2H, t, *J* = 7.1 Hz), 3.85 (4H, s), 4.17 (3H, s), 4.67 (2H, s), 6.61 (2H, d, *J* = 8.8 Hz), 7.09-7.12 (2H, m), 7.23-7.26 (3H, m), 7.42 (2H, d, *J* = 8.7 Hz), 7.51 (2H, d, *J* = 7.6 Hz), 7.72-7.74 (3H, m), 7.82 (1H, d, *J* =15 Hz), 8.02 (2H, d, *J* = 6.4 Hz), 8.49-8.52 (3H, m), 8.68 (2H, d, *J* = 6.3 Hz). ^{13}C NMR (125 MHz, DMSO-d_6): δ 46.350, 49.158, 50.122, 55.917, 60.043, 111.865, 117.194, 120.811, 122.134, 122.589, 122.754, 130.058, 136.457, 136.747, 141.619, 144.308, 148.740, 149.306, 149.858, 153.275, 158.144, 159.025. HRMS (FAB): m/e calcd. for $C_{34}H_{35}N_6$ [M^+] 527.2923, found 527.2916.

Characterization of **3B** ^{1}H NMR (500 MHz, DMSO-d_6): δ 2.75 (2H, t, *J* = 6.99 Hz), 3.72 (2H, t, *J* = 7.1 Hz), 3.85 (4H, s), 4.25 (3H, s), 4.69 (2H, s), 6.62 (2H, d, *J* = 9.0 Hz), 7.12-7.18 (2H, m), 7.23-7.26 (3H, m), 7.50-7.55 (4H, m), 7.68-7.75 (4H, m), 7.81 (1H, d, *J* = 15.7 Hz), 8.32 (1H, t, *J* = 7.2 Hz), 8.39 (1H, d, *J* = 9.3 Hz), 8.48-8.52 (3H, m), 8.72 (1H, d, *J* = 6.2 Hz). ^{13}C NMR (125 MHz, DMSO-d_6): δ 45.619, 49.225, 50.255, 55.991, 60.043, 110.754, 111.816, 120.888, 122.179, 122.229, 122.451, 122.777, 123.084, 123.587, 130.627, 136.502, 136.789, 143.135, 143.900, 145.317, 148.772, 149.334, 150.177, 153.160, 158.147, 159.034. HRMS (FAB): m/e calcd. for $C_{34}H_{35}N_6$ [M^+] 527.2923, found 527.2924.

Characterization of **3C** ^{1}H NMR (500 MHz, DMSO-d_6): δ 2.77 (2H, t, *J* = 6.9 Hz), 3.76 (2H, t, *J* = 6.9 Hz), 3.86 (4H, s), 4.42 (3H, s), 4.74 (2H, s), 6.68 (2H, d, *J* = 8.8 Hz), 7.15 (1H, d, *J* = 7.9 Hz), 7.24-7.26 (3H, m), 7.51-7.52 (3H, m), 7.69-7.74 (4H, m), 7.84 (1H, m), 8.10 (1H, t, *J* = 7.5 Hz), 8.18 (1H, d, *J* = 15 Hz), 8.23 (1H, d, *J* = 7.3 Hz), 8.41 (1H, d, *J* = 7.2 Hz), 8.50-8.53 (4H, m), 8.80 (1H, d, *J* = 6.3 Hz). ^{13}C NMR (125 MHz, DMSO-d_6): δ 49.240, 50.237, 55.965, 59.996, 112.010, 112.123, 118.814, 120.208, 120.954, 122.161, 122.279, 122.666, 122.766, 126.827, 128.037, 129.773, 131.826, 134.152, 136.478, 136.810, 139.193, 141.999, 148.565, 148.763, 149.345, 151.161, 156.278, 157.851, 158.976. HRMS (FAB): m/e calcd. for $C_{38}H_{37}N_6$ [M^+] 577.3080, found 577.3074.

Characterization of **3D** ^{1}H NMR (500 MHz, DMSO-d_6): δ 2.82 (2H, t, *J* = 6.9 Hz), 3.78 (2H, t, *J* = 6.9 Hz), 3.90 (4H, s), 4.44 (3H, s), 4.74 (2H, s), 6.68 (2H, d, *J* = 8.8 Hz), 7.19 (1H, d, *J* = 6.8 Hz), 7.25-7.27 (3H, m), 7.52 (2H, d, *J* = 7.8 Hz), 7.70-7.76 (5H, m), 7.97-7.98 (2H, m), 8.08 (1H, d, *J* = 15 Hz), 8.13 (1H, t, *J* = 7.2 Hz), 8.31-8.35 (2H, m), 8.50-8.53 (3H, m), 8.99 (1H, d, *J* = 7.8 Hz), 9.10 (1H, d, *J* = 6.7 Hz). ^{13}C NMR (125 MHz, DMSO-d_6): δ 41.597, 44.005, 50.276, 55.993, 59.879, 111.978, 113.366, 114.025, 119.028, 120.947, 122.250, 122.864, 123.292, 125.763, 126.256, 128.577, 131.188, 134.606, 136.554, 136.827, 138.773, 144.334, 146.841, 148.774, 149.317, 150.388, 153.086, 158.067. HRMS (FAB): m/e calcd. for $C_{38}H_{37}N_6$ [M^+] 577.3080, found 577.3087.

Characterization of **3E** ^{1}H NMR (500 MHz, DMSO-d_6): δ 2.85 (2H, t, *J* = 6.9 Hz), 3.80 (2H, t, *J* = 6.7 Hz), 3.93-4.00 (7H, m), 4.41 (3H, s), 4.73 (2H, s), 6.67 (2H, d, *J* = 8.7 Hz), 7.18 (1H, d, *J* = 8.3 Hz), 7.25-7.28 (3H, m), 7.41 (1H, d, *J* = 15 Hz), 7.51-7.52 (2H, m), 7.65-7.75 (8H, m), 8.04 (1H, d, *J* = 15 Hz), 8.35 (1H, d, *J* = 9.0 Hz), 8.42 (1H, d, *J* = 9.1 Hz), 8.49-8.52 (3H, m), 8.70 (1H, d, *J* = 6.8 Hz). ^{13}C NMR (125 MHz, DMSO-d_6): δ 48.995, 50.248, 55.959, 56.093, 59.733, 108.742, 111.960, 112.352, 120.651, 120.690, 120.994, 122.284, 122.331, 122.777, 122.965, 124.950, 128.710, 131.366, 134.409, 136.622, 136.870, 141.041, 146.949, 148.759, 149.300, 149.603, 150.693, 153.918, 157.932, 158.183. HRMS (FAB): m/e calcd. for $C_{39}H_{39}N_6O$[M^+] 607.3185, found 607.3179.

Characterization of **4A** ^{1}H NMR (500 MHz, DMSO-d_6): δ 2.55 (4H, t, *J* = 7.1 Hz), 3.46 (4H, covered with DMSO peak), 3.79 (8H, s), 4.17 (3H, s), 6.41 (2H, d, *J* = 8.9 Hz), 7.10 (1H, d, *J* = 15 Hz), 7.22-7.25 (4H, m), 7.35 (2H, d, *J* = 8.8 Hz), 7.47-7.48 (4H, m), 7.70-7.73 (4H, m), 7.80 (1H, d, *J* = 15 Hz), 8.01 (2H, d, *J* = 6.8 Hz), 8.47 (4H, d, *J* = 4.2 Hz), 8.64 (2H, d, *J* = 6.7 Hz). ^{13}C NMR (125 MHz, DMSO-d_6): δ 46.304, 48.439, 50.017, 60.024, 111.211, 116.643, 121.888, 122.000, 122.175, 122.683, 130.147, 136.482, 141.742, 144.167, 148.715, 149.476, 153.346, 158.978. HRMS (FAB): m/e calcd. for $C_{42}H_{45}N_8$[M^+] 661.3767, found 661.3772.

Characterization of **4B** ^{1}H NMR (500 MHz, DMSO-d_6): δ 2.57 (4H, t, *J* = 7.0 Hz), 3.46 (4H, covered with DMSO peak), 3.79 (8H, s), 4.28 (3H, s), 6.46 (2H, d, *J* = 8.9 Hz), 7.15 (1H, d, *J* = 15 Hz), 7.22-7.25 (4H, m), 7.46-7.49 (6H, m), 7.70-7.73 (4H, m), 7.80 (1H, d, *J* = 15 Hz), 8.30 (1H, t, *J* = 7.9 Hz), 8.41 (1H, d, *J* = 8.4 Hz), 8.47-8.48 (4H, m), 8.71 (1H, d, *J* = 6.2 Hz). ^{13}C NMR (125 MHz, DMSO-d_6): δ 45.615, 48.440, 50.107, 60.015, 110.081, 111.140, 121.759, 122.181, 122.674, 122.849, 123.489, 130.725, 136.489, 142.974, 144.008, 145.171, 148.727, 149.797, 153.202, 158.970. HRMS (FAB): m/e calcd. for $C_{42}H_{45}N_8[M^+]$ 661.3767, found 661.3773.

Characterization of **4C** ^{1}H NMR (500 MHz, DMSO-d_6): δ 2.64 (4H, t, *J* = 7.1 Hz), 3.52 (4H, t, *J* = 7.0 Hz), 3.81 (8H, s), 4.43 (3H, s), 6.54 (2H, d, *J* = 8.7 Hz), 7.23-7.26 (4H, m), 7.45-7.48 (5H, m), 7.63-7.65 (2H, m), 7.71-7.74 (4H, m), 7.83 (1H, t, *J* = 7.5 Hz), 8.08 (1H, t, *J* = 7.8 Hz), 8.15 (1H, d, *J* = 15 Hz), 8.22 (1H, d, *J* = 7.9 Hz), 8.40 (1H, d, *J* = 8.8 Hz), 8.47-8.50 (6H, m), 8.77 (1H, d, *J* = 6.8 Hz). ^{13}C NMR (125 MHz, DMSO-d_6): δ 48.555, 48.612, 50.206, 60.035, 111.479, 118.786, 120.202, 122.122, 122.232, 122.731, 126.777, 129.810, 132.047, 134.153, 136.525, 139.268, 141.804, 148.813, 150.920, 156.338, 159.014. HRMS (FAB): m/e calcd. For $C_{46}H_{47}N_8[M^+]$ 711.3924, found 711.3925.

Characterization of **4D** ^{1}H NMR (500 MHz, DMSO-d_6): δ 2.61 (4H, t, *J* = 7.0 Hz), 3.49 (4H, t, *J* = 7.0 Hz), 3.82 (8H, s), 4.43 (3H, s), 6.53 (2H, d, *J* = 8.7 Hz), 7.23-7.25 (4H, m), 7.48 (4H, d, *J* = 7.6 Hz), 7.65 (2H, d, *J* = 8.6 Hz), 7.71-7.74 (4H, m), 7.95-7.97 (2H, m), 8.08 (1H, d, *J* = 15 Hz), 8.20 (1H, t, *J* = 7.8 Hz), 8.30-8.34 (2H, m), 8.49 (4H, d, *J* = 4.9 Hz), 8.99 (1H, d, *J* = 8.6 Hz), 9.10 (1H, d, *J* = 6.7 Hz). ^{13}C NMR (125 MHz, DMSO-d_6): δ 43.926, 48.461, 50.162, 60.010, 111.338, 112.699, 113.772, 118.973, 122.159, 122.661, 125.684, 126.279, 128.484, 131.382, 134.550, 136.449, 138.771, 144.581, 146.636, 148.765, 150.130, 153.121, 158.998. HRMS (FAB): m/e calcd. For $C_{46}H_{47}N_8$ $[M^+]$ 711.3924, found 711.3925.

Characterization of **4E** ^{1}H NMR (500 MHz, DMSO-d_6): δ 2.60 (4H, t, *J* = 7.0 Hz),

3.50 (4H, t, J = 7.0 Hz), 3.82 (8H, s), 3.97 (3H, s), 4.42 (3H, s), 6.53 (2H, d, J = 8.9 Hz), 7.23-7.26 (4H, m), 7.47-7.49 (5H, m), 7.59 (2H, d, J = 8.8 Hz), 7.71-7.74 (6H, m), 8.02 (1H, d, J = 15 Hz), 8.38 (1H, d, J = 9.8 Hz), 8.43 (1H, d, J = 9.2 Hz), 8.49-8.50 (4H, m), 8.70 (1H, d, J = 9.2 Hz). ^{13}C NMR (125 MHz, DMSO-d_6): δ 48.465, 50.144, 56.075, 59.988, 108.797, 111.322, 111.614, 120.583, 120.633, 122.074, 122.164, 122.667, 124.797, 128.579, 131.545, 134.406, 136.454, 140.804, 147.174, 148.758, 150.462, 153.976, 158.120, 158.972. HRMS (FAB): m/e calcd. For $C_{47}H_{49}N_8O$ [M^+] 741.4029, found 741.4043.

Characterization of **5A** ^{1}H NMR (500 MHz, DMSO-d_6): δ 1.16 (6H, t, J = 7.5 Hz), 2.52-2.56 (4H, m), 2.71-2.72 (4H, m), 2.75-2.80 (8H, m), 3.61 (4H, J = 7.6 Hz), 4.18 (3H, s), 6.76 (2H, d, J = 8.9 Hz), 7.15 (1H, d, J = 16 Hz), 7.58 (2H, d, J = 8.8 Hz), 7.89 (1H, d, J = 16 Hz), 8.05 (2H, d, J = 6.7 Hz), 8.69 (2H, d, J = 6.4 Hz). ^{13}C NMR (125 MHz, DMSO-d_6): δ 14.754, 24.930, 28.405, 31.162, 31.533, 46.382, 50.561, 111.725, 117.386, 122.190, 122.838, 130.385, 141.552, 144.342, 148.876, 153.269. HRMS (FAB): m/e calcd. For $C_{26}H_{39}N_2S_4$ [M^+] 507.1996, found 507.2001.

Characterization of **5B** ^{1}H NMR (500 MHz, DMSO-d_6): δ 1.16 (6H, t, J = 7.2 Hz), 2.52-2.57 (4H, m), 2.71-2.79 (12H, m), 3.62 (4H, t, J = 7.6 Hz), 4.29 (3H, s), 6.78 (2H, d, J = 9.0 Hz), 7.22 (1H, d, J = 15.7 Hz), 7.70-7.73 (3H, m), 7.90 (1H, d, J = 15.7 Hz), 8.33 (1H, t, J = 7.9 Hz), 8.45 (1H, d, J = 8.3 Hz), 8.76 (1H, d, J = 6.2 Hz). ^{13}C NMR (125 MHz, DMSO-d_6): δ 14.756, 24.938, 28.432, 31.160, 31.559, 45.676, 50.537, 110.960, 111.602, 122.689, 123.154, 123.655, 130.958, 143.148, 143.817, 145.333, 149.181, 153.136. HRMS (FAB): m/e calcd. For $C_{26}H_{39}N_2S_4$ [M^+] 507.1996, found 507.1999.

Characterization of **5C** ^{1}H NMR (500 MHz, DMSO-d_6): δ 1.16-1.19 (6H, m), 2.53 (4H, t, J = 7.4 Hz), 2.72-2.81 (12H, m), 3.68 (4H, t, J = 7.4 Hz), 4.45 (3H, s), 6.82 (2H, d, J = 8.9 Hz), 7.55 (1H, d, J = 15.5 Hz), 7.71 (1H, m), 7.84-7.86 (3H, m), 8.09 (1H, m), 8.23-8.26 (2H, m), 8.42 (1H, d, J = 8.9 Hz), 8.50 (1H, d, J = 9.2 Hz), 8.82

(1H, d, J = 9.1 Hz). ^{13}C NMR (125 MHz, DMSO-d_6): δ 14.751, 24.837, 28.455, 31.150, 31.566, 45.637, 50.542, 111.810, 112.385, 118.848, 120.253, 123.628, 126.879, 128.096, 129.795, 132.139, 134.197, 139.206, 142.100, 148.488, 150.168, 156.320. HRMS (FAB): m/e calcd. For $C_{30}H_{41}N_2S_4$ [M^+] 557.2153, found 557.2148.

Characterization of **5D** ^{1}H NMR (500 MHz, DMSO-d_6): δ 1.17 (6H, t, J = 7.4 Hz), 2.50 (4H, t, J = 7.3 Hz), 2.72 (4H, t, J = 3.9 Hz), 2.78-2.82 (8H, m), 3.65 (4H, t, J = 7.5 Hz), 4.45 (3H, s), 6.81 (2H, d, J = 8.9 Hz), 7.85 (2H, d, J = 8.8 Hz), 7.96-7.99 (2H, m), 8.14-8.20 (2H, m), 8.33-8.35 (2H, m), 8.99 (1H, d, J = 8.6 Hz), 9.12 (1H, d, J = 6.7 Hz). ^{13}C NMR (125 MHz, DMSO-d_6): δ 14.757, 24.950, 28.487, 31.167, 31.578, 44.059, 50.578, 111.744, 113.512, 114.121, 119.026, 123.487, 125.765, 126.273, 128.592, 131.525, 134.610, 138.752, 144.255, 146.847, 149.400, 153.064. HRMS (FAB): m/e calcd. For $C_{30}H_{41}N_2S_4$ [M^+] 557.2153, found 557.2156.

Characterization of **5E** ^{1}H NMR (500 MHz, DMSO-d_6): δ 1.16-1.22 (6H, m), 2.50-2.58 (4H, m), 2.70-2.74 (4H, m), 2.77-2.82 (8H, m), 3.65 (4H, t, J = 7.6 Hz), 3.96 (3H, s), 4.44 (3H, s), 6.79 (2H, d, J = 8.8 Hz), 7.50 (1H, d, J = 15.6 Hz), 7.68-7.73 (2H, m), 7.79 (2H, d, J = 8.8 Hz), 8.09 (1H, d, J = 15.4 Hz), 8.37 (1H, d, J = 9.6 Hz), 8.46 (1H, d, J = 9.2 Hz), 8.72 (1H, d, J = 9.1 Hz). ^{13}C NMR (125 MHz, DMSO-d_6): δ 14.762, 24.953, 28.457, 31.167, 31.573, 50.553, 56.111, 108.740, 111.691, 112.444, 120.648, 120.706, 122.913, 124.947, 128.722, 131.703, 134.386, 141.034, 146.894, 149.753, 153.893, 158.175. HRMS (FAB): m/e calcd. For $C_{31}H_{43}N_2OS_4$ [M^+] 587.2258, found 587.2265.

Characterization of **6A** ^{1}H NMR (500 MHz, DMSO-d_6): δ 2.74-2.84 (16H, m), 3.61 (4H, t, J = 16.3 Hz), 4.18 (3H, s), 6.73 (2H, d, J = 8.8 Hz), 7.15 (1H, d, J = 16.1 Hz), 7.58 (2H, d, J = 8.7 Hz), 7.89 (1H, d, J = 16.1 Hz), 8.05 (2H, d, J = 6.5 Hz), 8.68 (2H, d, J = 6.4 Hz). ^{13}C NMR (125 MHz, DMSO-d_6): δ 27.116, 31.468, 31.846, 32.115, 46.365, 51.045, 111.455, 117.270, 122.170, 122.733, 130.544, 141.592, 144.314, 148.768, 153.276. HRMS (FAB): m/e calcd. For $C_{24}H_{33}N_2S_4$ [M^+]

477.1527, found 477.1533.

Characterization of **6B** ^{1}H NMR (500 MHz, DMSO-d_6): δ 2.74-2.83(16H, m), 3.61 (4H, t, *J* = 8.4 Hz), 4.28 (3H, s), 6.73 (2H, d, *J* = 8.9 Hz), 7.20 (1H, d, *J* = 15.7 Hz), 7.68-7.72 (3H, m), 7.88 (1H, d, *J* = 15.7 Hz), 8.32-8.36 (1H, m), 8.43 (1H, d, *J* = 8.3 Hz), 8.74 (1H, d, *J* = 6.1 Hz). ^{13}C NMR (125 MHz, DMSO-d_6): δ 27.114, 31.468, 31.829, 32.102, 45.617, 51.041, 110.853, 111.474, 122.594, 123.128, 123.628, 131.096, 143.138, 143.865, 145.331, 149.070, 153.156. HRMS (FAB): m/e calcd. For $C_{24}H_{33}N_2S_4$ [M^+] 477.1527, found 477.1529.

Characterization of **6C** ^{1}H NMR (500 MHz, DMSO-d_6): δ 2.77-7.84 (16H, m), 3.67 (4H, t, *J* = 8.4 Hz), 4.45 (3H, s), 6.81 (2H, d, *J* = 8.9 Hz), 7.55 (1H, d, *J* = 15.5 Hz), 7.83-7.85 (3H, m), 8.09 (1H, t, *J* = 8.6 Hz), 8.23-8.26 (2H, m), 8.42 (1H, d, *J* = 9.0 Hz), 8.50 (1H, d, *J* = 9.3 Hz), 8.83 (1H, d, *J* = 9.1 Hz). ^{13}C NMR (125 MHz, DMSO-d_6): δ 27.132, 31.489, 31.835, 32.114, 51.098, 54.867, 111.609, 112.304, 118.847, 120.255, 122.843, 126.877, 128.094, 129.799, 132.295, 134.194, 139.210, 142.085, 148.530, 150.036, 156.328. HRMS (FAB): m/e calcd. For $C_{28}H_{35}N_2S_4$ [M^+] 527.1683, found 527.1686.

Characterization of **6D** ^{1}H NMR (500 MHz, DMSO-d_6): δ 2.78-2.81 (16H, m), 3.64 (4H, t, *J* = 8.4 Hz), 4.45 (3H, s), 6.77 (2H, d, *J* = 8.9 Hz), 7.85 (2H, d, *J* = 8.8 Hz), 7.96-8.01 (2H, m), 8.14-8.22 (2H, m), 8.33-8.35 (2H, m), 8.99 (1H, d, *J* = 8.6 Hz), 9.12 (1H, d, *J* = 6.7 Hz) ^{13}C NMR (125 MHz, DMSO-d_6): δ 27.159, 31.477, 31.831, 32.107, 44.038, 51.089, 111.514, 113.435, 114.106, 119.043, 123.411, 125.769, 126.260, 128.609, 131.681, 134.621, 138.768, 144.317, 146.856, 149.289, 153.092. HRMS (FAB): m/e calcd. For $C_{28}H_{35}N_2S_4$ [M^+] 527.1683, found 527.1675.

Characterization of **6E** ^{1}H NMR (500 MHz, DMSO-d_6): δ 2.76-2.82 (16H, m), 3.65 (4H, t, *J* = 8.4 Hz), 3.97 (3H, s), 4.44 (3H, s), 6.77 (2H, d, *J* = 9.1 Hz), 7.50 (1H, d, *J* = 15.5 Hz), 7.71-7.74 (2H, m), 7.79 (2H, d, *J* = 8.9 Hz), 8.10 (1H, d, *J* = 15.5 Hz),

8.37 (1H, d, J = 9.5 Hz), 8.45 (1H, d, J = 9.3 Hz), 8.71 (1H, d, J = 9.2 Hz). ^{13}C NMR (125 MHz, DMSO-d_6): δ 27.126, 31.471, 31.825, 32.102, 51.076, 56.091, 108.736, 111.498, 112.395, 120.656, 120.717, 122.848, 124.967, 128.729, 131.851, 134.413, 141.056, 146.941, 149.636, 153.935, 158.195. HRMS (FAB): m/e calcd. For $C_{29}H_{37}N_2OS_4$ [M^+] 557.1789, found 557.1796.

Characterization of **7A** ^{1}H NMR (500 MHz, DMSO-d_6): δ 2.73 (4H, t, J = 5.3 Hz), 2.81 (4H, t, J = 7.6 Hz), 3.57 (4H, s), 3.68-3.70 (8H, m), 4.17 (3H, s), 6.70 (2H, d, J = 8.8 Hz), 7.13 (1H, d, J = 16 Hz), 7.57 (2H, d, J = 8.7 Hz), 7.87 (1H, d, J = 16 Hz), 8.04 (2H, d, J = 6.6 Hz), 8.67 (2H, d, J = 6.6 Hz). ^{13}C NMR (125 MHz, DMSO-d_6): δ 29.053, 30.752, 46.362, 51.239, 69.977, 72.869, 111.765, 117.265, 122.157, 122.680, 130.448, 141.623, 144.312, 148.900, 153.281. HRMS (FAB): m/e calcd. For $C_{24}H_{33}N_2O_2S_2$ [M^+] 445.1983, found 445.1977.

Characterization of **7B** ^{1}H NMR (500 MHz, DMSO-d_6): δ 2.74 (4H, t, J = 5.3 Hz), 2.82 (4H, t, J = 7.6 Hz), 3.56-3.58 (4H, m), 3.67-3.71 (8H, m), 4.28 (3H, s), 6.72 (2H, d, J = 8.9 Hz), 7.20 (1H, d, J = 15.7 Hz), 7.69-7.72 (3H, m), 7.88 (1H, d, J = 15.7 Hz), 8.32 (1H, t, J = 7.9 Hz), 8.43 (1H, d, J = 8.0 Hz), 8.74 (1H, d, J = 6.1 Hz). ^{13}C NMR (125 MHz, DMSO-d_6): δ 29.069, 30.779, 45.632, 51.256, 69.978, 72.877, 110.832, 111.663, 122.528, 123.097, 123.613, 130.996, 143.122, 143.874, 145.310, 149.201, 153.149. HRMS (FAB): m/e calcd. For $C_{24}H_{33}N_2O_2S_2$ [M^+] 445.1983, found 445.1988.

Characterization of **7C** ^{1}H NMR (500 MHz, DMSO-d_6): δ 2.75 (4H, t, J = 5.2 Hz), 2.86 (4H, t, J = 7.7 Hz), 3.56-3.58 (4H, m), 3.69-3.75 (8H, m), 4.44 (3H, s), 6.78 (2H, d, J = 8.9 Hz), 7.54 (1H, d, J = 15.6 Hz), 7.84-7.86 (3H, m), 8.07 (1H, t, J = 16.3 Hz), 8.22 (2H, t, J = 7.4 Hz), 8.42 (1H, d, J = 9.0 Hz), 8.50 (1H, d, J = 9.3 Hz), 8.81 (1H, d, J = 9.1 Hz). ^{13}C NMR (125 MHz, DMSO-d_6): δ 29.161, 30.888, 51.358, 69.988, 72.866, 111.917, 112.277, 118.847, 120.255, 122.776, 126.879, 128.089, 129.09, 132.210, 134.201, 139.230, 142.078, 148.572. HRMS (FAB): m/e calcd. For

$C_{28}H_{35}N_2O_2S_2$ [M^+] 495.2140, found 495.2139.

Characterization of **7D** ^{1}H NMR (500 MHz, DMSO-d_6): δ 2.75 (2H, t, *J* = 5.0 Hz), 2.84 (6H, t, *J* = 7.6 Hz), 3.55 (4H, s), 3.63-3.73 (8H, m), 4.44 (3H, s), 6.75 (2H, d, *J* = 8.7 Hz), 7.84 (2H, d, *J* = 8.7 Hz), 7.96-8.01 (2H, m), 8.13-8.22 (2H, m), 8.33 (2H, d, *J* = 7.9 Hz), 8.99 (1H, d, *J* = 8.6 Hz), 9.10 (1H, d, *J* = 6.6 Hz). ^{13}C NMR (125 MHz, DMSO-d_6): δ 30.428, 30.809, 50.929, 51.312, 69.979, 72.872, 111.816, 113.406, 114.064, 119.020, 123.333, 125.761, 126.242, 128.595, 131.568, 134.611, 138.763, 144.323, 146.835, 149.428, 153.078. HRMS (FAB): m/e calcd. For $C_{28}H_{35}N_2O_2S_2$ [M^+] 495.2140, found 495.2139.

Characterization of **7E** ^{1}H NMR (300 MHz, $CDCl_3$): δ 2.79 (4H, t, *J* = 7.2 Hz), 2.90 (4H, s), 3.68 (8H, m), 3.83 (4H, t, *J* = 5.1 Hz), 3.99 (3H, s), 4.60 (3H, s) 6.58 (2H, d, *J* = 8.7 Hz), 7.37 (1H, d, *J* = 2.7 Hz), 7.56 (2H,t, *J* = 3.0 Hz), 7.73-7.84 (3H, m), 7.79 (1H, t *J* = 15.3 Hz), 8.07 (1H, d, *J* = 9.6 Hz), 8.31 (1H, d, *J* = 9.0Hz), 8.63 (1H, d, *J* = 9.3Hz). ^{13}C NMR (125 MHz, DMSO-d_6): δ 29.104, 30.818, 51.308, 56.089, 69.980, 72.881, 108.743, 111.776, 112.337, 120.641, 120.694, 122.769, 124.933, 128.708, 131.748, 134.400, 141.015, 146.967, 149.770, 153.914, 158.178. HRMS (FAB): m/e calcd. For $C_{29}H_{37}N_2O3S_2$ [M^+] 525.2246, found 525.2248.

Determination of the Dissociation Constants of the Complexes

In the case of a stoichiometry of 1:1, the dissociation constant $K_d = 1/K_a$ which controls the equilibrium between the free ligand [*L*] and the metal cation complex [*ML*], [*M*] + [*L*] = [*ML*] can be written as

$$K_a = \frac{[ML]}{[L][M]} \qquad (1)$$

The measurements are carried out under conditions where the fluorescence intensity of the free ligand X_{free} is proportional to the concentration c_{free}:

$$X_{free} = ac_{free} \qquad (2)$$

The fluorescence intensity becomes X when a given amount of metal cation at a concentration c_M added

$$X = a[L] + b[ML] \qquad (3)$$

Now we have this relation

$$c_{free} = [L] + [ML] \qquad (4)$$
$$c_M = [M] + [ML] \qquad (5)$$

In the presence of an excess of metal cation, the ligand is thoroughly complexed with metal cation, X reaches the maximum value X_{max}:

$$X_{\max} = bc_0 \qquad (6)$$

From equations (1) to (6), now we can derive the relation

$$\frac{X_{free} - X}{X - X_{\max}} = K_a[M] \qquad (7)$$

(X_{free} - X)/(X - X_{max}) is often plotted as a function of the overall concentration in metal cation c_M, assuming that the concentration in free cation $[M] \cong c_M$; the slope yields K_a.

The complexation of the ligand in buffered solution strong enough that $[M]$ may not be approximated to c_M, then the following relation derived from the above equations should be used:

$$X = X_{free} + \frac{X_{\max} - X_{free}}{2c_0}\left[c_0 + c_M + 1/K_a - \left[(c_0 + c_M + 1/K_d)^2 - 4c_0c_M\right]^{\frac{1}{2}}\right] \qquad (8)$$

K_a can be obtained by a nonlinear least-squares analysis of X versus c_M. Computed dissociation constants between styryl dye ligand and metal cations listed in **Table 2.2.1**.

Table2.2. 1. Dissociation constants (K_d) between probes and metal ions

K_d (μM)	**Zn^{2+}**	**Cd^{2+}**	**Pb^{2+}**	**Hg^{2+}**	**Ag^{+}**
1D	.*	.	.	235	.
2A	0.0319	.	.	0.0103	.
2B	0.274	0.649	0.816	0.0888	33.6
2D	.	.	.	0.281	.
3A	0.406	0.191	0.506	2.36	.
3B	0.0951	0.0170	0.158	0.00108, (1.77)**	.
3C	0.378	0.947	2.31	7.25	.
3D	0.511	0.879	5.06	.	.
3E	0.734	0.685	2.85	.	.
4A	0.292, (2.93)	0.000211	20.6	0.205	.
4B	0.375	0.567	5.21	0.776	.
4C	0.00180, (12.8)	0.205	4.65	0.0448	.
4D	0.0505	0.259	6.02	6.69	.
4E	0.00977,	0.0399	4.03	4.48	.

	(12.1)				
5A	.	.	.	5.90	2.80
5B	.	.	.	3.29	2.74
5C	.	.	.	4.84	0.710
5D	.	.	.	5.49	8.11
5E	.	.	.	11.9	15.3
6A	.	.	.	15.4	11.8
6B	.	.	.	0.298, (13.2)	3.86
6C	.	.	.	27.0	5.22
6D	.	.	.	37.3	13.6
6E	.	.	.	26.2	10.1
7A	.	.	.	.	7.42
7B	.	.	.	.	16.2
7C	.	.	.	859	26.7
7D	.	.	.	16.0	17.1
7E	.	.	.	.	49.3

*n.d. (not determined).

** Values in parentheses were obtained when the second metal ion was added to the 1:1 complex of the probe and metal ion (in other words, when one metal ion was

removed from the 1:2 complex of the probe and metal ion).

Metal cation sensing experiment protocol

1. Prepare a 5 mM stock solution of probe by in spectroscopymetry-grade DMSO, respectively.

2. Prepare 100 μl of 10 μM probe in HEPES (10 mM, pH 7.4, 25°C. 0.1 v % DMSO) by adding the 5 mM stock solution of probe to a micro plate well.

3. Twenty-micro liter of metal cation (Na^{+}, Mg^{2+}, K^{+}, Ca^{2+}; each 1 M. Cr^{3+}, Mn^{3+}, Fe^{3+}, Fe^{2+}, Co^{2+}, Ni^{2+}, Cu^{2+}, Cu^{+}, Zn^{2+}, Ag^{+}, Cd^{2+}, Hg^{2+}, Pb^{2+}; each 500 μM) in buffer solution (10 mM, pH 7.4, 25°C. 0.1 v % DMSO) is added to the solution in the micro plate well, respectively.

4. Add 80 μL of HEPES buffer solution (10 mM, pH 7.4, 25°C. 0.1 v% DMSO) to the well for adjusting solution concentration.

5. Record the fluorescence intensity of the solution just prepared by using a micro plate reader.

Producing of a Heat Map

1.Convert each recorded intensity of fluorescence spectrum to false color intensity image by using Microsoft Excel program. See **Scheme 2.2.4**.

Scheme 2.2.4. Detailed view of the excitation fluorescence spectrum changes of probe **7A** upon addition of various metal cations and its false-color intensity image for a simple view. The highest and lowest values of the fluorescence intensity were determined from the total titration values for each probe.

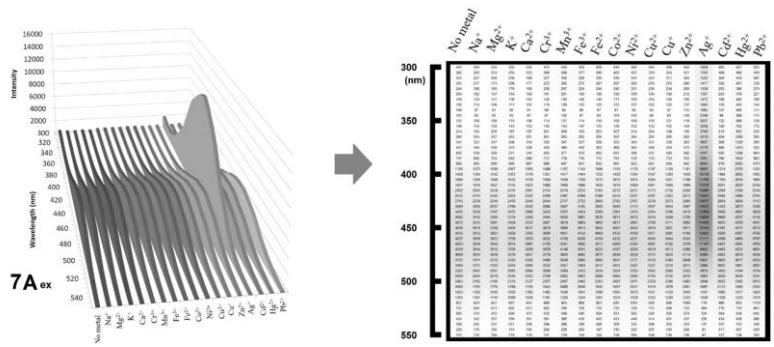

2.Sort images by name of probe.

2.2.4 References

1. Fernandez-Suarez, M.; Ting, A. Y., Fluorescent probes for super-resolution imaging in living cells. *Nat Rev Mol Cell Biol* **2008,** *9* (12), 929-43.

2. Kobayashi, H.; Ogawa, M.; Alford, R.; Choyke, P. L.; Urano, Y., New Strategies for Fluorescent Probe Design in Medical Diagnostic Imaging. *Chemical Reviews* **2010,** *110* (5), 2620-2640.

3. Chan, J.; Dodani, S. C.; Chang, C. J., Reaction-based small-molecule fluorescent probes for chemoselective bioimaging. *Nat Chem* **2012,** *4* (12), 973-84.

4. Long, F.; Zhu, A.; Shi, H., Recent advances in optical biosensors for environmental monitoring and early warning. *Sensors (Basel)* **2013,** *13* (10), 13928-48.

5. Im, C.-N.; Kang, N.-Y.; Ha, H.-H.; Bi, X.; Lee, J. J.; Park, S.-J.; Lee, S. Y.; Vendrell, M.; Kim, Y. K.; Lee, J.-S.; Li, J.; Ahn, Y.-H.; Feng, B.; Ng, H.-H.; Yun, S.-W.; Chang, Y.-T., A Fluorescent Rosamine Compound Selectively Stains Pluripotent Stem Cells. *Angewandte Chemie International Edition* **2010,** *49* (41), 7497-7500.

6. Nakano, S.; Tamura, T.; Das, R. K.; Nakata, E.; Chang, Y.-T.; Morii, T., A Diversity-Oriented Library of Fluorophore-Modified Receptors Constructed from a Chemical Library of Synthetic Fluorophores. *ChemBioChem* **2017,** *18* (22), 2212-2216.

7. Vendrell, M.; Lee, J.-S.; Chang, Y.-T., Diversity-oriented fluorescence library approaches for probe discovery and development. *Current Opinion in Chemical Biology* **2010,** *14* (3), 383-389.

8. Wang, S.; Chang, Y.-T., Discovery of heparin chemosensors through diversity oriented fluorescence library approach. *Chemical Communications* **2008,** (10), 1173-1175.

9. Rosania, G. R.; Lee, J. W.; Ding, L.; Yoon, H.-S.; Chang, Y.-T., Combinatorial Approach to Organelle-Targeted Fluorescent Library Based on the Styryl Scaffold.

Journal of the American Chemical Society **2003,** *125* (5), 1130-1131.

10. Peng, X.; Du, J.; Fan, J.; Wang, J.; Wu, Y.; Zhao, J.; Sun, S.; Xu, T., A Selective Fluorescent Sensor for Imaging Cd2+ in Living Cells. *Journal of the American Chemical Society* **2007,** *129* (6), 1500-1501.

11. Coskun, A.; Deniz, E.; Akkaya, E. U., A sensitive fluorescent chemosensor for anions based on a styryl–boradiazaindacene framework. *Tetrahedron Letters* **2007,** *48* (31), 5359-5361.

12. Zeng, L.; Miller, E. W.; Pralle, A.; Isacoff, E. Y.; Chang, C. J., A Selective Turn-On Fluorescent Sensor for Imaging Copper in Living Cells. *Journal of the American Chemical Society* **2006,** *128* (1), 10-11.

13. Rurack, K.; Kollmannsberger, M.; Resch-Genger, U.; Daub, J., A Selective and Sensitive Fluoroionophore for HgII, AgI, and CuII with Virtually Decoupled Fluorophore and Receptor Units. *Journal of the American Chemical Society* **2000,** *122* (5), 968-969.

14.Yuan, M.; Li, Y.; Li, J.; Li, C.; Liu, X.; Lv, J.; Xu, J.; Liu, H.; Wang, S.; Zhu, D., A Colorimetric and Fluorometric Dual-Modal Assay for Mercury Ion by a Molecule. *Organic Letters* **2007,** *9* (12), 2313-2316.

15. Wu, J.; Liu, W.; Ge, J.; Zhang, H.; Wang, P., New sensing mechanisms for design of fluorescent chemosensors emerging in recent years. *Chemical Society Reviews* **2011,** *40* (7), 3483-3495.

16. de Silva, A. P.; Gunaratne, H. Q. N.; Gunnlaugsson, T.; Huxley, A. J. M.; McCoy, C. P.; Rademacher, J. T.; Rice, T. E., Signaling Recognition Events with Fluorescent Sensors and Switches. *Chemical Reviews* **1997,** *97* (5), 1515-1566.

2.3 Fluorescent thymidine triphosphate probe

2.3.1 Introduction

Various intracellular metabolisms are related with small molecules including carbohydrate, metal cation, amino acid, and phosphorylated molecules.[1] Because of importance roles of the phosphorylated molecules in cell, many researchers have attempted to describe chemical reactions that involved the phosphorylated molecules. Fluorescent probes are one of the most helpful tools for biological study. However, developing selective probe which shows specific signal for certain phosphorylated molecule is complicated, because of their structural similarity and common to each phosphorylated molecule, the phosphate![2-9]

Recently, for detecting phosphorylated biomolecules, bis(Zn^{2+}-2,2′-dipicolylamine) complex (bis(Zn^{2+}-DPA)) has been widely used.[4-6] However, probes using the bis(Zn^{2+}-DPA) as a binding agent are not appropriate method for distinguish phosphorylated molecules. Because bis(Zn^{2+}-DPA) recognize phosphoryl group through strong binding affinity, consequently, almost every phosphorylated molecules showed response for it. Thus, we sought to develop a new probe for the selective detection of NTP from among other phosphorylated biomolecules.

Herein, we prepared small fluorescent library, which is composed of styryl based metal cation chelated fluorescent dyes, for developing NTP selective probe (see **Scheme 2.3.1** and Experimental section for preparation protocol). Each candidate has fully conjugated fluorophore structure with a chelated metal cation with the ligand. Therefore, fluorescence of the dye is changed upon proper binding a specific anion through intramolecular charge transfer mechanism (ICT). Through screening of the 264 candidates, we found 2′-deoxythymidine triphosphate (dTTP) selective fluorescent probe and utilized successfully for discriminating thymidine containing oligonucleotide.

Scheme 2.3.1. Schematic strategy of preparing probes for anion based on styryl dye based metal chelated fluorescent dye and anion sensing.

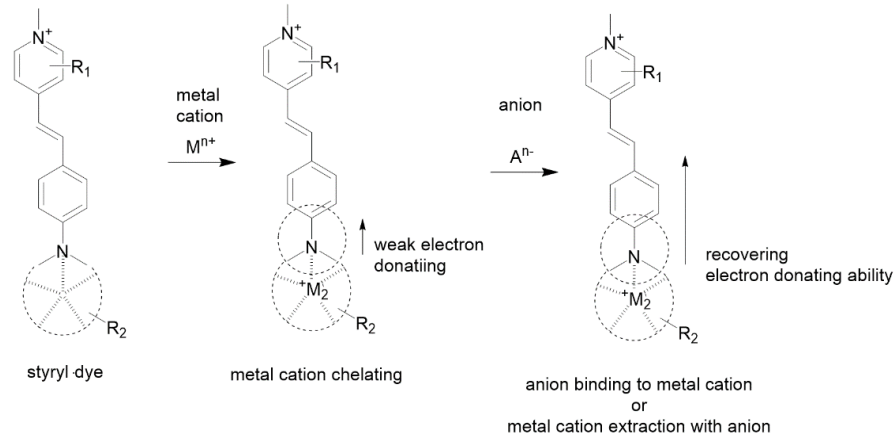

2.3.2 Data & results

As depicted in **Figure 2.3.1**, several candidates showed fluorescence response for a certain NTP. We verified sensing properties of these identified probes. 7A-Zn^{2+} and 7A-Pb^{2+} exhibited sensitivity for AMP, but with a decrease in fluorescence intensity and the change was not significant. Several other metal chelated probes (4A-Ni^{2+}, 4A-Co^{2+}, and 4A-Cu^{2+}) showed enhanced fluorescence intensity toward biological phosphates due to the removal of metal ions by phosphorylated molecules. In contrast, we found 6A-Hg^{2+} is a selective probe for dTTP showing a unique 5-fold increase in fluorescence emission.

Excess amounts of other nucleotides and PPi did not show significant fluorescence response with **6A**-Hg^{2+}(**Figure 2.3.2A**). The sequential addition of excess thiols, which are known as mercury chelators, efficiently quenched the enhanced fluorescence from the **6A**-Hg^{2+}-dTTP complex (**Figure 2.3.2B**). Interestingly, **6A**-Hg^{2+} was also found to bind to thymidine and uridine with affinities (Kd = 1.7 and 2.6 μM, respectively) similar to that for dTTP and UTP (**Figure 2.3.2D**). These evident the Hg^{2+} ion in **6A**-Hg^{2+} complex is directly coordinated to the thymine unit, but not to the phosphate group of dTTP.

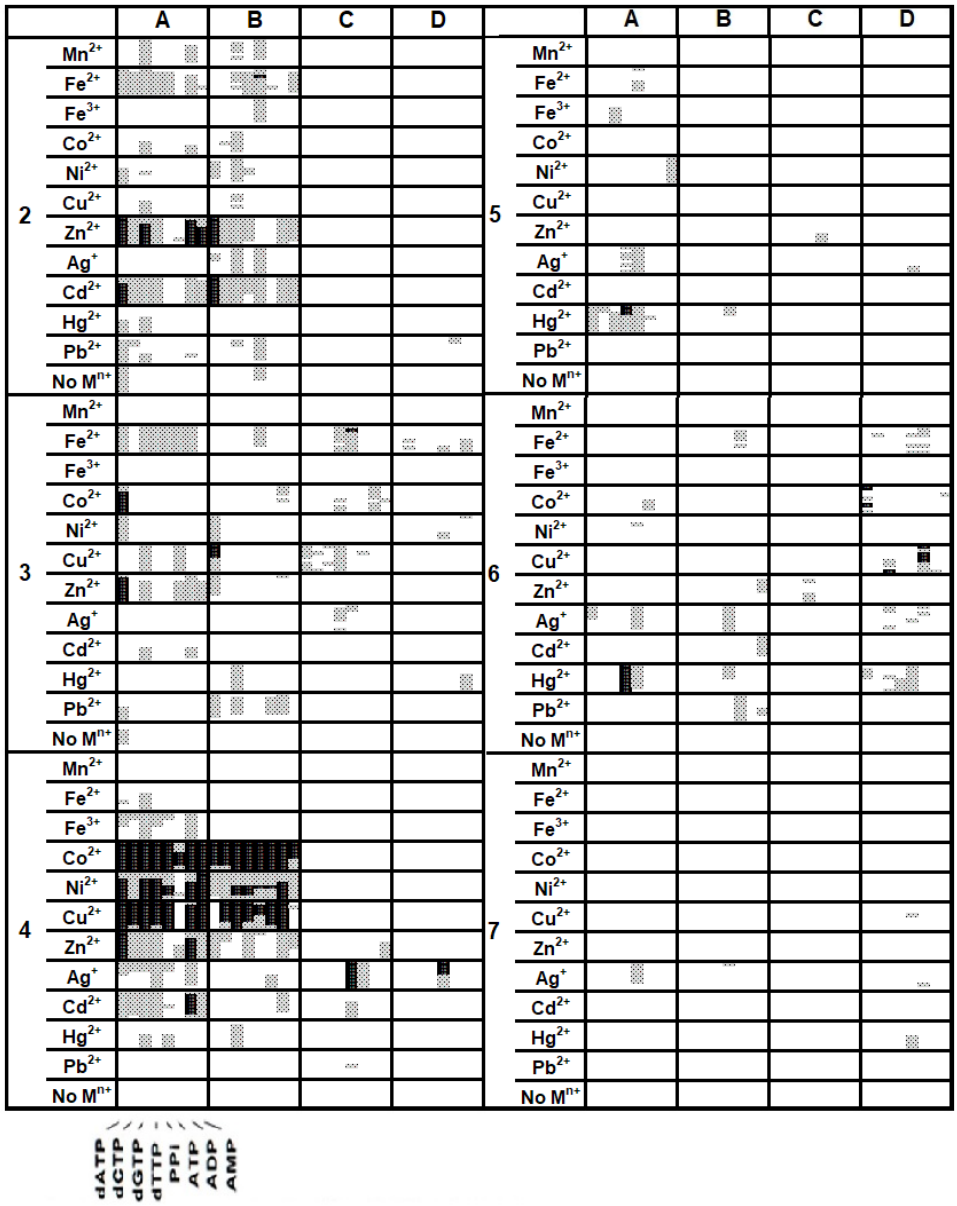

Figure 2.3.1. Hit map of primary screening for biological anions (dATP, dCTP, dGTP, dTTP, PPi, ATP, ADP, and AMP; each 100 μM, 10 mM HEPES buffer, pH 7.4, 25 °C) against 264 anion probes; Anion probes were prepared by combination 24 metal ion probes (each 10 μM) and 1 eq of 11 metal cations (denoted in figure).

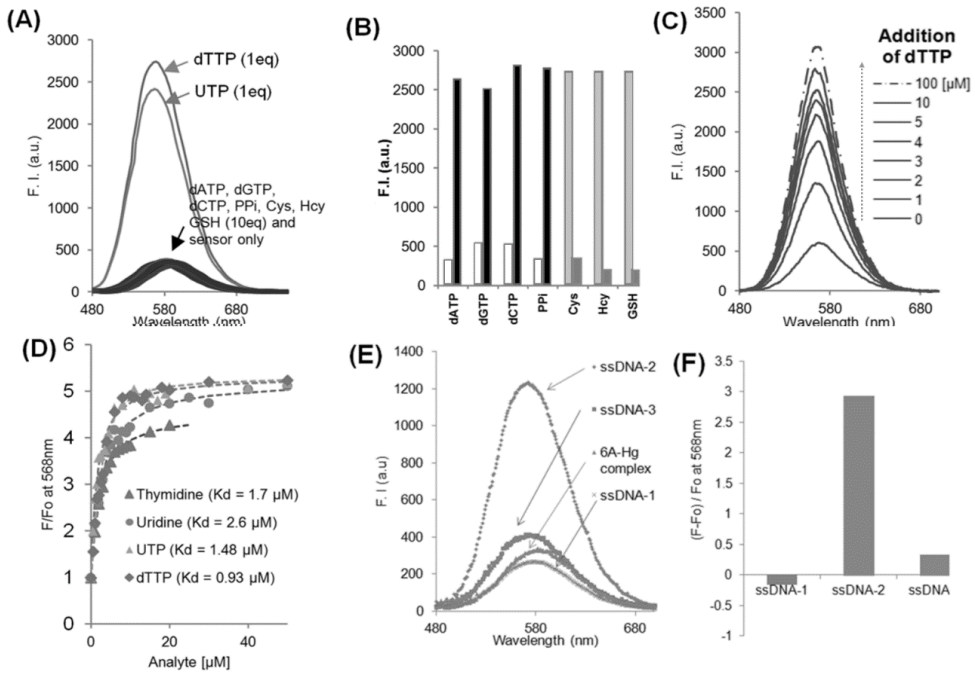

Figure 2.3.2. (A) Fluorescence emission spectra of **6A**-Hg^{2+} (10 μM) upon addition of dTTP, UTP, dATP, dGTP, dCTP, PPi, cysteine (Cys), homocysteine (Hcy) and glutathione (GSH). (B) Sequential fluorescence change of **6A**-Hg^{2+} upon addition of various anions (10 eq) and dTTP (1 eq). White colored bar represents the first addition of 10 eq of nucleotides and black colored bar represents the sequential addition of 1 eq of dTTP to **6A**-Hg^{2+} solution in the presence of other nucleotide. Light gray colored bar represents the first addition of 1 eq of dTTP and dark gray colored bar represents the sequential addition of 10 eq of each thiol into **6A**-Hg^{2+} solution, which contains 1 eq of dTTP. (C) Fluorescence emission titration spectra of **6A**-Hg^{2+} (10 μM) upon addition of dTTP (0, 1, 2, 3, 4, 5, 10, 100 μM). (D) titration curves of **6A**-Hg^{2+} (10 μM) with dTTP, UTP, thymidine and uridine. All these data were acquired in 10 mM HEPES buffer (pH 7.4) with excitation at 425 nm. (E) Fluorescence spectra of **6A**-Hg^{2+} in the presence of 30 μM of ssDNA (ssDNA-1: 5′-$(AG)_5$-3′, ssDNA-2: 5′-$(TC)_5$-3′, ssDNA-3: 5′-$(GC)_5$-3′. (F) Relative fluorescence change of **6A**-Hg^{2+} in the presence of ssDNA.

The binding between **6A**-Hg^{2+} and thymidine was supported from the NMR and absorption spectra (see **Figures 2.3.3 and 2.3.4**). As seen in **Figure 2.3.3**, a part of aromatic protons (H_b, H_c, H_f, and H_g: 6.5 ~ 8.5 ppm) exhibited changes in the chemical shifts and aliphatic protons in the azathia crown ether ring (H_h and H_i: 3.2 ~ 3.8 ppm) were broadened after 1 eq of Hg^{2+} was added to **6A** (**Figure 2.3.3A and 2.3.3B**). After addition of 1 eq of thymidine to the **6A**-Hg^{2+} complex, broadened peaks of the azathia crown ether ring were split slightly (**Figure 2.3.3C**). Also, as seen in **Figure 2.3.4**, the Hg^{2+} was not extracted from ligand in presence of excess thymine, therefore, the cause of fluorescence increase is not from metal cation removal. Meanwhile, other candidates did not showed selectivity toward dTTP, that having the same ligand **6** and Hg^{2+} (**6B**-Hg^{2+}, **6C**-Hg^{2+}, and **6D**-Hg^{2+}). This denoted the selectivity is not controlled by the metal ion binding unit alone, but by the whole molecular structure of **6A**.

Next, thymine selective **6A**-Hg^{2+} was utilized as probe for selective sensing of thymine-rich DNA. Meanwhile, picolinium/quinolinium styryl dyes are usually known as stainer for double-stranded DNA (dsDNA)[10]. Fluorescence of **6A**-Hg^{2+} was also increased in the presence of dsDNA (0.2 mg/mL), but **6A**-Hg^{2+} showed a selective and stronger fluorescence response in presence of thymine-rich single-stranded DNA (ssDNA) (**Figure 2.3.5**). This enhancement was accompanied by more than 10 nm blue-shifted maximum emission wavelength. Upon the addition of 10 μM of ssDNA (sequence: 5′-$(TC)_5$-3′), fluorescence of **6A**-Hg^{2+} was enhanced with its maximum intensity from 582 nm to 568 nm.

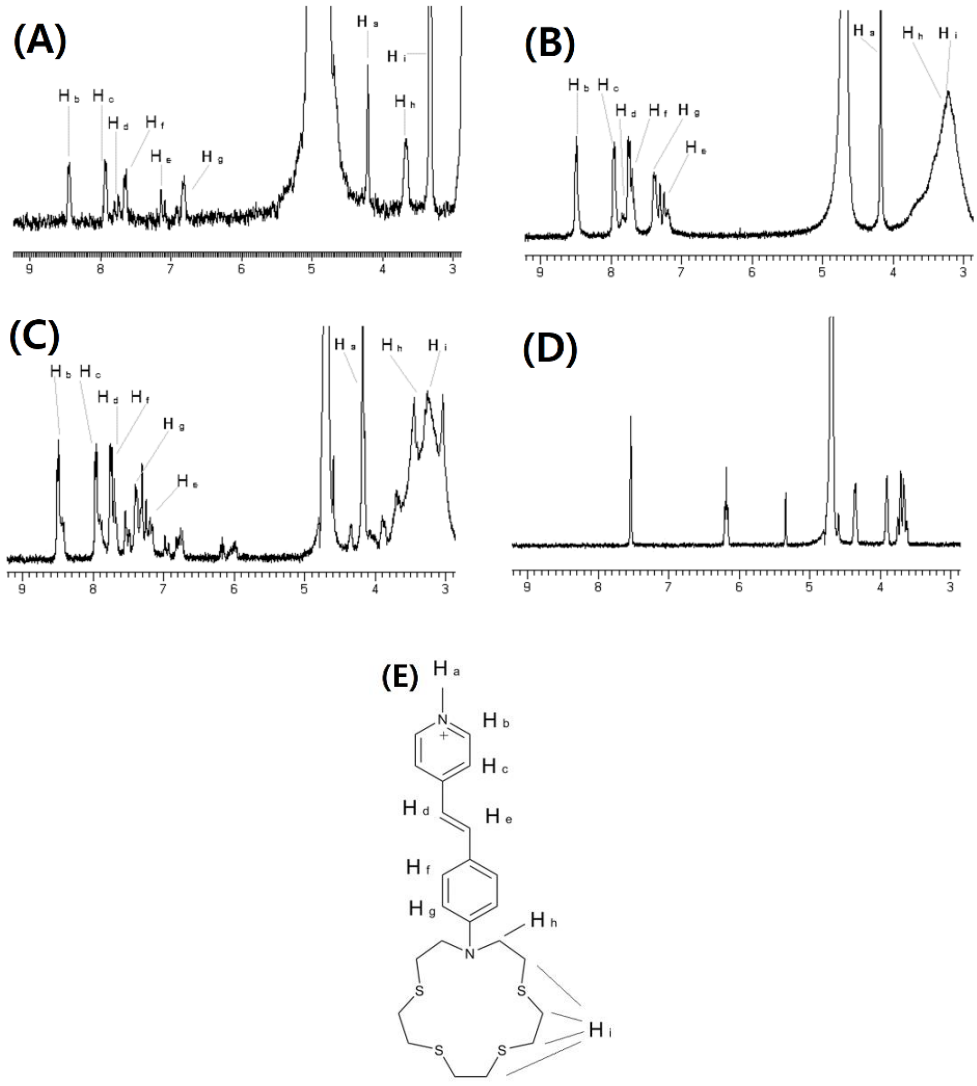

Figure 2.3.3. NMR spectra of thymidine and **6A** complexes in a mixture of D_2O and DMSO-d_6 (v/v, 9:1) (A) NMR spectrum of **6A** (B) NMR spectrum **6A**–Hg^{2+} (C) NMR spectrum **6A**–Hg^{2+} and thymidine (D) NMR spectrum of thymidine in D_2O. (E) Structure of **6A**.

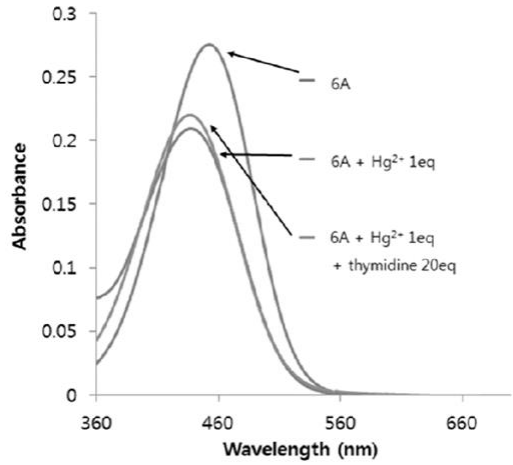

Figure 2.3.4. Absorption spectra of **6A** (5 μM) in the presence of Hg^{2+} and thymidine. All these data were recorded in 10 mM HEPES buffer (pH 7.4).

These results suggest that **6A**-Hg^{2+} may be useful in the detection of DNA lesions for example thymidine dimer.[11] Although Hg^{2+} ion or Zn^{2+}-cyclen are known to interact with thymine-rich DNA helices or thymidine triphosphate, to the best of our knowledge, **6A**-Hg^{2+} is the first selective probe for thymidine over other NTPs with a strong binding affinity in neutral aqueous buffer solutions.[12-13]

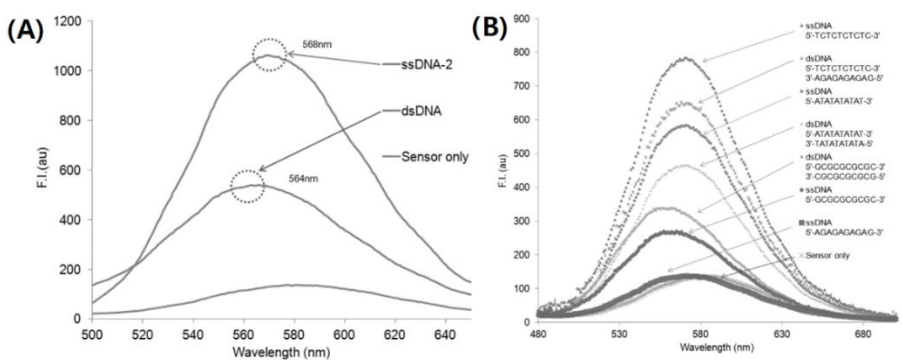

Figure 2.3.5. Fluorescence spectra of **6A**-Hg^{2+} (sensor, 5 μM) in the presence of various DNA. All these spectra were recorded in 10 mM HEPES buffer (pH 7.4) with excitation at 425 nm.

In summary, thymidine triphosphate selective probe, **6A**-Hg^{2+}, was developed

from the metal cation chelated fluorescent styryl dye library. The recognition mechanism was examined by NMR titration, absorption and fluorescence spectra. This probe showed selective fluorescence response for TTP among the NTPs and thymidine rich nucleic acid among the non-thymidine nucleic acid.

2.3.3 Experimental section

Materials & Methods

Chemical reagents, and solvents were purchased from Sigma-Aldrich co., Samchun, TCI. Single-stranded DNAs and double-stranded DNAs were purchased from IDT Co. The microplate reader was Spectra Max M2 from Molecular Device co. ^{1}H NMR spectra of **6A**–Hg^{2+} complex titration were recorded by using Bruker 300 MHz NMR spectrometer.

Anion probe preparation

Anion probes were prepared by the addition of 1 equiv. of each of 11 metal cations (Zn^{2+}, Ag^{+}, Cd^{2+}, Hg^{2+}, Pb^{2+}, Mn^{2+}, Fe^{3+}, Fe^{2+}, Cu^{2+}, Co^{2+}, and Ni^{2+}) to each of the 24 metal cation probes (see Experimental section 2.3 page XX). Seven phosphorylated nucleotides (dATP, dCTP, dGTP, dTTP, ATP, ADP, and AMP), and PPi were screened against this probe library.

Anion sensing experiment protocol

1. Prepare a 5 mM stock solution of styryl dye ligand by in spectroscopymetry-grade DMSO.

2. Prepare 100 μM of styryl dye ligand in HEPES buffer (10 mM, pH 7.4, 25°C) with the 5 mM stock solution of styryl dye ligand.

3. Add 10 μL of metal cation (Zn^{2+}, Ag^{+}, Cd^{2+}, Hg^{2+}, Pb^{2+}, Mn^{2+}, Fe^{3+}, Fe^{2+}, Cu^{2+}, Co^{2+}, and Ni^{2+}; each 50 μM) in HEPES buffer solution (10 mM, pH 7.4, 25°C) to micro plate well, respectively.

4. Add 10 μL of the 100 μM of styryl dye ligand in HEPES buffer to the micro plate

well, respectively.

5. Shake the micro plate for 1 minute.

6. Add 20 μL of 1 mM phosphoryl anion solution in HEPES buffer (10 mM, pH 7.4, 25°C) to the well, respectively.

7. Add 160 μL of HEPES buffer solution (10 mM, pH 7.4, 25°C. 0.1 v% DMSO) to the well for adjusting solution concentration.

8. Read fluorescence intensity of the solution just prepared by using a micro plate reader.

Producing of a primary screening Map

1.Convert each recorded intensity change of fluorescence to ratio value ((fluorescence intensity of probe + anion) : (fluorescence intensity of probe)) by using Microsoft Excel program.

2. Using Microsoft Excel program to convert ratio value to false-color image. See **Scheme 2.3.2**.

Scheme 2.3.2. Converting ratio value to false-color image with Microsoft Excel Program.

1. Sort images by name of anion probe.

2.3.4 References

1. Berg, J. M.; Tymoczko, J. L.; Gatto, G. J.; Stryer, L., *Biochemistry*. Eighth edition. ed.; W.H. Freeman & Company, a Macmillan Education Imprint: New York, 2015; 8th ed. page 424-442. 424-442.

2. Sarkar, H. S.; Das, S.; Mandal, D.; Uddin, M. R.; Mandal, S.; Sahoo, P., "Turn-on" fluorescence sensing of cytosine: development of a chemosensor for quantification of

cytosine in human cancer cells. *RSC Advances* **2017,** *7* (85), 54008-54012.

3. Lu, S.-H.; Phang, R.; Fang, J.-M., Fluorescent Sensing of Guanine and Guanosine Monophosphate with Conjugated Receptors Incorporating Aniline and Naphthyridine Moieties. *Organic Letters* **2016,** *18* (8), 1724-1727.

4. Jolliffe, K. A., Pyrophosphate Recognition and Sensing in Water Using Bis[zinc(II)dipicolylamino]-Functionalized Peptides. *Accounts of Chemical Research* **2017,** *50* (9), 2254-2263.

5. Zwicker, V. E.; Liu, X.; Yuen, K. K. Y.; Jolliffe, K. A., Triazole–containing zinc(II)dipicolylamine-functionalised peptides as highly selective pyrophosphate sensors in physiological media. *Supramolecular Chemistry* **2016,** *28* (1-2), 192-200.

6. Lee, S.; Yuen, K. K. Y.; Jolliffe, K. A.; Yoon, J., Fluorescent and colorimetric chemosensors for pyrophosphate. *Chemical Society Reviews* **2015,** *44* (7), 1749-1762.

7. Park, C.; Hong, J.-I., A new fluorescent sensor for the detection of pyrophosphate based on a tetraphenylethylene moiety. *Tetrahedron Letters* **2010,** *51* (15), 1960-1962.

8. Tedsana, W.; Tuntulani, T.; Ngeontae, W., A highly selective turn-on ATP fluorescence sensor based on unmodified cysteamine capped CdS quantum dots. *Analytica Chimica Acta* **2013,** *783* (Supplement C), 65-73.

9. Huang, F.; Hao, G.; Wu, F.; Feng, G., Fluorescence sensing of ADP over ATP and PPi in 100% aqueous solution. *Analyst* **2015,** *140* (17), 5873-5876.

10. Li, Q.; Kim, Y.; Namm, J.; Kulkarni, A.; Rosania, G. R.; Ahn, Y.-H.; Chang, Y.-T., RNA-Selective, Live Cell Imaging Probes for Studying Nuclear Structure and Function. *Chemistry & Biology* **2006,** *13* (6), 615-623.

11. Kim, S.-i.; Jin, S.-G.; Pfeifer, G. P., Formation of cyclobutane pyrimidine dimers at dipyrimidines containing 5-hydroxymethylcytosine. *Photochemical & Photobiological Sciences* **2013,** *12* (8), 1409-1415.

12. Schmidt, F.; Stadlbauer, S.; Konig, B., Zinc-cyclen coordination to UTP, TTP or pyrophosphate induces pyrene excimer emission. *Dalton Transactions* **2010,** *39* (31), 7250-7261.

13. Kwon, T.-H.; Kim, H. J.; Hong, J.-I., Phosphorescent Thymidine Triphosphate Sensor Based on a Donor–Acceptor Ensemble System using Intermolecular Energy Transfer. *Chemistry – A European Journal* **2008,** *14* (31), 9613-9619.

2.4 Fluorescent nucleic acid probes

2.4.1 Introduction

Real-time monitoring of nucleic acids (NA) in living cells are essential to understand role of NA dynamics in cellular functions.[1-5] Living cell assays are considered as most reliable procedure to study NA dynamics. Fluorophores, which show fluorescence signal selectively toward to NA, have been widely utilized in the study of vital rolls of NA in cell.[1, 5-18] Many classes of DNA selective probes have been developed and utilized, however, only a few RNA selective probes over DNA in living cell are reported and there are still need to develop new probes.[6, 10, 19-23]

Previously, we developed metal cation fluorescent probes from a focused styryl dye library (see section 2.1) and observed unexpected fluorescent signals while conducting cellular metal cation imaging experiments. Most styryl dyes of the library do not showed intense fluorescence in DMSO solution and a few of them fluoresced in cells without target metal cation. Thus, the main factor of fluorescence enhancement of the probe was not hydrophobic environment in cells and we sought to investigate cause of this phenomenon.

More than 20 years ago, styryl dye DSMI[24] was reported as minor groove binder of dsDNA. Recently, Chang and his colleagues developed RNA selective styryl dye based probes from diversity oriented fluorescent library.[19] However, an investigation into the mechanism of their fluorescence response was not carried out. The fluorescent RNA selective staining feature of the probe[19] in cytosol and nucleoli that cannot be explained by minor groove binding mechanism and this must be reconsidered.[25-26]

Several styryl dyes, that were developed for fluorescent metal cation probes, showed enhanced fluorescence in presence of ssDNA. Among them, probe **1** was picked out for study of NA sensing mechanism which showed most intense fluorescence with NA. From the investigation of NA sensing properties of the probe **1**, we found appropriate positive planar structure is essential for nucleic acid backbone recognition. Based on this hypothesis, we prepared an oxonium containing

planar fluorescent molecule and the molecule fluoresced with NA.[27] Finally, cellular imaging experiments were performed with probe **1,** which stained cytosol and nucleoli selectively. The RNA sensing properties of the probe were confirmed by NA digest experiments.

2.4.2. Data & Results

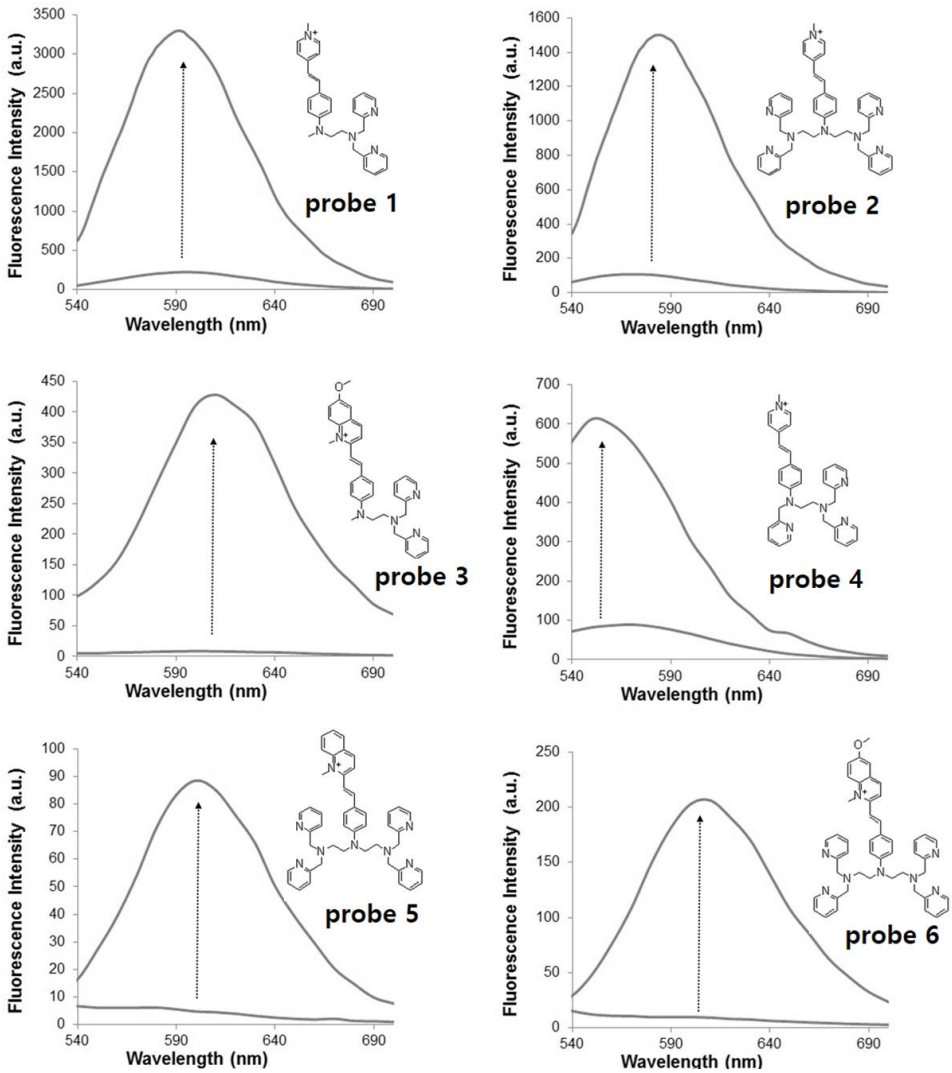

Figure 2.4.1. Fluorescence emission spectra of styryl dyes (5 μM) and styryl dyes with ssDNA (5'- TGC TTG AAG CAG CTC TGG A -3', 5 μM) in 10 mM HEPES buffer (pH 7.4). λ_{ex}=495 nm.

Among 35 styryl dyes, a few of them showed significant fluorescence response in presence of ssDNA. Interestingly, even though probe **1**, probe **2**, and probe **3** had same picolinium styryl structure, they showed different fluorescence intensity. Among them, probe **1** was chosen for further study since its strong fluorescence with ssDNA.

The probe **1** showed significant fluorescence increase with RNA (from λ_{abs}=470 nm, ε= 20500/ M·cm, λ_{em}=586 nm, Φ_f=0.002 to λ_{abs}=495 nm, ε= 26000/ M·cm, λ_{em}=590 nm Φ_f=0.15 in presence of 0.2 mg/ml of RNA. Quantum yield was computed from relative brightness to fluorescein and ε of probe **1**). To demonstrate NA sensing performance of probe **1**, we prepared additional styryl dyes that were known for fluorescent NA sensor (see **Scheme 2.4.1** in Experimental section)[19, 24]. As seen in **Figure 2.4.1**, that styryl dyes showed a fluorescence enhancement upon NA addition. These properties were reported earlier,[19] but the fluorescence of these dyes are very weak compared to fluorescence of probe **1**.

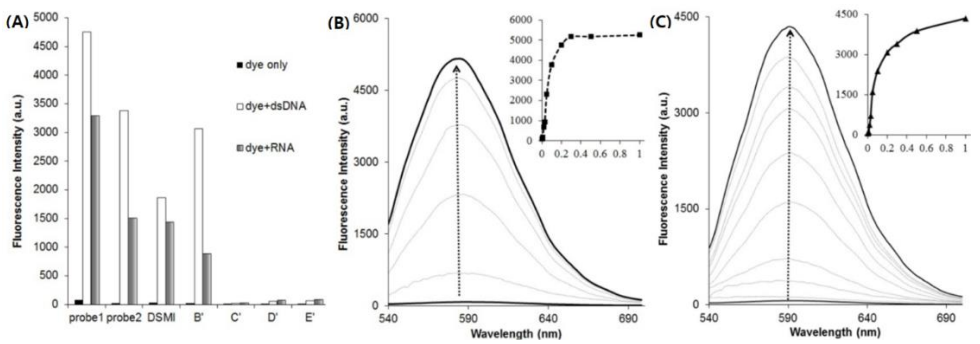

Figure 2.4.2. (A) Fluorescent response of styryl dyes with; blank (control), 0.2 mg/ml of dsDNA, and 0.2 mg/ml or RNA. λ_{ex}=495 nm for probe **1**, probe **2**, DSMI and B', λ_{ex}=550 nm for C', D', and E'. Revealed fluorescence intensity is maximum fluorescence intensity value. (B) Fluorescence emission spectra of probe **1** with dsDNA at various concentrations. (C) Fluorescence emission spectra of probe **1** with RNA at various concentrations. 10 μM of styryl dyes were used. Inset graphs: fluorescent NA dependency titration curve; x-axis= fluorescence intensity, y-axis= NA contents in solution (mg/ml).

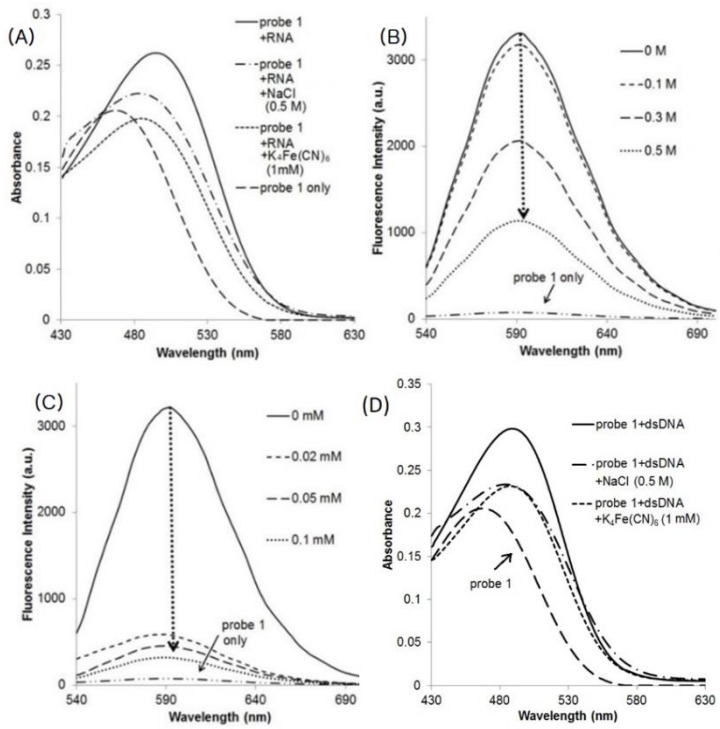

Figure 2.4.3. (A) Absorption spectra of probe **1** with RNA (0.2 mg/ml) and salt. (B) Fluorescence emission titration of probe **1** with RNA upon addition of NaCl (0, 0.1, 0.3, 0.5 M). (C) Fluorescence emission titration of probe **1** with RNA upon addition of $K_4Fe(CN)_6$ (0, 0.02, 0.05, 0.1 mM). (D) Absorption spectra of probe **1** (10 μM) with salt in presence of dsDNA. These spectra were recorded in HEPES buffer (10 mM, pH 7.4, 0.1% DMSO).

To examine NA sensing mechanism of probe **1**, effect of salt on the interaction between NA and the probe **1** was investigated. Strong charge-charge interaction combines sodium ion and NA together, but as seen in **Figure 2.4.3A**, probe **1** was not drive out and fluorescence of probe **1** was not quenched efficiently.[24] Thus, the interaction between probe **1** and NA is not simple electrostatic interaction. Meanwhile, small amount of $K_4Fe(CN)_6$, which is known for strong fluorescence quenching ion, deeply quenched fluorescence of the probe **1**. Thus, probe **1** did not intercalated in NA base. [28] Although fluorescence of probe **1** was quenched, absorption spectra showed that probe **1** was not isolated from NA in presence of

$K_4Fe(CN)_6$. These effects of salt titration experiment have been studied with dsDNA regularly, but that of with RNA were not well known.

Many fluorescent molecules showed weak fluorescence in polar solvents including acetone, acetonitrile, DMSO, ethanol, and water. Also, styryl dyes (probe **1**, probe **2** and **DSMI**) fluoresced weakly in polar solvent (**Figure 2.4.4**). We found no distinct differences between them, so, we concluded hydrophobic environment could not be main cause of strong fluorescence of probe **1** with NA. Long RNA would form partial stem-loop base pairing, which possibly form minor groove instantly, may cause fluorescence enhancement. However, probe **1** still fluoresced strongly with short ssDNA (**Figure 2.4.5A**). Although there are slight differences of probe **1**'s fluorescence intensity depending on the sequence that makes up the NA, any noticeable feature of probe **1** was not detected.

From these, high fluorescence intensity of the probe **1** with NA would be explained by efficient blocking of non-radiative deactivation with appropriate bulky groups.[29] NA recognition part is marked with a dotted square and bulky groups are marked with a dotted oval in **Figure 2.4.5B**.On the other hand, lower fluorescence intensity of probe **2** may from additional bulky groups that decreased affinity of styryl dye to phosphate backbone of NA.

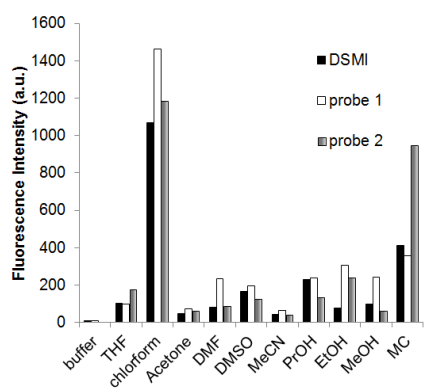

Figure 2.4.4 Fluorescence intensity of DSMI, probe 1, and probe 2 (10 μM) in diverse organic solvents. Each fluorescence intensity was obtained from with maximum excitation wavelength.

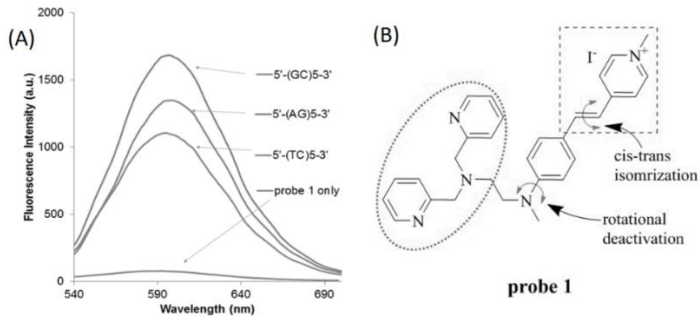

Figure 2.4.5 (A) Fluorescent spectra of probe **1** (10 μM) in presence of different ssDNA (20 μM) in HEPES buffer (10 mM, pH 7.4). (B) Non-radiative decay channels (marked with arrows) of **probe 1**.

We hypothesized that a fluorescent molecule, which has electronically delocalized positive charge planar structure, rotational radiation deactivation channel, and similar fluorescence response tendency in organic solvent to probe **1**, would be a fluorescent NA sensor. As our expectation, oxonium containing molecule[27] (**Aa**, see Experimental section) fluoresced strongly in upon NA added (**Figure 2.4.6**).

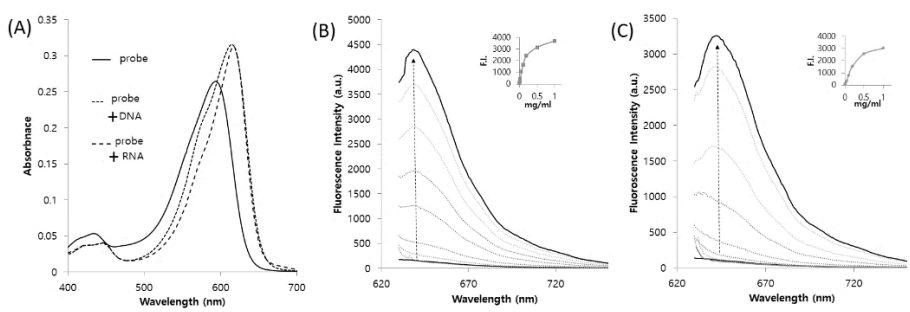

Figure 2.4.6. (A) Absorption spectra of **Aa** and with NA (0.2 mg/ml) (λ_{abs} : 595 nm → 616 nm, extinction coefficient : 52800→63000 $(cm \cdot M)^{-1}$) (B) Fluorescence emission spectra of oxonium NA sensor with dsDNA at various concentrations. (C) Fluorescence emission spectra of oxonium NA sensor with RNA at various concentrations. 5 μM of sensor was used. Inset graphs: fluorescent NA dependency titration curve; x-axis= fluorescence intensity, y-axis= NA contents in solution (mg/ml). λ_{ex} :616 nm.

However, π-extended oxonium containing fluorophore derivatives' (Ab and Ac) were extremely weak (**Figure 2.4.7**). Maybe, these and NA seem to had failed to achieve adequate complex for fluorescence.

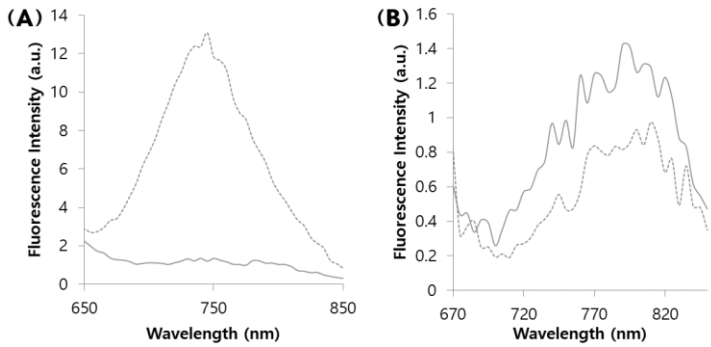

Figure 2.4.7. Fluorescent response of Ab (A) and Ac (B) with; blank (control, solid line) and 0.2 mg/ml of dsDNA (dotted line).

Cellular imaging experiments were conducted to confirm specificity of the probe **1** towards NA in cells.[19-20] As seen in **Figure 2.4.8**, probe **1** stained cytoplasm and nucleolus (pointed with white arrow) in fixed cells. Although probe **1** showed brighter fluorescence response to dsDNA *in vitro* than that of RNA, the cellular imaging showed that probe **1** stained RNA more efficiently in cells. The probe **1** showed fluorescent nucleoli and cytoplasm staining, but negligible nucleus staining. Also, similar results were obtained from cellular experiments with live HeLa cells. Next, nucleic acid digest experiments were performed with fixed and permeabilized myoblast C2C12 cell to confirm RNA staining property of probe **1** in cells. In the DNase digest, only the DNAs in the cell would be digested. On the other hand, only RNAs would be digested with RNase. Hoechst DNA staining was also conducted as controls (**Figure 2.4.8A**). The fluorescence of probe **1** quenched in the RNase digest (**Figure 2.4.9** and **2.4.10A**), but the nucleus fluorescence intensity of Hoechst decreased very slightly. Also, slightly decreased fluorescence of probe **1** was observed with DNase, but the variation was not obvious (**Figure 2.4.10A**). These

results support the probe **1** stained RNA in the cell efficiently. Also cytotoxicity of the probe **1** was analyzed (**Figure 2.4.10B**).

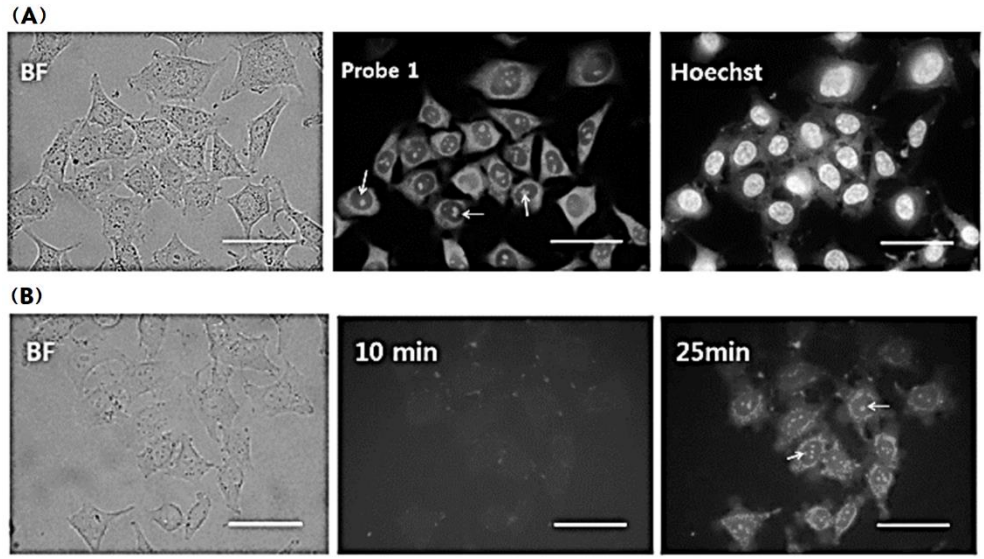

Figure 2.4.8. Fixed cell (A), and Live cell (B) NA staining with probe **1** (10 μM) and Hoechst (4 μM). The scale bar represents 50 μm. Image brightness and contrast were slightly adjusted to improve picture quality.

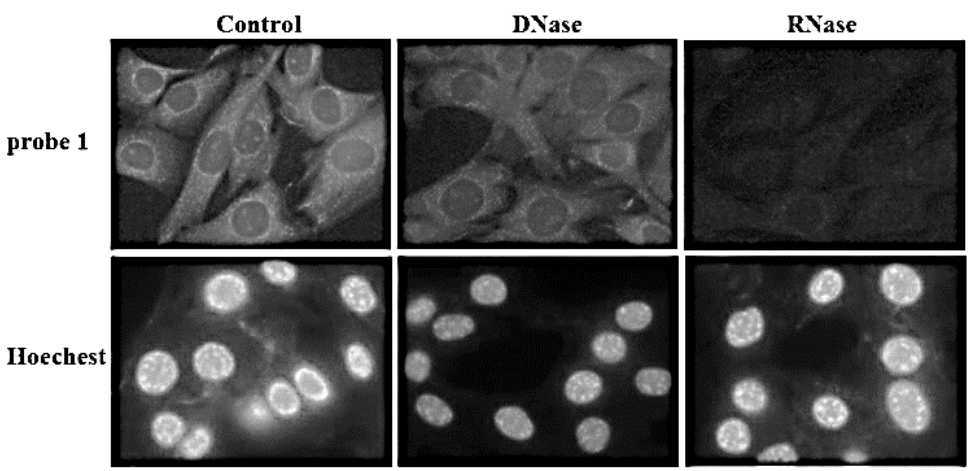

Figure 2.4.9. Images of probe **1** (10 μM) and as well as Hoechst (4 μM) are shown as comparison experiments; equal exposure was used for the same dye imaging. The brightness and contrast of the control and DNase images of probe **1** were adjusted to improve picture quality.

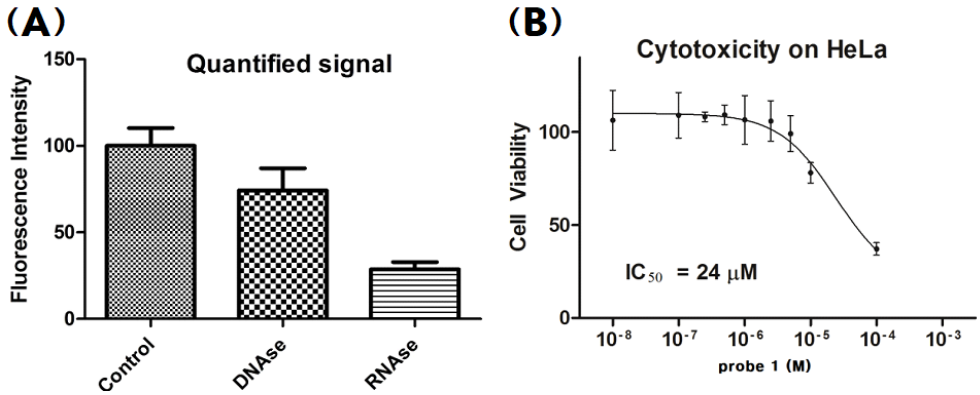

Figure 2.4.10. (A) Quantified fluorescence response of probe **1** from NA digest experiments. (B) Calculation of cell viability.

In summary, we discovered RNA sensitive cell staining styryl dye probe **1,** which fluoresced strongly in presence of NA in buffer solution. Photophysical properties of the probe **1** were investigated and titration experiments were conducted to examine the interaction of the probe **1** with RNA. Our experiment suggests efficient blocking non-radiative channel of the probe **1** with phosphate backbone would be the appropriate elucidation of RNA sensing event. Our fluorescent probe **1** stained cytoplasm and nucleoli in cells selectively. RNA selective and sensitive cell staining properties of probe **1** were analyzed and confirmed with NA digest experiments.

2.4.3 Experimental section

Materials and methods

Chemical reagents, deoxyribonucleic acid (dsDNA) from calf thymus, ribonucleic acid (RNA) from torular yeast, DNase (D4138. Sigma-Aldrich Co), and RNase (R6513. Sigma-Aldrich Co) were purchased from Samchun Chemical and Sigma-Aldrich Co. Synthesized single stranded DNA (ssDNA) was purchased from Integrated and DNA Technologies, Inc.

Preparation of styryl dyes

Scheme 2.4.1. (A) Synthesis of five *p*-dimethyl amino styryl dyes. (B) Structure of five styryl dyes.

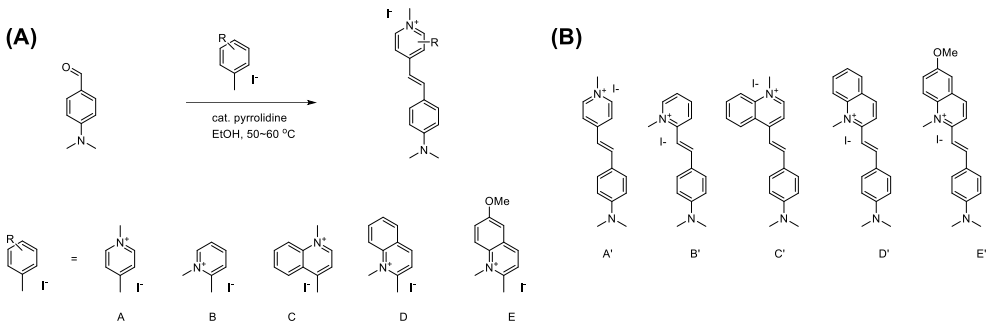

General synthetic procedure of styryl dyes

Para-dimethylamino benzaldehyde derivative (11 mmol) was added to a 100ml round bottom flask. A magnetic stirring bar and 30ml of absolute ethanol were added. After then, 10mmol of picolinium or quinolinium iodide was added to the RBF. With stirring, 3-4 drops of pyrrolidine was added to the RBF and heated to 50~60℃. The reaction mixture was stirred overnight. Checked by TLC if p-benzaldehyde was consumed, the reaction mixture was poured to 50ml of water. Reaction mixture was washed with water and dichloromethane. Decanted organic layer carefully, isolated organic layer, dried over by sodium sulfate and removed organics in low pressure. Remained viscous crude compound was dissolved in small amount of methylene chloride. Well dissolved mixture was slowly added to 100 mL of EA in a beaker dropwise. Filtered precipitate then rinsed with EA to get pure product. Other styryl dyes contained ligand were synthesized according to the previous report. (ref).

NMR characteristics of **A'** ^{1}H NMR (300 MHz, DMSO-d_6) δ 3.02 (6H, s), 4.18 (3H, s), 6.79 (2H, d, *J* = 8.538 Hz), 7.18 (1H, d, *J* = 16.083 Hz), 7.60 (2H, d, *J* = 8.523 Hz), 7.92 (1H, d, *J* = 16.119 Hz), 8.05 (2H, d, *J* = 6.384 Hz), 8.69 (2H, d, *J* = 6.366 Hz). ^{13}C NMR (75 MHz, DMSO-d_6) δ 40.182, 46.848, 112.424, 117.596, 122.591, 122.933, 130.598, 142.357, 144.804, 152.345, 153.827

NMR characteristics of **B'** ^{1}H NMR (300 MHz, DMSO-d_6) δ 3.04 (6H, s), 4.30

(3H, s), 6.78 (2H, d, *J* = 8.598 Hz), 7.23 (1H, d, *J* = 15.72 Hz), 7.710-7.737 (3H, m), 7.93 (1H, d, *J* = 15.717 Hz), 8.33 (1H, t, *J* = 7.91 Hz), 8.46 (1H, d, *J* = 8.28 Hz), 8.77 (1H, d, *J* = 6.07 Hz). ^{13}C NMR (75 MHz, DMSO-d_6) δ 40.208, 46.235, 111.041, 112.225, 122.756, 123.488, 124.063, 131.218, 143.527, 144.610, 145.724, 152.556, 153.681.

NMR characteristics of **C'** ^{1}H NMR (300 MHz, DMSO-d_6) δ 3.08 (6H, s), 4.45 (3H, s), 6.82 (2H, d, *J* = 8.664 Hz), 7.55 (1H, d, *J* = 15.408 Hz), 7.822-7.843 (3H, m), 8.07 (1H, t, *J* = 8.052 Hz), 8.231-8.283 (2H, m), 8.43 (1H, d, *J* = 9.00 Hz) , 8.51 (1H, d, *J* = 9.12 Hz) , 8.81 (1H, d, *J* = 9.02 Hz). ^{13}C NMR (75 MHz, DMSO-d_6) δ 40.188, 55.399, 112.317, 119.302, 120.699, 122.871, 127.268, 128.478, 130.256, 132.457, 134.596, 139.676, 142.336, 149.388, 153.327, 156.793

NMR characteristics of **D'** ^{1}H NMR (300 MHz, DMSO-d_6) δ 3.07 (6H, s), 4.43 (3H, s), 6.80 (2H, d, *J* = 8.706 Hz), 7.54 (1H, d, *J* = 15.429 Hz), 7.816-7.862 (3H, m), 8.07 (1H, t, *J* = 7.881 Hz), 8.250-8.276 (2H, m), 8.42 (1H, d, *J* = 8.91 Hz) , 8.50 (1H, d, *J* = 9.14 Hz) , 8.80 (1H, d, *J* = 9.05 Hz). ^{13}C NMR (75 MHz, DMSO-d_6) δ 40.179, 55.402, 112.282, 119.287, 120.666, 122.861, 127.257, 128.454, 130.232, 132.450, 134.580, 139.656, 142.304, 149.382, 153.294, 156.766

NMR characteristics of **E'** ^{1}H NMR (300 MHz, DMSO-d_6) δ 3.05 (6H, s), 3.97 (3H, s), 4.42 (3H, s), 6.78 (2H, d, *J* = 8.622 Hz), 7.49 (1H, d, *J* = 15.498 Hz), 7.666-7.715 (2H, m), 7.79 (2H, d, *J* = 8.691 Hz), 8.12 (1H, d, *J* = 15.468 Hz), 8.36 (1H, d, *J* = 9.252 Hz), 8.45 (1H, d, *J* = 9.18 Hz), 8.69 (1H, d, *J* = 9.105 Hz). ^{13}C NMR (75 MHz, DMSO-d_6) δ 40.157, 56.089, 56.590, 109.233, 111.522, 112.231, 112.420, 121.102, 122.893, 125.309, 129.110, 131.986, 134.842, 141.338, 147.773, 152.977, 154.416, 158.602.

General synthetic procedure of oxonium dyes

Eleven-mmol of salicylaldehyde derivative was added to a 100ml round bottom

flask. To the RBF, 30ml of conc. H_2SO_4 was added. After then, 10 mm of acetophenone derivative was added. The mixture was heated to 50~60℃. After 20 min, the reaction mixture was poured to 50ml of iced water. To the mixture, 10 mL of $HClO_4$ was added. Precipitated dark solid was filtered and rinsed with acetic acid. The solid was washed with EA. No more purification was needed.

Scheme 2.4.2. Synthesis (A) and structure (B) of three oxonium containing molecules.

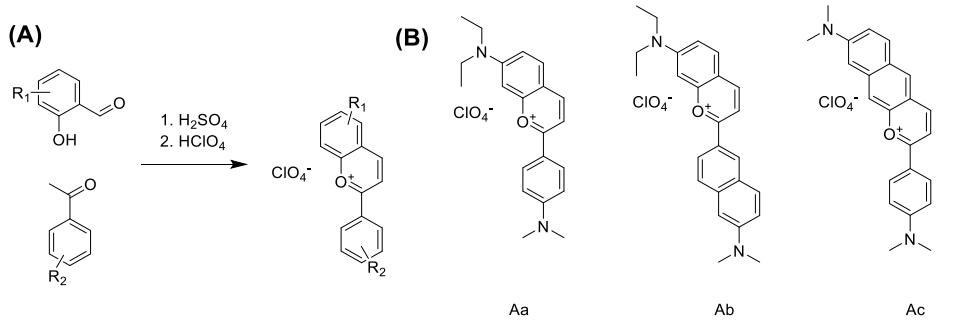

NMR characteristics of **Aa** ^{1}H NMR (300 MHz, $CDCl_3$) 1.36 (6H, t, *J* =6.813 Hz), 3.199 (6H, s), 3.639 (4H, q, *J* = 6.39 Hz), 6.84 (2H, d, *J* = 8.265 Hz), 6.995-7.064 (2H, m), 7.61 (1H, d, *J* = 8.286 Hz), 7.71 (1H, d, *J* = 9.08 Hz), 8.14 (2H, d, *J* = 8.91 Hz), 8.32 (1H, d, *J* = 8.43 Hz). (It is similar to previous report.)

NMR characteristics of **Ab** ^{1}H NMR (300 MHz, $CDCl_3$) 1.29 (6H, t, *J* =6.93 Hz), 3.03 (6H, s), 3.639 (4H, q, *J* = 6.48 Hz), 6.49 (1H, s), 6.853-6.958 (3H, m), 7.28-7.38 (2H, m), 7.42 (1H, d, *J* = 8.985 Hz), 7.59 (1H, d, *J* = 7.38 Hz), 7.78 (1H, d, *J* = 9.15 Hz), 8.11 (1H, d, *J* = 7.83 Hz), 8.35 (1H, s).

NMR characteristics of **Ac** ^{1}H NMR (300 MHz, $CDCl_3$) 2.99 (6H, s), 3.10 (6H, s), 5.84 (1H, d, *J* = 9.69 Hz), 6.693-6.824 (4H, m), 7.02 (H, d, *J* = 8.99 Hz), 7.249-7.282 (2H, m), 7.474-7.504 (2H, m), 7.64 (1H, d, *J* = 8.94 Hz).

Analysis photophysical properties of styryl dyes

Firstly, each styryl dye DMSO stock solution with the same concentration (0.1 M) for spectral analysis was prepared then diluted for studying photophysical properties. Absorption spectra were recorded with Spectrophotometer (Du-800, Beckman Coulter) and fluorescence spectra were recorded with Microplate reader (Spectra Max M2, Molecular Device). All spectra were recorded in 10 mM HEPES buffer (pH 7.4, 0.1 % DMSO, 25 ˚C) except when 100% organic solvent was used.

Cellular imaging experiment

All cellular experiment progress including cell culture, fixed and live cell staining, cytotoxicity on HeLa cell test, and DNase and RNase Digest Test followed the previously reported protocol.[19-20]

4.4. References

1. Liu, Z.; Lavis, Luke D.; Betzig, E., Imaging Live-Cell Dynamics and Structure at the Single-Molecule Level. *Molecular Cell* **2015,** *58* (4), 644-659.

2. Marras, S. A. E.; Tyagi, S.; Kramer, F. R., Real-time assays with molecular beacons and other fluorescent nucleic acid hybridization probes. *Clinica Chimica Acta* **2006,** *363* (1), 48-60.

3. Martí, A. A.; Jockusch, S.; Stevens, N.; Ju, J.; Turro, N. J., Fluorescent Hybridization Probes for Sensitive and Selective DNA and RNA Detection. *Accounts of Chemical Research* **2007,** *40* (6), 402-409.

4. Santangelo, P. J.; Nix, B.; Tsourkas, A.; Bao, G., Dual FRET molecular beacons for mRNA detection in living cells. *Nucleic Acids Research* **2004,** *32* (6), e57-e57.

5. Urbanek, M. O.; Galka-Marciniak, P.; Olejniczak, M.; Krzyzosiak, W. J., RNA imaging in living cells – methods and applications. *RNA Biology* **2014,** *11* (8), 1083-1095.

6. Bao, G.; Rhee, W. J.; Tsourkas, A., Fluorescent Probes for Live-Cell RNA Detection. *Annual Review of Biomedical Engineering* **2009,** *11* (1), 25-47.

7. Liu, X.; Sun, Y.; Zhang, Y.; Miao, F.; Wang, G.; Zhao, H.; Yu, X.; Liu, H.; Wong, W.-Y., A 2,7-carbazole-based dicationic salt for fluorescence detection of nucleic acids and two-photon fluorescence imaging of RNA in nucleoli and cytoplasm. *Organic &*

Biomolecular Chemistry **2011,** *9* (10), 3615-3618.

8. Su, X.; Xiao, X.; Zhang, C.; Zhao, M., Nucleic Acid Fluorescent Probes for Biological Sensing. *Applied Spectroscopy* **2012,** *66* (11), 1249-1261.

9. Dumat, B.; Bordeau, G.; Faurel-Paul, E.; Mahuteau-Betzer, F.; Saettel, N.; Metge, G.; Fiorini-Debuisschert, C.; Charra, F.; Teulade-Fichou, M.-P., DNA Switches on the Two-Photon Efficiency of an Ultrabright Triphenylamine Fluorescent Probe Specific of AT Regions. *Journal of the American Chemical Society* **2013,** *135* (34), 12697-12706.

10. Guo, L.; Chan, M. S.; Xu, D.; Tam, D. Y.; Bolze, F.; Lo, P. K.; Wong, M. S., Indole-based Cyanine as a Nuclear RNA-Selective Two-Photon Fluorescent Probe for Live Cell Imaging. *ACS Chemical Biology* **2015,** *10* (5), 1171-1175.

11. Li, D.; Tian, X.; Wang, A.; Guan, L.; Zheng, J.; Li, F.; Li, S.; Zhou, H.; Wu, J.; Tian, Y., Nucleic acid-selective light-up fluorescent biosensors for ratiometric two-photon imaging of the viscosity of live cells and tissues. *Chemical Science* **2016,** *7* (3), 2257-2263.

12. Feng, X. J.; Wu, P. L.; Bolze, F.; Leung, H. W. C.; Li, K. F.; Mak, N. K.; Kwong, D. W. J.; Nicoud, J.-F.; Cheah, K. W.; Wong, M. S., Cyanines as New Fluorescent Probes for DNA Detection and Two-Photon Excited Bioimaging. *Organic Letters* **2010,** *12* (10), 2194-2197.

13. Hong, Y.; Chen, S.; Leung, C. W. T.; Lam, J. W. Y.; Tang, B. Z., Water-Soluble Tetraphenylethene Derivatives as Fluorescent "Light-Up" Probes for Nucleic Acid Detection and Their Applications in Cell Imaging. *Chemistry – An Asian Journal* **2013,** *8* (8), 1806-1812.

14. Zhao, C.; Zhang, Y.; Wang, X.; Cao, J., Development of BODIPY-based fluorescent DNA intercalating probes. *Journal of Photochemistry and Photobiology A: Chemistry* **2013,** *264* (Supplement C), 41-47.

15. Zheng, Y.-C.; Zheng, M.-L.; Chen, S.; Zhao, Z.-S.; Duan, X.-M., Biscarbazolylmethane-based cyanine: a two-photon excited fluorescent probe for DNA and selective cell imaging. *Journal of Materials Chemistry B* **2014,** *2* (16), 2301-2310.

16. Gaur, P.; Kumar, A.; Dalal, R.; Bhattacharyya, S.; Ghosh, S., Emergence through delicate balance between the steric factor and molecular orientation: a highly bright and photostable DNA marker for real-time monitoring of cell growth dynamics. *Chemical Communications* **2017,** *53* (17), 2571-2574.

17. Gaur, P.; Kumar, A.; Dalal, R.; Kumar, R.; Bhattacharyya, S.; Ghosh, S., Selectivity

advancement through chemical structure engineering: Long-term intracellular DNA recognition, chromosomal staining and micronuclei detection. *Sensors and Actuators B: Chemical* **2017,** *248* (Supplement C), 690-698.

18. Peng, X.; Wu, T.; Fan, J.; Wang, J.; Zhang, S.; Song, F.; Sun, S., An Effective Minor Groove Binder as a Red Fluorescent Marker for Live-Cell DNA Imaging and Quantification. *Angewandte Chemie International Edition* **2011,** *50* (18), 4180-4183.

19. Li, Q.; Kim, Y.; Namm, J.; Kulkarni, A.; Rosania, G. R.; Ahn, Y.-H.; Chang, Y.-T., RNA-Selective, Live Cell Imaging Probes for Studying Nuclear Structure and Function. *Chemistry & Biology* **2006,** *13* (6), 615-623.

20. Li, Q.; Chang, Y.-T., A protocol for preparing, characterizing and using three RNA-specific, live cell imaging probes: E36, E144 and F22. *Nature Protocols* **2007,** *1*, 2922.

21. O'Connor, N. A.; Stevens, N.; Samaroo, D.; Solomon, M. R.; Marti, A. A.; Dyer, J.; Vishwasrao, H.; Akins, D. L.; Kandel, E. R.; Turro, N. J., A covalently linked phenanthridine-ruthenium(ii) complex as a RNA probe. *Chemical Communications* **2009,** (19), 2640-2642.

22. Zhang, X.; Chen, A.; Tsourkas, A. In *Imaging RNA in Single Living Cells: Recent Advances and Future Outlook*, Biomedical Optics and 3-D Imaging, Miami, Florida, 2012/04/28; Optical Society of America: Miami, Florida, 2012; p BM2A.2.

23. Li, Z.; Sun, S.; Yang, Z.; Zhang, S.; Zhang, H.; Hu, M.; Cao, J.; Wang, J.; Liu, F.; Song, F.; Fan, J.; Peng, X., The use of a near-infrared RNA fluorescent probe with a large Stokes shift for imaging living cells assisted by the macrocyclic molecule CB7. *Biomaterials* **2013,** *34* (27), 6473-6481.

24. Kumar, C. V.; Turner, R. S.; Asuncion, E. H., Groove binding of a styrylcyanine dye to the DNA double helix: the salt effect. *Journal of Photochemistry and Photobiology A: Chemistry* **1993,** *74* (2), 231-238.

25. Almaqwashi, A. A.; Paramanathan, T.; Rouzina, I.; Williams, M. C., Mechanisms of small molecule–DNA interactions probed by single-molecule force spectroscopy. *Nucleic Acids Research* **2016,** *44* (9), 3971-3988.

26. Armitage B.A. () Cyanine Dye–DNA Interactions: Intercalation, Groove Binding, and Aggregation. In: Waring M.J., Chaires J.B. (eds) DNA Binders and Related Subjects. Topics in Current Chemistry, vol 253. Springer, Berlin, Heidelberg

27. Czerney, P.; Graneß, G.; Birckner, E.; Vollmer, F.; Rettig, W., Molecular

engineering of cyanine-type fluorescent and laser dyes. *Journal of Photochemistry and Photobiology A: Chemistry* **1995,** *89* (1), 31-36.

28. Wu, J.-Z.; Yuan, L., Synthesis and DNA interaction studies of a binuclear ruthenium(II) complex with 2,9-bis(2-imidazo[4,5-f][1,10]phenanthroline)-1,10-phenanthroline as bridging and intercalating ligand. *Journal of Inorganic Biochemistry* **2004,** *98* (1), 41-45.

29. Lin, C.-K.; Wang, Y.-F.; Cheng, Y.-C.; Yang, J.-S., Multisite Constrained Model of trans-4-(N,N-Dimethylamino)-4′-nitrostilbene for Structural Elucidation of Radiative and Nonradiative Excited States. *The Journal of Physical Chemistry A* **2013,** *117* (15), 3158-3164.

2.5 Ratiometric fluorescent hydrogen peroxide probes

2.5.1 Introduction

Hydrogen peroxide (H_2O_2) is generated without cessation from various sources.[1-4] Although H_2O_2 is well known for its cytotoxic effects, many recent studies reported importance of H_2O_2 its regulatory roll of eukaryotic signal transduction.[1-2, 5-8] To understand H_2O_2-related biochemical mechanisms better, probe for detection of H_2O_2 precisely is inevitable. One of the most widely used optical method for measuring H_2O_2 in molecular biology study is horseradish peroxidase (HRP)-catalyzed oxidation of fluorogenic substrates.[9] However, this method is rather expensive and requires purified enzymes, although it is considered sensitive and precise. Recently, Chang's group developed boronate-based fluorescent probes and many researchers reported that enabled detection of H_2O_2. These are designed to quench fluorescence due to the presence of a directly conjugated electron-deficient boronic ester group and the broken π-conjugation of xanthene by the closed spirolactam ring.[10-12] When this boronate group reacts with H_2O_2 to yield a hydroxyl moiety, the fluorescence of the probe is turned on by regeneration of a "push–pull" pair in the fluorophore. However, quantitative assay of H_2O_2 is still challenging because of this off/on property of the sensors whose whereabouts are not clear in many applications.[13] To meet practical requirements, the seesaw-type ratiometric change,[14-16] which simultaneous recording of two measurable fluorescence intensities, would be an alternative for the quantitative detection of H_2O_2.[17]

Recently, ratiometric sensors for H_2O_2, that based on Förster resonance energy-transfer (FRET) strategy or an intramolecular charge-transfer (ICT) strategy, were reported. However, the emission ratio change based on FRET is limited (less than 8-fold) since intrinsic characteristics of FRET,[18-20] and an ICT-based sensor using H_2O_2-mediated deprotection of carbobenzyloxy (Cbz) boronate exhibits 75-fold emission ratio changes,[21-22] but the probe's fluorescence change rate is much slower ($t_{1/2}$>45 min) than a directly conjugated aryl boronate sensor without the Cbz moiety

(t1/2<30 min).[23] The electronic state change of boronate-based H_2O_2 probes can be rationally designed from the electron push–pull strategy, however, it is hard to predict whether the resulting H_2O_2 probes would generate detectable fluorescence upon reaction with H_2O_2. Consequently, we sought to develop directly conjugated aryl boronic ester based probes which enable dramatic ratiometric sensing of H_2O_2 in a short time.

One of the fluorescent probe development strategy is diversity-oriented fluorescent library approach, which recently yielded unexpected but fruit full results that can not be acquired from rational design. We thought a focused library would minimize the size of the library and increasing the probability of success, rather than laborious synthesizing and screening hundreds of fluorescent molecules to find fluorescent probes. Thus, we aimed to find ratiometric fluorescent probes for H_2O_2 through a focused styryl-dye library which was prepared with combinatorial building blocks. H_2O_2 reactive formylphenyl boronic ester derivatives were used (**1**–**3,** Group **1**) as combinatorial building block(s) for better chance of finding `hit' molecules. For the structural diversity of the library, we chose five different N-methylpicolinium and N-methylquinolinium blocks (**A**–**E,** Group **2**) (see **Figure 2.5.1**), and that have a positive net charge which enhances its solubility in water. The Knoevenagel condensation reaction between two groups (Group **1** and Group **2**) provided 15 fluorescent styryl dyes, that have fully π-bond conjugated structure containing electron push-pull structure. Thus, their fluorescence would be directly changed through the intramolecular charge transfer (ICT) mechanism after reaction with H_2O_2. As our expectation, most styryl-dyes showed fluorescence response with H_2O_2 and one of them was utilized further for quantification of glucose.

2.5.2 Data & results

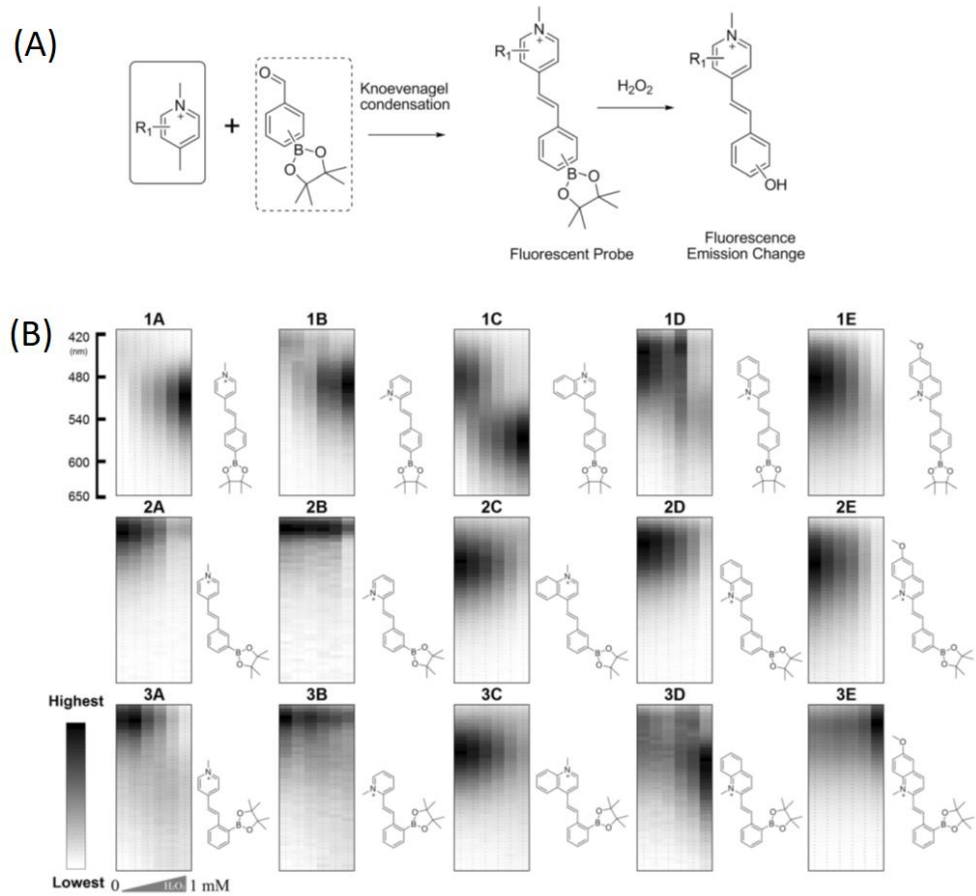

Figure 2.5.1. (A) Focused library synthesis of fluorescent probes for H_2O_2. (B) Fluorescence response of probes (50 μM) at each fluorescence emission wavelength after 30 min incubation with H_2O_2 (0, 50, 100, 200, 500, 1000 μM). Fluorescence intensity at each wavelength was depicted as an artificial color standard, which is shown as a bar graph. The highest and lowest fluorescence values were determined in each probe's fluorescence data. λ_{ex} = 375 nm. Each probe's observed mass, absorption wavelength, emission wavelength, and quantum yield are listed in Experimental section.

Each condensation reaction of building block leaded a fully conjugated fluorophore (see **Figure 2.5.1**). Twelve of 15 styryl dyes have a higher quantum yield than 0.010 (photophysical properties of styryl dyes are listed in **Table 2.5.1** in Experimental

Section.). Upon addition of H_2O_2, most of styryl dyes (each 50 μM) showed a distinct fluorescence change and the fluorescent properties were depicted in false-color images in **Figure 2.5.1**. Among them, **1A**, **1B**, **1C**, and **3D** underwent redshifts within 30 min of incubation with H_2O_2. Fortunately, two of them (**1A** and **1C)** showed a red shifted fluorescence at the maximum wavelength (over 70 nm) in the fluorescence emission spectrum and the UV/Vis spectrum upon addition of H_2O_2 (**Figure 2.5.2**). Interestingly, **1D** and **1E** have the same para-substituted boronic ester as **1A** and **1C**, that showed quenched fluorescence after H_2O_2 addition.

All five styryl dyes with meta-positioned boronate (**2A**–**E**) showed decreased fluorescence after H_2O_2 addition. Among ortho-positioned boronate probes, **3D** and **3E** showed increased fluorescence with H_2O_2, whereas three other probes (**3A**, **3B**, and **3C**) showed decreased fluorescence with H_2O_2. In short, the fluorescence change of each probe, upon H_2O_2 addition, is largely affected by the position of boronate and its conjugated structure with the picolinium/quinolinium blocks.

To demonstrate the utility of styryl dye based probe, **1A** and **1C** were selected for their superior photophysical properties including fluorescence intensity and changes in the intensity ratio upon H_2O_2 addition. Reactivity of **1A** and **1C** towards other ROSs were examined and only negligible fluorescence responses were observed within a 75 min incubation period (**Figure 2.5.2C, D**).

The kinetics of **1A** was measured with various concentrations of H_2O_2 and depicted in **Figure 2.5.3.** In the absence of H_2O_2, any significant changes of the fluorescence intensity ratio of the **1A** were not observed in neutral aqueous buffer solution. However, **1A** showed rapid fluorescence response after 1 mM of H_2O_2 addition (calculated pseudo-first-order rate constant is $k_{obs} = 1.3 \times 10^{-3}$ sec^{-1} with 1 mM of H_2O_2, $t_{1/2} < 5$ min).

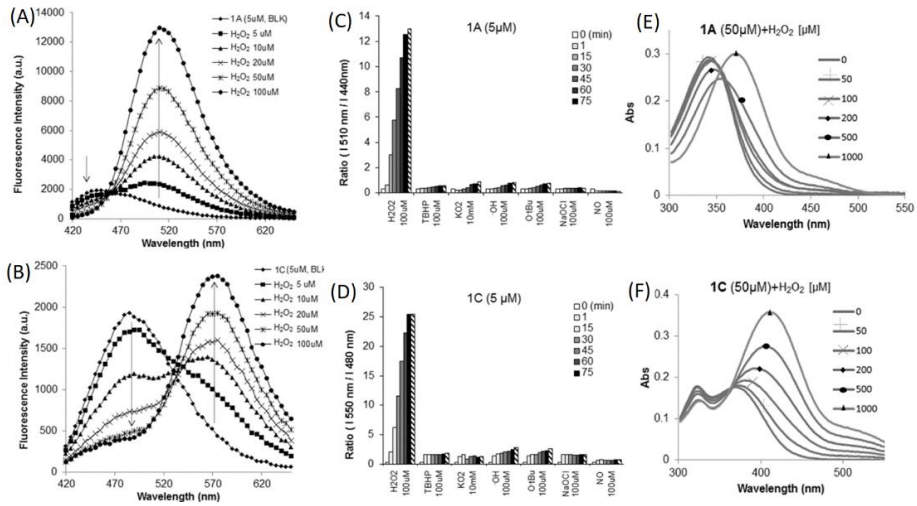

Figure 2.5.2. Fluorescence emission spectra **1A** (5 μM, A) and **1C** (5 μM, B) upon addition of H_2O_2 after 30 min incubation with various concentrations of H_2O_2. Fluorescence ratio changes of **1A** (5 μM, C) and **1C** (5 μM, D) toward ROSs at indicated time. UV/Vis spectra of **1A** (50 μM, E) and **1C** (50 μM, F) upon addition of H_2O_2 after 30 min incubation with various concentrations of H_2O_2. λ_{ex} = 375 nm.

Next, we utilized **1A** to quantify glucose with fluorescence response in real time through glucose oxidation by Glucose Oxidase (GOx) through whose resulting metabolite, H_2O_2.[24] Glucose (0.05 mM to 1.5 mM), **1A** (5 μm), and GOx (1 μm) were mixed in a cuvette. Every 10 minutes, changes in fluorescence emission ratio ($I_{520\ nm}/I_{420\ nm}$, excitation wavelength 375 nm) of the solution were recorded. After the addition of GOx into glucose solution (1 mM), fluorescence ratio ($I_{520\ nm}/I_{420\ nm}$) increased from 0.3 to 8 by H_2O_2 produced from glucose oxidation (**Figure 2.5.3b**). Further, the emission ratio changes with time were obviously dependent on the glucose concentration (remaining) between 0.1 and 1 mM (**Figure 2.5.3b**). Interestingly, when glucose concentration was higher than 1 mM, glucose oxidation rate did not increased significantly. Because only a limited pool of molecular oxygen (ca. 0.3 mM) existed in the solution which could be depleted during the oxidation. Notably, the fluorescence change of **1A** was totally blocked in this reaction by the addition of catalase (**Figure 2.5.3d**), which catalyzes the decomposition of H_2O_2 in

the solution. This is solid evidence that the fluorescence change of the probe was caused by H_2O_2, and not by the direct oxidation reaction between GOx and the probe. Using **1A**, we could also check the selectivity of GOx for other saccharide molecules, namely, 2-deoxy-d-glucose and galactose. As indicated in **Figure 2.5.3c**, GOx oxidized 2-deoxy-d-glucose as well, but more slowly than d-glucose, producing H_2O_2. On the other hand, galactose showed a negligible change in fluorescence because galactose is not a good substrate for GOx, as reported earlier.[25]

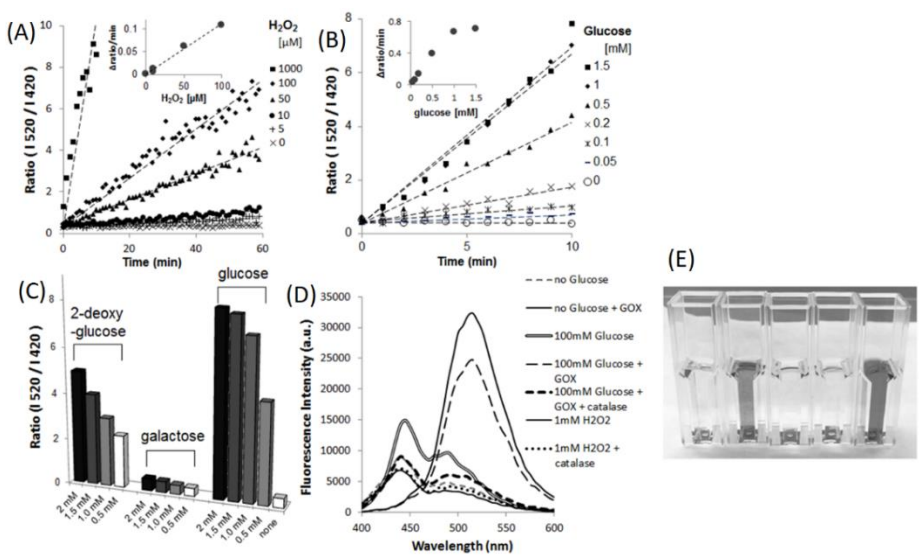

Figure 2.5.3. **(A)** Ratiometric fluorescence emission changes ($I_{520\ nm}/I_{420\ nm}$) upon reaction of **1A** (5 μM) with H_2O_2 with time; inset graph, x-axis: H_2O_2 concentration, y-axis: average ratio change per min. (B) Real-time monitoring of glucose oxidation by GOx (1 μM) with **1A** (5 μM); inset graph, x-axis: glucose concentration, y-axis: average ratio change per min. (C) Reactivity of GOx (1 μM) toward 2-deoxy-D-glucose, D-galactose, and D-glucose. GOx/**1A** (5 μM) was incubated with these sugars (0.5–2 mM) for 10 min. (D) Fluorescence emission spectra of **1A** (10 μM) in various condition. The mixture was incubated for 30 min at room temperature. λ_{ex} = 375 nm. (E) Photograph of **1A** (50 μM) with 100 mM glucose, 100 mM glucose + 0.5 μM GOx, 0.5 μM GOx, probe only (no glucose + no GOx), 1 mM H_2O_2 (left to right). This photo was taken using an iPhone4® camera under room light.

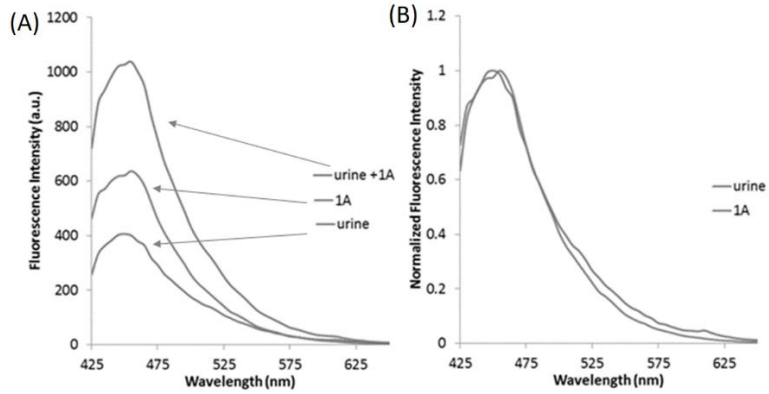

Figure 2.5.4. (A) Fluorescence and (B) normalized fluorescence spectra of 10-fold diluted urine solution and probe **1A** (100 μM). Spectra were recorded in 10 mM phosphate buffer (pH 7.4). λ_{ex} = 375 nm.

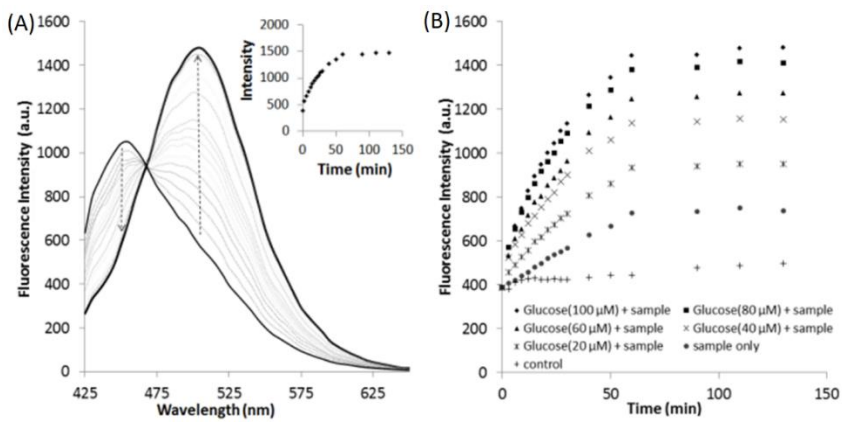

Figure 2.5.5. (A) Real-time monitoring of fluorescence changes of **1A** (100 μM) upon addition of GOx (0.5 μM) and glucose (100 μM) in 10-fold diluted human urine. Inset graph, x-axis: elapsed time from 3 min to 130 min, y-axis: fluorescence intensity at 510 nm. (B) Real-time monitoring of glucose (20, 40, 60, 80 and 100 μM) oxidation by GOx (0.5 μM) with **1A** (100 μM) in 10-fold diluted human urine. See Experimental section for detailed procedures. All experiments were performed in phosphate buffer solution (10 mM, pH 7.4). λ_{ex} = 375 nm.

From these results, we utilized **1A** for precisely quantifying of the glucose level of diabetes patients in a sample, and **1A** was successfully detected and quantified glucose in a human urine sample. The human urine was collected from a healthy volunteer and tested. Coincidentally, the fluorescence spectrum of healthy human urine was very similar to that of **1A** itself.[26-27] Therefore, we analyzed data of urine samples using a fluorescence intensity of 510 nm, instead quantifying by ratiometric change (see **Figure 2.5.4** and **2.5.5**). Since the concentration of glucose in the urine of a diabetic patient is above 1 mM, our probe, **1A**, would be useful in diagnosing diabetes.[28] By using **1A** and GOx, enhanced and redshifted fluorescence emission spectra were obtained from glucose-containing (20–100 μM) urine samples, as seen in **Figure 2.5.5**. Moreover, we could quantify a small amount of glucose in human urine (diluted 10-fold) by using standard addition plots (19.7±2.4 μM, see **Figure 2.5.6**).

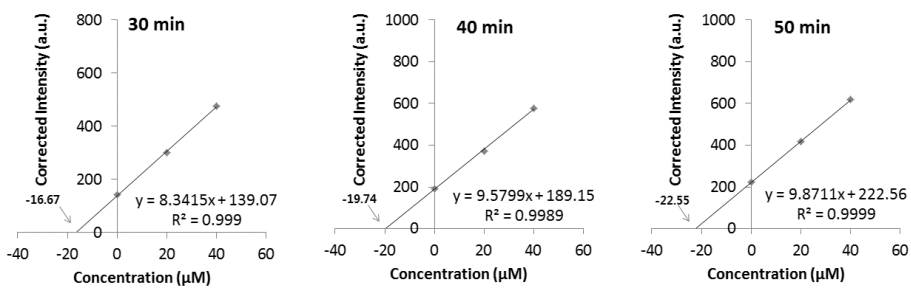

Figure 2.5.6. Standard addition plots for estimating glucose concentration in samples. Data were selected from glucose containing (0, 20, 40 μM) 10-fold diluted urine with phosphate buffer solution. Corrected Intensity: fluorescence intensity of the sample (urine (10% (v/v)) + 100 μM **1A** + 0.5 μM GOx + glucose) – fluorescence intensity of the control sample (urine 10% (v/v)) + 100 μM **1A**), Concentration: glucose concentration of the sample was added. λ_{em} = 510 nm.

In the same way, fluorescence intensity of **1A** was increased proportional to the amount of cholesterol in presence of cholesterol oxidase (**Figure 2.5.7**).[29]

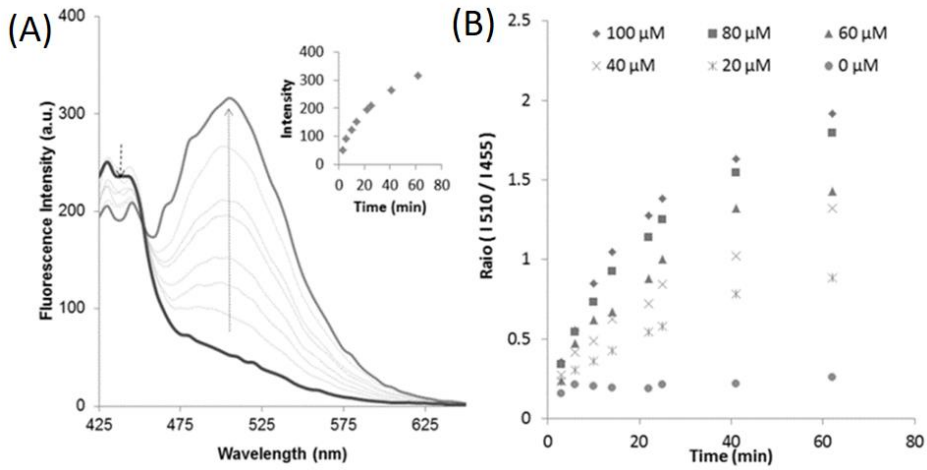

Figure 2.5.7. (A) Fluorescence spectra (λ_{ex} = 375 nm) of cholesterol in phosphate buffer (10 mM, pH 7.4) solution. Solution contained 10 μM **1A** + 80 μM cholesterol + 0.5 μM cholesterol oxidase. Inset graph; x-axis: time, y-axis: fluorescence intensity at 510 nm. (B) Real-time monitoring of cholesterol oxidation by cholesterol oxidase (0.1 μM) with **1A** (10 μM) in the presence of various concentrations of cholesterol with fluorescence intensity ratio changes. Inset graph, x-axis: elapsed time from 3 to 62 min, y-axis: fluorescence intensity at 510 nm.

Many biomolecules including lactate,[30] xanthine,[31] monoamine,[32] and choline[33] are related with H_2O_2, since these oxidases produce H_2O_2 as a byproduct after oxidation. By using **1A** that can detect the activity of these oxidases, as well as the presence and the quantity of specific biomolecules. Our probe would be a low cost method relative to HRP-catalyzed oxidation a method that requires additional enzymes. Probe **1A** is also strongly chromogenic (see **Figure 2.5.3E**) when reacting with H_2O_2, and therefore, H_2O_2 generating metabolic reaction can be detected by the naked eye in the real-life environment.

In summary, we have developed ratiometric fluorescent probes for H_2O_2 from a focused library. Upon the addition of H_2O_2, probe **1A** shows a redshift of over 100 nm in the maximum fluorescence emission wavelength and an increase in ratio of over 30-fold. Probe **1A** was successfully utilized for the real time monitoring of glucose with oxidation by GOx.

2.5.3 Experimental section

Materials & Methods

Materials and solvents were obtained from commercial suppliers (Sigma-Aldrich, TCI, Acros and Alfa Aesar) and were used without further purification. The plate reader was Biotek SYNERGY Microplate Reader. Combinatorial block **A** and **B** were purchased from Sigma-Aldrich and **C**, **D**, **E** blocks were prepared by following the previous procedure (see Experimental section 2.4). **1**, **2**, and **3** blocks, Glucose oxidase (Sigma G2133), and catalase (Sigma C1345) were purchased from Sigma-Aldrich.

Hydrogen peroxide (H_2O_2), tert-butyl hydrogenperoxide (TBHP), and hypochlorite (OCl^-) were delivered as 30%, 70%, and 5% aqueous solutions, respectively. Superoxide (O_2^-) was added as solid KO_2. Hydroxyl radical (•OH) and tert-butoxy radical (•OtBu) were generated by reaction of 1 mM Fe^{2+} with 100 μM H_2O_2 or 100 μM TBHP, respectively. Nitric oxide (NO) was added using NO gas. [34]

General Procedure for Synthesis of the Library

Each building block was dissolved separately in absolute ethanol (40mM) as stock solutions In a 20 ml glass vial, 80 μmol of each reactant (each 2.0 ml) and 10 μL pyrrolidine were slowly added at room temperature and stirred at 65°C for 1hr to overnight. The reaction was monitored by TLC and LC-MS. LC−MS characterization was performed on a LC-MS-IT-TOF Prominence Shimadzu Technology, using a DAD (SPD-M20A) detector, and a C18 column (20 mm × 4.0 mm, 100Å, Phenomenex Inc.), with 7 min elution using a gradient solution of CH_3CN-H_2O (containing 0.1% TFA) and an electrospray ionization source. When the reaction was completed, the organic solvent was evaporated under a low-pressured rotary evaporator, and dried the mixture complete *in vacuo*. Then, reaction mixture was purified by flash column chromatography (Merck Silica Gel 60, particle size: 0.040−0.063 mm, 230−400 mesh ASTM) and was further purified by reverse

phase semi-prep HPLC (Gilson RP-HPLC with a C18 column, 100 mm × 21.2 mm, Axia column from Phenomenex Inc.) using water and acetonitrile as eluents. NMR spectra of the products (1A and 1C) were recorded on a Bruker NMR spectroscopy (300 MHz for ^{1}H-NMR and 75 MHz ^{13}C-NMR). High-resolution mass spectra were recorded by Gas Chromatography-Mass Spectrometer (Mass System: JEOL, JMS-600W, GC System Agilent, 6890 Series). The chemical structures of the products are shown in **Scheme 2.5.1**.

Scheme 2.5.1. Focused library synthesis of fluorescent probes for H_2O_2.

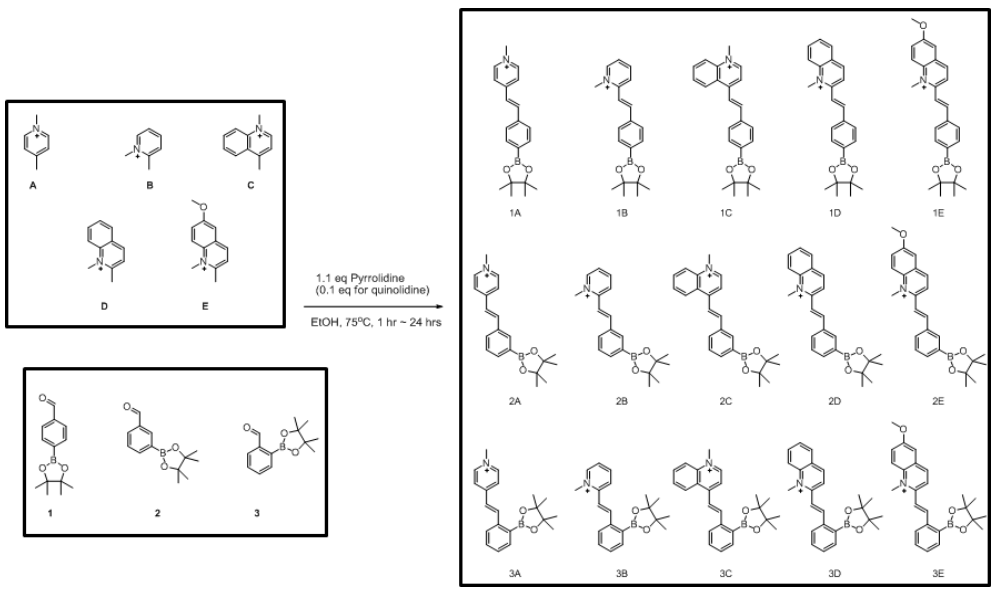

Table 2.5.1. Spectroscopic properties and mass data for H_2O_2 sensor library: absorbance maximum (λ_{abs}), fluorescent emission maximum (λ_{em}), extinction coefficient, quantum yield.

name	mass(calc)	m/z (exp)	λ_{abs}(nm)	λ_{em} (nm)	ε ($M^{-1}cm^{-1}$)	Φ[a]
1A	322.2	322.0	342	445	4430	0.012
1B	322.2	322.0	328	435	3250	0.004
1C	372.2	372.0	368	480	2885	0.022
1D	372.2	372.0	360	450	3450	0.013
1E	402.2	402.0	376	485	5490	0.032
2A	322.2	322.0	336	440	2150	0.011
2B	322.2	322.0	328	435	1970	0.003
2C	372.2	372.0	364	480	2590	0.020
2D	372.2	372.0	360	455	5050	0.011
2E	402.2	402.1	376	480	6210	0.022
3A	322.2	322.1	338	435	3650	0.013
3B	322.2	322.1	328	435	1170	0.013
3C	372.2	372.1	318	480	3180	0.012
3D	372.2	372.1	320	440	3650	0.003
3E	402.2	402.1	310	460	2740	0.14

All absorbance and fluorescence excitation and emission data were recorded by a Synergy 4, Biotek Inc. Fluorescent plate reader (5 μM compounds in PBS (100 μl) for λ_{abs}, 5 μM compounds in PBS (100 μL) for λ_{em}, excitation at 375 nm) in 96-well polypropylene plates. Mass was calculated as (M^+), and found mass (M^+) was observed in ESI-MS of LC-MS. [a] The fluorescence quantum yields of the dyes were determined by the reference standard (rhodamine B, Φ_F=0.49 in ethanol at 25 °C).

Urinary glucose detection experiment procedure

1. 100 μL of human urine was added to a 5 mL vial.
2. 700 μL of 10 mM phosphate buffer (pH 7.4) was added to the vial.
3. Appropriate amount of aqueous glucose solution (10 mM, in phosphate buffer) was added to the vial.
4. 10 μL of probe **1A** (10 mM DMSO stock solution) was added to the vial.
5. 90 μL of 10 mM phosphate buffer (pH 7.4) was added to the above solution to make the total volume of 0.9 mL.
6. 100 μL of GOx (5 μM in phosphate buffer) was added to the vial and well mixed.
7. Photophysical properties were recorded with Microplate reader.

NMR, Mass Characteristics and NMR Spectra of 1A and 1C

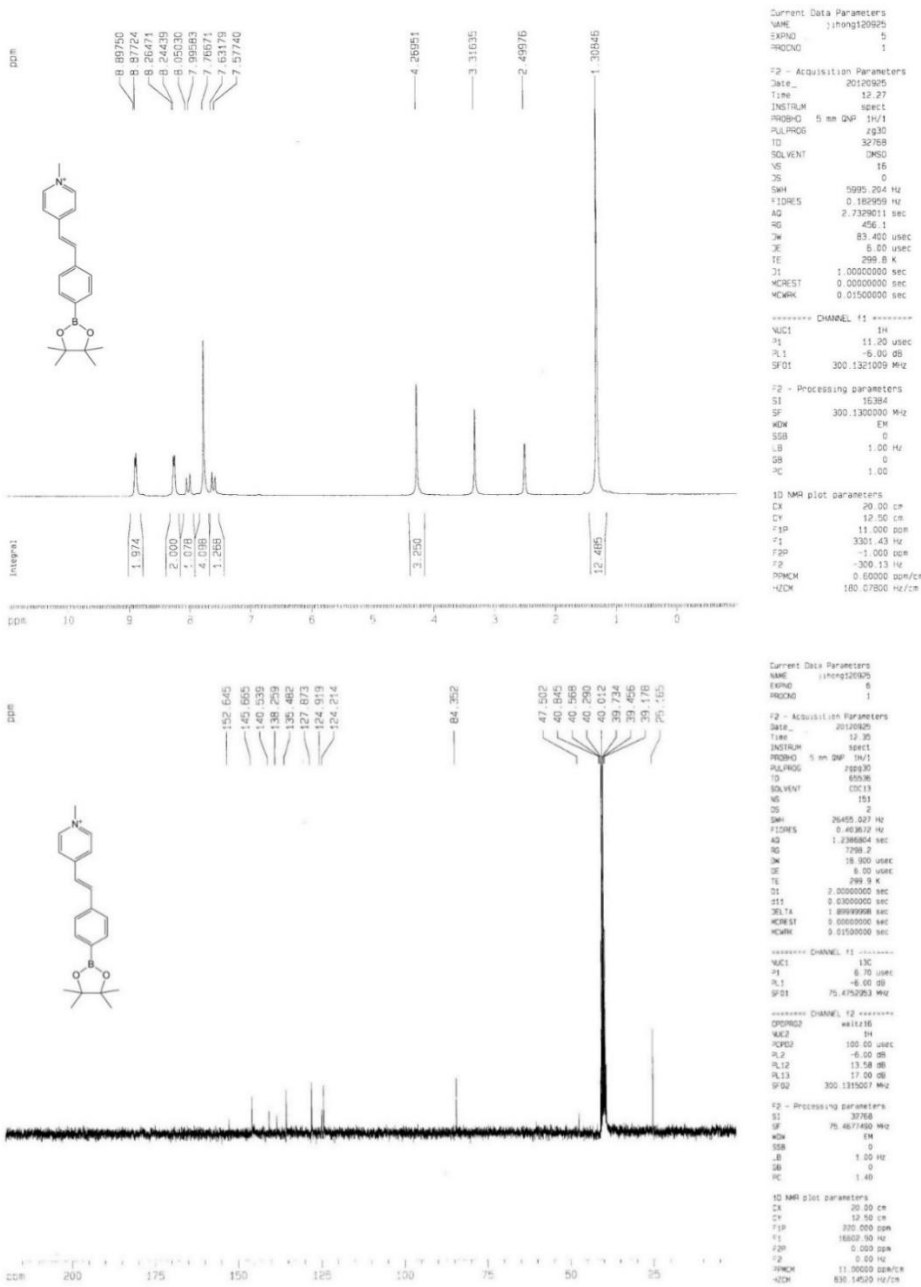

^{1}H NMR (DMSO-d_6, 300 MHz) 8.88 (d, J = 6.08 Hz, 2H), 8.25 (d, J = 6.10 Hz, 2H), 8.03 (d, J = 16.34 Hz, 1H), 7.77 (s, 4H), 7.60 (d, J = 16.32 Hz, 1H), 4.27 (s, 3H), 1.31 (s, 12H). ^{13}C NMR (DMSO-d_6, 75 MHz) 152.65, 145.67, 140.54, 138.26, 135.49, 127.87, 124.92, 124.21, 84.35, 47.50, 25.17. HR–FAB–Mass m/z calcd. for $C_{20}H_{25}BNO_2$[M]: 322.1987, found 322.1985.

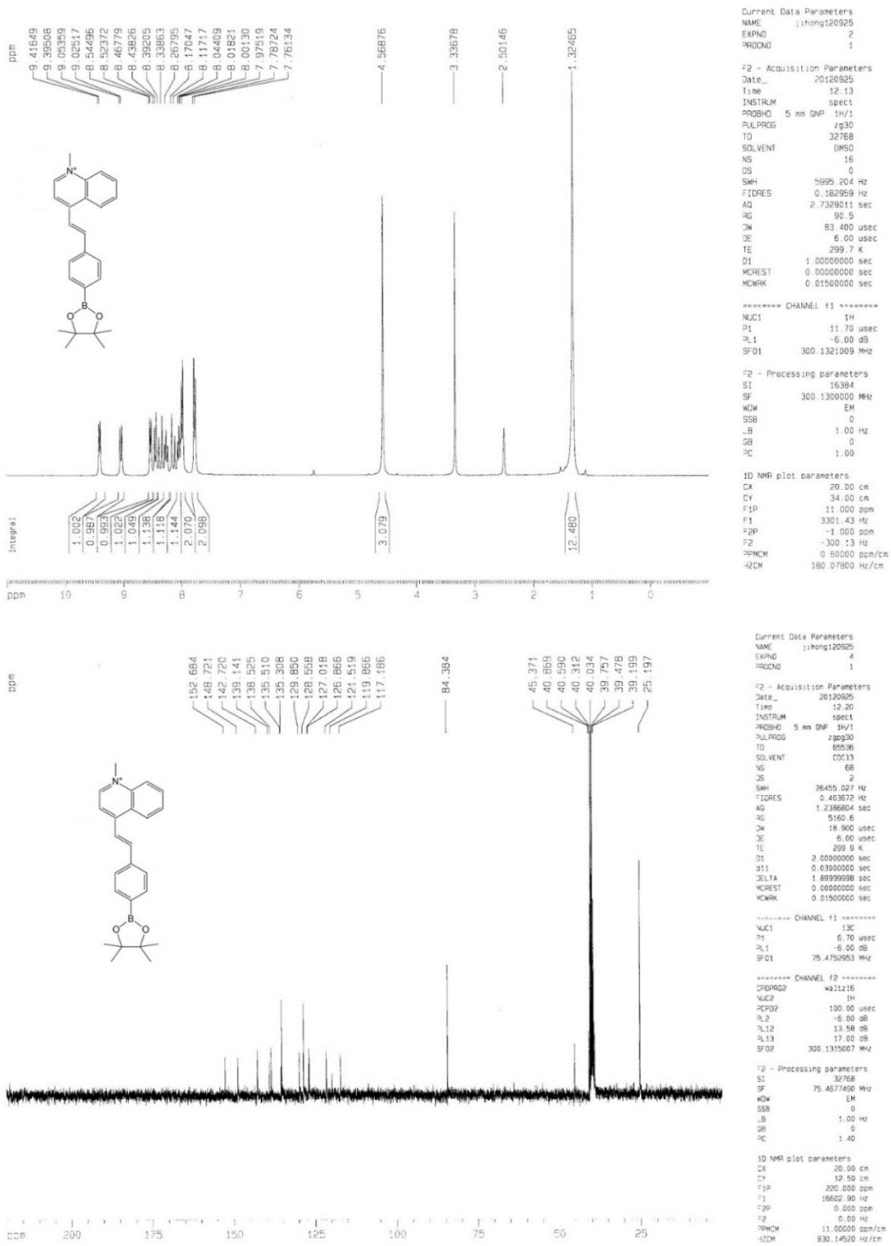

^{1}H NMR (DMSO-d_6, 300 MHz) 9.41 (d, J = 6.42 Hz, 1H), 9.03 (d, J = 9.53 Hz, 1H), 8.53 (d, J = 6.37 Hz, 1H), 8.45 (d, J = 8.86 Hz, 1H), 8.37 (d, J = 16.03 Hz, 1H), 8.27 (t, J = 7.84 Hz, 1H), 8.14 (d, J = 15.99 Hz, 1H), 8.04 (t, J = 7.80 Hz, 1H), 7.99 (d, J = 7.83 Hz, 2H), 7.77 (d, J = 7.77 Hz, 2H), 4.57 (s, 3H), 1.32 (s, 12H). ^{13}C NMR (DMSO-d_6, 75 MHz) 152.68, 148.72, 142.72, 139.141, 138.53, 135.51, 135.31, 129.85, 128.56, 127.02, 126.87, 121.52, 119.87, 117.19, 84.38, 45.37, 25.20. HR–FAB–MS m/z calcd. for $C_{24}H_{27}BNO_2$[M]: 372.2135, found 372.2146.

2.5.4 Reference

1. Murphy, Michael P., How mitochondria produce reactive oxygen species. *Biochemical Journal* **2009,** *417* (1), 1.

2. Lennicke, C.; Rahn, J.; Lichtenfels, R.; Wessjohann, L. A.; Seliger, B., Hydrogen peroxide – production, fate and role in redox signaling of tumor cells. *Cell Communication and Signaling* **2015,** *13* (1), 39.

3. Halliwell, B.; Clement, M. V.; Long, L. H., Hydrogen peroxide in the human body. *FEBS Letters* **2000,** *486* (1), 10-13.

4. Boveris, A.; Cadenas, E., Mitochondrial Production of Hydrogen Peroxide Regulation by Nitric Oxide and the Role of Ubisemiquinone. *IUBMB Life* **2000,** *50* (4-5), 245-250.

5. Baumann, K., Letting H2O2 work. *Nature Reviews Molecular Cell Biology* **2010,** *11*, 234.

6. Gough, D. R.; Cotter, T. G., Hydrogen peroxide: a Jekyll and Hyde signalling molecule. *Cell Death &Amp; Disease* **2011,** *2*, e213.

7. Neill, S.; Desikan, R.; Hancock, J., Hydrogen peroxide signalling. *Current Opinion in Plant Biology* **2002,** *5* (5), 388-395.

8. Veal, E. A.; Day, A. M.; Morgan, B. A., Hydrogen Peroxide Sensing and Signaling. *Molecular Cell 26* (1), 1-14.

9. Zhou, M.; Diwu, Z.; Panchuk-Voloshina, N.; Haugland, R. P., A Stable Nonfluorescent Derivative of Resorufin for the Fluorometric Determination of Trace Hydrogen Peroxide: Applications in Detecting the Activity of Phagocyte NADPH Oxidase and Other Oxidases. *Analytical Biochemistry* **1997,** *253* (2), 162-168.

10. Dickinson, B. C.; Chang, C. J., Chemistry and biology of reactive oxygen species in signaling or stress responses. *Nature Chemical Biology* **2011,** *7*, 504.

11. Dickinson, B. C.; Peltier, J.; Stone, D.; Schaffer, D. V.; Chang, C. J., Nox2 redox signaling maintains essential cell populations in the brain. *Nature Chemical Biology* **2010,** *7*, 106.

12. Lippert, A. R.; Van de Bittner, G. C.; Chang, C. J., Boronate Oxidation as a Bioorthogonal Reaction Approach for Studying the Chemistry of Hydrogen Peroxide in Living Systems. *Accounts of Chemical Research* **2011,** *44* (9), 793-804.

13. Chan, J.; Dodani, S. C.; Chang, C. J., Reaction-based small-molecule fluorescent probes for chemoselective bioimaging. *Nature Chemistry* **2012,** *4*, 973.

14. Bianchi-Smiraglia, A.; Rana, M. S.; Foley, C. E.; Paul, L. M.; Lipchick, B. C.; Moparthy, S.; Moparthy, K.; Fink, E. E.; Bagati, A.; Hurley, E.; Affronti, H. C.; Bakin, A. V.; Kandel, E. S.; Smiraglia, D. J.; Feltri, M. L.; Sousa, R.; Nikiforov, M. A., Internally ratiometric fluorescent sensors for evaluation of intracellular GTP levels and distribution. *Nature Methods* **2017,** *14*, 1003.

15. Wu, P.; Hou, X.; Xu, J.-J.; Chen, H.-Y., Ratiometric fluorescence, electrochemiluminescence, and photoelectrochemical chemo/biosensing based on semiconductor quantum dots. *Nanoscale* **2016,** *8* (16), 8427-8442.

16. Feng, S.; Fang, Y.; Feng, W.; Xia, Q.; Feng, G., A colorimetric and ratiometric fluorescent probe with enhanced near-infrared fluorescence for selective detection of cysteine and its application in living cells. *Dyes and Pigments* **2017,** *146* (Supplement C), 103-111.

17. Chen, X.; Tian, X.; Shin, I.; Yoon, J., Fluorescent and luminescent probes for detection of reactive oxygen and nitrogen species. *Chemical Society Reviews* **2011,** *40* (9), 4783-4804.

18. Du, F.; Min, Y.; Zeng, F.; Yu, C.; Wu, S., A Targeted and FRET-Based Ratiometric Fluorescent Nanoprobe for Imaging Mitochondrial Hydrogen Peroxide in Living Cells. *Small* **2014,** *10* (5), 964-972.

19. Huang, X.; Wang, J.; Liu, H.; Lan, T.; Ren, J., Quantum dot-based FRET for sensitive determination of hydrogen peroxide and glucose using tyramide reaction. *Talanta* **2013,** *106* (Supplement C), 79-84.

20. Guo, H.; Aleyasin, H.; Dickinson, B. C.; Haskew-Layton, R. E.; Ratan, R. R., Recent advances in hydrogen peroxide imaging for biological applications. *Cell & Bioscience* **2014,** *4* (1), 64.

21. Chung, C.; Srikun, D.; Lim, C. S.; Chang, C. J.; Cho, B. R., A two-photon fluorescent probe for ratiometric imaging of hydrogen peroxide in live tissue. *Chemical Communications* **2011,** *47* (34), 9618-9620.

22. Srikun, D.; Miller, E. W.; Domaille, D. W.; Chang, C. J., An ICT-Based Approach to Ratiometric Fluorescence Imaging of Hydrogen Peroxide Produced in Living Cells. *Journal of the American Chemical Society* **2008,** *130* (14), 4596-4597.

23. Shen, Y.; Zhang, X.; Zhang, Y.; Wu, Y.; Zhang, C.; Chen, Y.; Jin, J.; Li, H., A

mitochondria-targeted colorimetric and ratiometric fluorescent probe for hydrogen peroxide with a large emission shift and bio-imaging in living cells. *Sensors and Actuators B: Chemical* **2018,** *255* (Part 1), 42-48.

24. Bankar, S. B.; Bule, M. V.; Singhal, R. S.; Ananthanarayan, L., Glucose oxidase — An overview. *Biotechnology Advances* **2009,** *27* (4), 489-501.

25. Bartlett, P. N.; Bradford, V. Q.; Whitaker, R. G., Enzyme electrode studies of glucose oxidase modified with a redox mediator. *Talanta* **1991,** *38* (1), 57-63.

26. Leiner, M. J. P.; Hubmann, M. R.; Wolfbeis, O. S., The total fluorescence of human urine. *Analytica Chimica Acta* **1987,** *198* (Supplement C), 13-23.

27. Rajasekaran, R.; Aruna, P. R.; Koteeswaran, D.; Padmanabhan, L.; Muthuvelu, K.; Rai, R. R.; Thamilkumar, P.; Murali Krishna, C.; Ganesan, S., Characterization and Diagnosis of Cancer by Native Fluorescence Spectroscopy of Human Urine. *Photochemistry and Photobiology* **2013,** *89* (2), 483-491.

28. Molitch ME. Diabetes Mellitus. In: Walker HK, Hall WD, Hurst JW, editors. Clinical Methods: The History, Physical, and Laboratory Examinations. 3rd edition. Boston: Butterworths; 1990. Chapter 136. Available from: https://www.ncbi.nlm.nih.gov/books/NBK242

29. Richmond, W., Use of cholesterol oxidase for assay of total and free cholesterol in serum by continuous-flow analysis. *Clinical Chemistry* **1976,** *22* (10), 1579-1588.

30. Sztajer, H.; Wang, W.; Lünsdorf, H.; Stocker, A.; Schmid, R. D., Purification and some properties of a novel microbial lactate oxidase. *Applied Microbiology and Biotechnology* **1996,** *45* (5), 600-606.

31. Czupryna, J.; Tsourkas, A., Xanthine oxidase-generated hydrogen peroxide is a consequence, not a mediator of cell death. *FEBS Journal* **2012,** *279* (5), 844-855.

32. Simonson, S. G.; Zhang, J.; Andrew T. Canada, J.; Su, Y.-F.; Benveniste, H.; Piantadosi, C. A., Hydrogen Peroxide Production by Monoamine Oxidase during Ischemia-Reperfusion in the Rat Brain. *Journal of Cerebral Blood Flow & Metabolism* **1993,** *13* (1), 125-134.

33. Rozwadowski, K. L.; Khachatourians, G. G.; Selvaraj, G., Choline oxidase, a catabolic enzyme in Arthrobacter pascens, facilitates adaptation to osmotic stress in Escherichia coli. *Journal of Bacteriology* **1991,** *173* (2), 472-478.

34. Miller, E. W.; Albers, A. E.; Pralle, A.; Isacoff, E. Y.; Chang, C. J., Boronate-Based

Fluorescent Probes for Imaging Cellular Hydrogen Peroxide. *Journal of the American Chemical Society* **2005,** *127* (47), 16652-16659.

Part 3. Development of fluorescent mitochondria targeting imaging probes based on styryl BODIPY

After their introduction in 1968,[1] 4,4-difluoro-4-bora-3a,4a-diaza-*s*-indacene (BODIPY, the BODIPY's name originated from **bo**ron **dipy**rromethene) fluorophores have been intensively studied by the academia in multidisciplinary due to their superior photophysical properties.[2-6] In this part, we described development of fluorescent probes based on styryl BODIPY and cancer treatment studies using them. Before taking up the main subject, let's look at a brief concept of BODIPY and characteristics of cancer cell.

3.1.1 Introduction to basic concept of BODIPY

This strong fluorescent dye, BODIPY, represents structural analogues of porphyrins. The distinct photophysical properties of BODIPY dyes can be ascribed to high rigidity of the BODIPY core which explains high ε and Φ_{fl}. The complexation of boron trifluoride with dipyrromethene unit forms a dipyrrometheneboron difluoride structure (**Figure 3.1.1**). BODIPY is rigidized by the bridging BF_2 unit which has high oscillating strength of the transition from S_0 to S_1 and very low probability for vibrational relaxation processes. Methylation in the meso position makes the BODIPY more planar and enhances the fluorescence quantum yield.

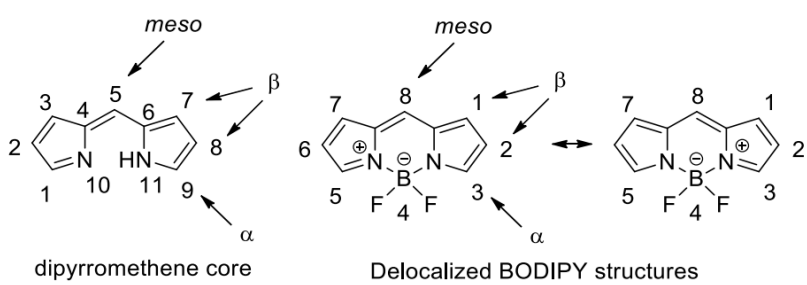

Figure 3.1.1. Structures and IUPAC numbering of dipyrromethene and BODIPY

Since their simple synthesis and derivatization, many BODIPY derivatives has been reported in last 50 years.[5, 7] Dipyrromethane intermediate is readily attacked by

nucleophile and can be polymerized in acidic condition. For this reason, the starting pyrrole has methyl substituents which prohibits side reaction, improves the photostability, and enhances yield of the resulting BODIPY derivatives. Interestingly, the methyl groups in α-position of the BODIPY are slightly acidic and can be modified further.

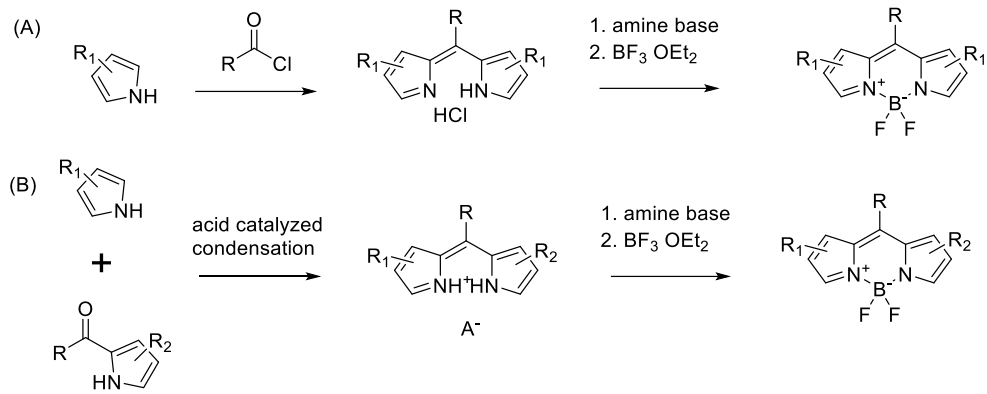

Figure 3.1.2. General approaches for the BODIPY synthesis. (A) Meso-substituted BODIPY, (B) Non-meso-substituted BODIPY.

Derivatization of the BODIPY Platform

The photophysical properties of BODIPY are highly influenced by π-conjugated substituents that extent electronic delocalization of the BODIPY. Many research groups, including Akkaya,[8] Burgess,[9] Carreira,[10] Dehaen,[11] Nagano,[12] Rurack,[13] Vicente,[14] Ziessel[7] and numerous researchers investigated strategies intensively for modifying the photophysical properties and the function of BODIPYs. Here, a few examples of modified BODIPY dyes.[15]

1. Electrophilic substitutions at the 2,6-position

Scheme 3.1.1. Possible resonance structures of BODIPY core.

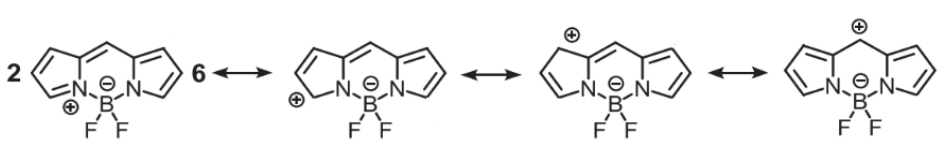

As illustrated in **Scheme 3.1.1**, the 2- and 6-positions of the BODIPY core bear the least positive charges. This electron rich character of the 2- and 6-positions are receptive to electrophilic substitution reactions, halogenation, formylation, and sulfonation.

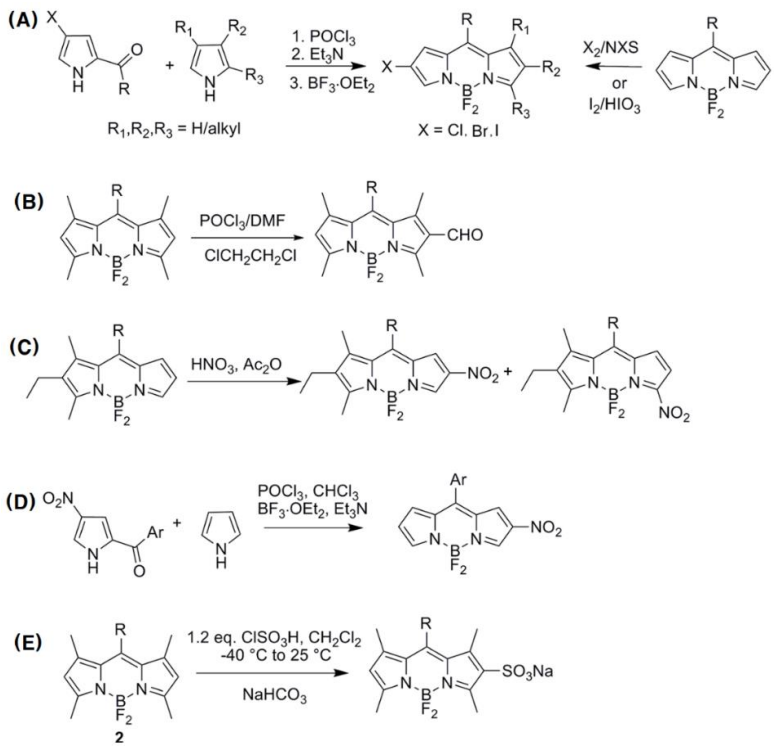

Figure 3.1.3. Synthesis of (**A**) 2-halo, (**B**) 2-formyl, (**C**) and (**D**) 2-nitro and (**E**) 2-sulfonyl functionalized BODIPYs. NXS: N-halosuccinimide.

2. Addition of functionalized styryl groups at the 3,5-positions

Acidic proton of methyl substituents at 3,5-positions can participate in Knoevenagel condensation reactions.

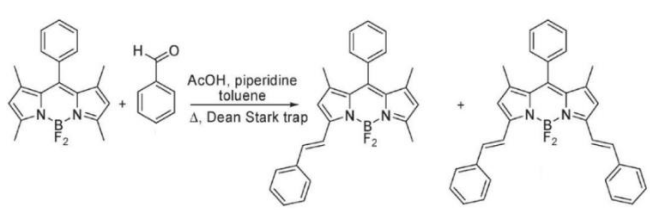

Figure 3.1.4. Typical synthesis of styryl BODIPY.

3. **Nucleophilic substitution of fluorine at the boron center.**

Fluorine atoms on boron center of BODIPY core can be replaced via nucleophilic substitution reactions.[16-18]

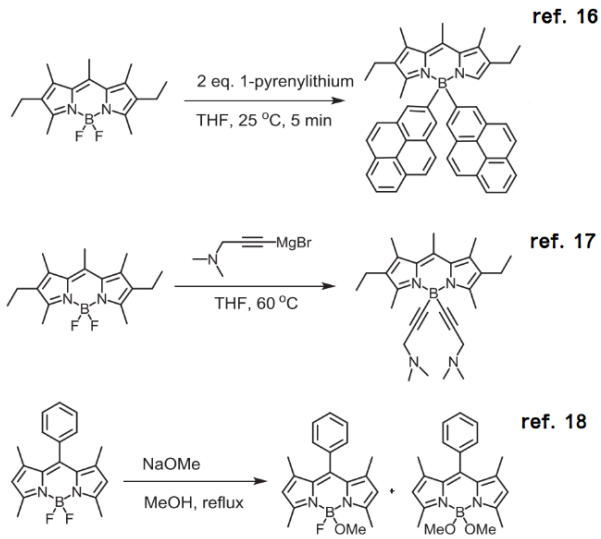

Figure 3.1.5. Substitution reactions on boron centers of BODIPY.

3. **Substitution nitrogen for meso-carbon (aza-BODIPY)**[19]

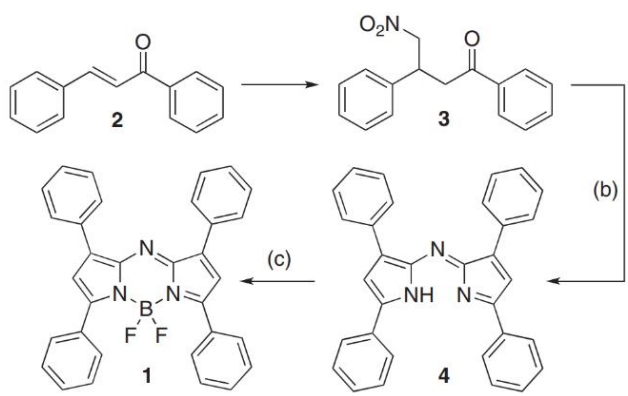

(a)	(b)	(c)
CH_3NO_2, DEA, MeOH, Δ, **24h**,	NH_4OAc, EtOH, Δ, **48h**,	BF_3-OEt_2O, DIEA, DCM, rt, **24h**.

Figure 3.1.6. Typical synthesis of aza-BODIPY.

4. **Substitution indole derivatives for pyrrole (isoindole)**[20]

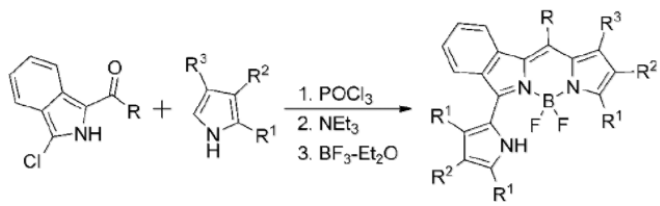

Figure 3.1.7. 3-pyrrole/indole substituted isoindole-BODIPY.

In addition to these, a huge number of derivatives are known, and the development of new BODIPY derivatives is still underway.

3.1.2 Introduction to cancer cells

People who cause public criticism in human society, are referred to as cancers. In fact, influences of antisocial humans on society are very similar to the effects of cancer on living organism (mischief to other beings, depleting resources,). Interestingly, the solution of "the cancer problem" (diagnosis, extraction and kill cancer) is also similar to the way of the dealing with the offenders (judging by law, imprisoning, punishment or execution). The pursuit of boundless self-interest for the public good (energy resource for cancer) is not only about society (living organism) but also its own ruin.[21] Then, what is the cancer and why does it matter to living thing? What makes the cancer cells so malevolently different from their normal predecessors? How we can treat this troublemaker? Also, can we observe this process in real time? To begin with, let us examine the characteristics of cancer cells.

Growth without regulation, the capacity to invade tissue and colonize distant sites, these are two typical features of cancer cells. The uncontrolled growth of abnormal cells is property of all neoplasm, which can be benign or malignant either. Benign neoplasm does not invade other parts of the body and it can be extracted surgically. Fortunately, it is not life threatening and not cancerous. However, malignant neoplasm cells grow become cancerous after mutations accumulate in the various

genes. Instead of growing by external stimulation, cancer cells stimulate their own growth, disable tumor-suppressor genes, and even ignore external signals of forbidding proliferation. The cancer cells multiply endless as long as energy supplement is sufficient. Thus, that stimulate the growth of new blood vessels to support their increasing size (angiogenesis) and make use of abnormal metabolic pathways to generate energy. The cancer cell goes so far as to break away from their site of origin, travel through the blood stream, invade surrounding local tissue and spread to distant parts of the body (metathesis). In sever case, cancers evade and mutate the body's immune system to prevent T cells from attacking them.

According to Cancer Genome Project, most cancer cells possess dozens of mutations.[22-23] However, identifying of these mutations are formidable that responsible for particular kinds of cancer, because many of the mutations exist in cancer cells are not related to cancer growth. Different kinds of cancers have different mutational peculiarity, but, most tumor types have divulged that certain mutated genes are expressed more often in cancer cells than others. The gene mutations accumulate over time in a consequence of independent events. This progression of cancer is a microevolutionary process.

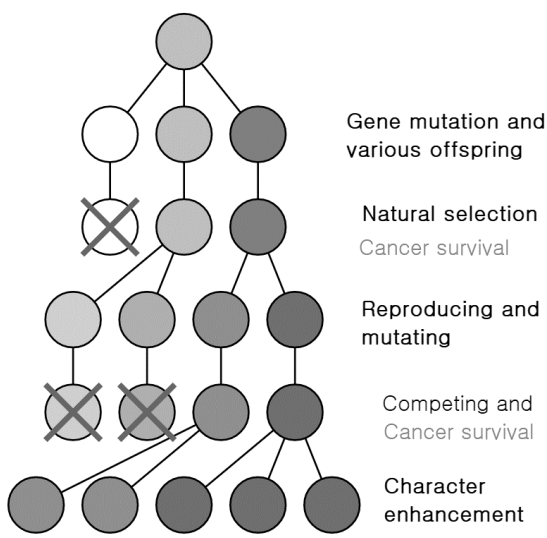

Figure 3.1.8. Schematic microevolution of cancer cells

To understand this better, consider these following processes

1. Genetically mutated cells arose.
2. When a mutation makes cancer cells growth faster, it can make more offspring than normal cells can.
3. The offspring can survive in the competition for resources.
4. A second mutation provide the cancer cell with another reproductive advantage.
5. This process continues with every new mutation that offers such benefits.

We have examined the characteristics of cancer cells so far. Then, how can we handle this mess?

Diagnosis and treatment of cancer: attacking cancer with counterplot

Millions of people are living with cancer, although it is not recognized.[24] Most types of cancer can be reduced by changes in a person's lifestyle. However, if the cancer developed, how can we treat this mess? To solve this problem, we must start from characteristics of the cancer.

Table 3.1.1. Cancer cell & Normal cell Characteristics

	Cancer cell	Normal cell
Nucleus	large	proportionated size
Growth	uncontrolled	controlled
Lifespan	Immortal	apoptosis
Cell signal	ignore	communicate
Immune cell	do not recognize	recognize
Oxygen	require or don't' like	require
Energy source	glucose (main)	diverse
Energy efficiency	low (~ 5%)	very high (~ 95%)
Environment	acidic	slightly alkaline (pH ~7.4)

Above all, cancer cells devote all their energies to increase the number of cancer

cells. As a result, cancer cells are immatured and look as follows (only genetic information related to growth is needed).

1. Lagging chromosomes and Coarse chromatin
2. Variable cell shapes and sizes
3. Multinucleated, multiple and large nucleoli
4. Multipolar, arrested mitosis
5. Small cytoplasmic volume relative to nuclei
6. Loss of normal specialized cell features (immatured cell)
7. Immatured membrane ; poorly defined tumor boundary
8. Overexpression of growth related gene, enzyme and micro-organelle (**Figure 3.1.9**)

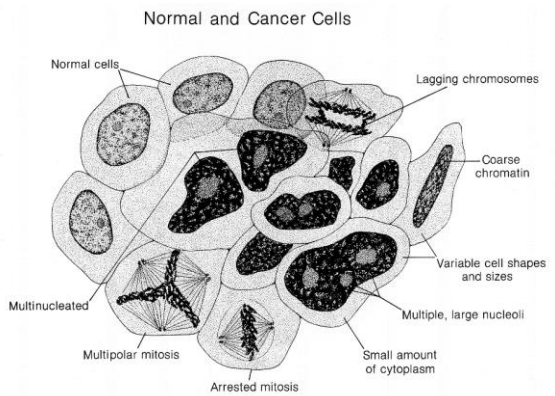

Figure 3.1.9. Schematic appearance of tumor cells. This image was released by the National Cancer Institute, an agency part of the National Institutes of Health.

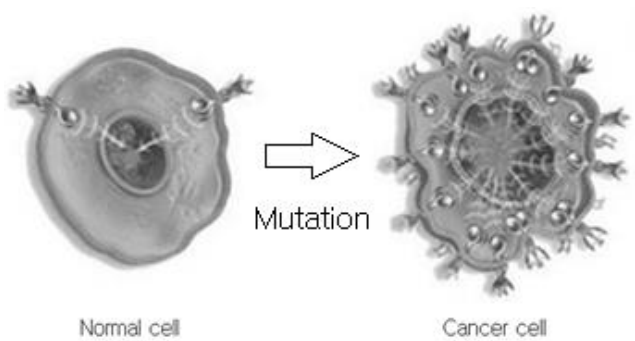

Figure 3.1.10. Mutations lead to epidermal growth factor receptor (EGFR) overexpression and its constant activation, which produces uncontrolled cell division.

Fortunately, reprocessing of metabolic schemes of mutated cell contributes to the development of cancers which can be a counterplot to treat cancer. The immature cell membrane of can the cancer cell allows the transmission of anti-cancer drugs readily (from small molecule to macro molecule). Recent studies provided genetic evidence that mitochondrial metabolism is essential for tumorigenesis, in other words, targeting drug to mitochondria of tumor cells can inhibit tumor growth.[25-27]

Herein, we have designed and synthesized styryl BODIPY derivatives that can be used as fluorescent sensor. Their synthesis, photophysical properties, and application for fluorescent probe were described in section 3.2 and 3.3.

3.1.3References

1. Treibs, A.; Kreuzer, F.-H., Difluorboryl-Komplexe von Di- und Tripyrrylmethenen. *Justus Liebigs Annalen der Chemie* **1968,** *718* (1), 208-223.

2. Yuriy, S. M.; Alexey, V. S.; Alexander, S. T.; Evgeniy, V. R., Recent Advances of Individual BODIPY and BODIPY-Based Functional Materials in Medical Diagnostics and Treatment. *Current Medicinal Chemistry* **2017,** *24* (25), 2745-2772.

3. Rezende, L. C. D.; Emery, F. S., *A review of the synthetic strategies for the development of BODIPY dyes for conjugation with proteins*. 2013.

4. Singh, S. P.; Gayathri, T., Evolution of BODIPY Dyes as Potential Sensitizers for Dye-Sensitized Solar Cells. *European Journal of Organic Chemistry* **2014,** *2014* (22), 4689-4707.

5. Loudet, A.; Burgess, K., BODIPY Dyes and Their Derivatives: Syntheses and Spectroscopic Properties. *Chemical Reviews* **2007,** *107* (11), 4891-4932.

6. Kowada, T.; Maeda, H.; Kikuchi, K., BODIPY-based probes for the fluorescence imaging of biomolecules in living cells. *Chemical Society Reviews* **2015,** *44* (14), 4953-4972.

7. Ulrich, G.; Ziessel, R.; Harriman, A., The Chemistry of Fluorescent Bodipy Dyes: Versatility Unsurpassed. *Angewandte Chemie International Edition* **2008,** *47* (7), 1184-1201.

8. Erten-Ela, S.; Yilmaz, M. D.; Icli, B.; Dede, Y.; Icli, S.; Akkaya, E. U., A Panchromatic Boradiazaindacene (BODIPY) Sensitizer for Dye-Sensitized Solar Cells.

Organic Letters **2008,** *10* (15), 3299-3302.

9. Kamkaew, A.; Lim, S. H.; Lee, H. B.; Kiew, L. V.; Chung, L. Y.; Burgess, K., BODIPY dyes in photodynamic therapy. *Chemical Society Reviews* **2013,** *42* (1), 77-88.

10. Zhao, W.; Carreira, E. M., Conformationally Restricted Aza-Bodipy: A Highly Fluorescent, Stable, Near-Infrared-Absorbing Dye. *Angewandte Chemie International Edition* **2005,** *44* (11), 1677-1679.

11. Boens, N.; Leen, V.; Dehaen, W., Fluorescent indicators based on BODIPY. *Chemical Society Reviews* **2012,** *41* (3), 1130-1172.

12. Sunahara, H.; Urano, Y.; Kojima, H.; Nagano, T., Design and Synthesis of a Library of BODIPY-Based Environmental Polarity Sensors Utilizing Photoinduced Electron-Transfer-Controlled Fluorescence ON/OFF Switching. *Journal of the American Chemical Society* **2007,** *129* (17), 5597-5604.

13. Hecht, M.; Fischer, T.; Dietrich, P.; Kraus, W.; Descalzo, A. B.; Unger, W. E. S.; Rurack, K., Fluorinated Boron-Dipyrromethene (BODIPY) Dyes: Bright and Versatile Probes for Surface Analysis. *ChemistryOpen* **2013,** *2* (1), 25-38.

14. Wang, H.; Fronczek, F. R.; Vicente, M. G. H.; Smith, K. M., Functionalization of 3,5,8-Trichlorinated BODIPY Dyes. *The Journal of Organic Chemistry* **2014,** *79* (21), 10342-10352.

15. Lakshmi V, Sharma R, Ravikanth M., Functionalized boron-dipyrromethenes and their applications.Dovepress 2015, 1-24.

16. Goze, C.; Ulrich, G.; Mallon, L. J.; Allen, B. D.; Harriman, A.; Ziessel, R., Synthesis and Photophysical Properties of Borondipyrromethene Dyes Bearing Aryl Substituents at the Boron Center. *Journal of the American Chemical Society* **2006,** *128* (31), 10231-10239.

17. Niu, S.-L.; Ulrich, G.; Retailleau, P.; Harrowfield, J.; Ziessel, R., New insights into the solubilization of Bodipy dyes. *Tetrahedron Letters* **2009,** *50* (27), 3840-3844.

18. Gabe, Y.; Ueno, T.; Urano, Y.; Kojima, H.; Nagano, T., Tunable design strategy for fluorescence probes based on 4-substituted BODIPY chromophore: improvement of highly sensitive fluorescence probe for nitric oxide. *Analytical and Bioanalytical Chemistry* **2006,** *386* (3), 621-626.

19. Gorman, A.; Killoran, J.; O'Shea, C.; Kenna, T.; Gallagher, W. M.; O'Shea, D. F., In Vitro Demonstration of the Heavy-Atom Effect for Photodynamic Therapy. *Journal of the*

American Chemical Society **2004,** *126* (34), 10619-10631.

20. Yu, C.; Xu, Y.; Jiao, L.; Zhou, J.; Wang, Z.; Hao, E., Isoindole-BODIPY Dyes as Red to Near-Infrared Fluorophores. *Chemistry – A European Journal* **2012,** *18* (21), 6437-6442.

21. Hardin, G., The Tragedy of the Commons. *Science* **1968,** *162* (3859), 1243-1248.

22. Loeb, K. R.; Loeb, L. A., Significance of multiple mutations in cancer. *Carcinogenesis* **2000,** *21* (3), 379-385.

23. Ledford, H., End of cancer-genome project prompts rethink. *Nature* **2015,** *517* (7533), 128-9.

24. https://www.cancer.gov/about-ancer/understanding/statistics Date : Nov. 30. 2017.

25. Weinberg, F.; Hamanaka, R.; Wheaton, W. W.; Weinberg, S.; Joseph, J.; Lopez, M.; Kalyanaraman, B.; Mutlu, G. M.; Budinger, G. R. S.; Chandel, N. S., Mitochondrial metabolism and ROS generation are essential for Kras-mediated tumorigenicity. *Proceedings of the National Academy of Sciences* **2010,** *107* (19), 8788-8793.

26. Guo, J. Y.; Chen, H. Y.; Mathew, R.; Fan, J.; Strohecker, A. M.; Karsli-Uzunbas, G.; Kamphorst, J. J.; Chen, G.; Lemons, J. M.; Karantza, V.; Coller, H. A.; Dipaola, R. S.; Gelinas, C.; Rabinowitz, J. D.; White, E., Activated Ras requires autophagy to maintain oxidative metabolism and tumorigenesis. *Genes Dev* **2011,** *25* (5), 460-70.

27. Fogal, V.; Richardson, A. D.; Karmali, P. P.; Scheffler, I. E.; Smith, J. W.; Ruoslahti, E., Mitochondrial p32 protein is a critical regulator of tumor metabolism via maintenance of oxidative phosphorylation. *Mol Cell Biol* **2010,** *30* (6), 1303-18.

3.2 Synthesis and photophysical properties of mono styryl BODIPY dyes

3.2.1 Introduction

Over the past 20 years, BODIPY fluorophores have attracted considerable interest in fluorescence imaging study due to their superior photophysical properties (e.g. high extinction coefficient and narrow bandwidth, photostability, high brightness in biological condition). However, BODIPY also has drawbacks including small Stokes shift and low solubility in aqueous solution. To overcome water solubility problems, hydrophilic soluble functional groups have been adopted to BODIPY core (for example, poly ethylene glycol, quaternary ammonium, and sulfate.) (please see related references in Part 3.). Also, wavelength and Stokes shift of BODIPY can be systematically tuned by modifying conjugation length of the molecule. However, increasing π-conjugation length of the BODIPY makes it more hydrophobic and less water soluble. Then, with maintaining the benefits of BODIPY's strong fluorescence, how we can develop biocompatible BODIPY, which has larger Stokes shift, longer fluorescence emission wavelength, and good water solubility without additional hydrophilic functional group?

Recently, Chang group developed BODIPY libraries and successfully utilized for several biological researches.[1-2] These BODIPYs have styryl structure, which showed distinct photophysical properties and dissolved well in aqueous solution without additional hydrophilic moiety. However, only fragmentary photophysical properties of the fluorophores were listed in this report. We thought a functional group of the styryl structure effects on electron distribution of BODIPY core and the photophysical properties of the BODIPY will develop a tendency to depend on that.

Herein, we demonstrate synthesis and photophysical properties of styryl BODIPYs. The products of Knoevenagel condensation reactions extend absorption, fluorescence emission and Stokes shift of BODIPYs. Each BODIPY has mono styryl structure with electron donating/withdrawing group. Each electron push-pull group

is π-linked to styryl benzene ring and influence directly on the electronic structure of BODIPY's core. Among the styryl BODIPYs, py-BDP showed intense fluorescence and good solubility in water. The py-BDP was functionalized more by alkylation which showed more red-shifted fluorescence and utilized for fluorescent probe.

3.2.2 Data & results

Photophysical properties of styryl BODIPYs

Scheme 3.2.1. Synthesis and structure of styryl BODIPY derivatives

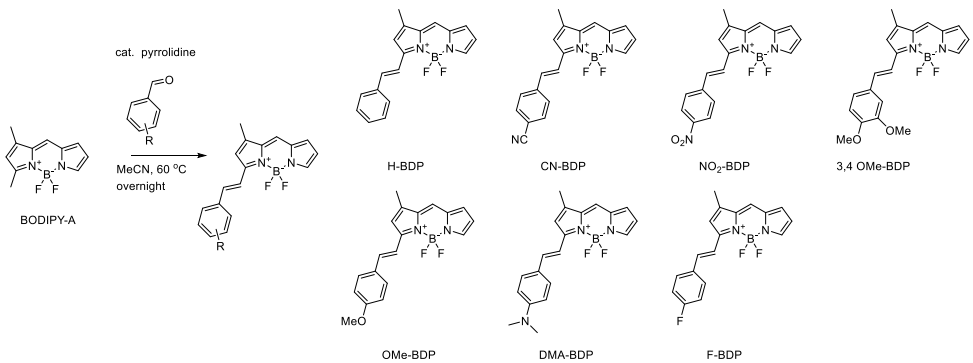

To begin with, we synthesized seven styryl BODIPYs and recorded their photophysical properties, that are listed in **Table 3.2.1** (see absorption and fluorescence spectra in **Figure 3.2.1**). Functionalized styryl BODIPYs showed red-shifted absorption and fluorescence emission wavelength regardless of functional group's character. The effect of e^- withdrawing group on photophysical properties of the styryl BODIPY was not significant (~ 10 nm). However, the effect of e^- donating group on the styryl BODIPY was dramatically increased with the strength of e^- donating ability (**Figure 3.2.1 and 3.2.2**). Interestingly, the fluorescence of the styryl BODIPY, which adopted dimethyl amine group, in acetonitrile was quenched. The fluorescence was not quenched in chloroform, so, it is difficult to pinpoint PeT as the cause for the fluorescence quenching. Meanwhile, styryl BODIPY, which introduced methoxide, fluoresced still in acetonitrile. In other words, by adjusting e^- donating ability to styryl BODIPY, modifying fluorescence of the styryl BODIPY is

possible. Thus, amine group functionalized styryl BODIPY would be utilized for metal cation fluorescent probe. In fact, although there is no detailed description of this assumption, amine group functionalized styryl BODIPYs were utilized for metal cation sensor.[3-4]

Table 3.2.1. Photophysical properties of styryl BODIPYs*

BODIPY	Solvent	$\lambda_{abs\cdot max}$ [nm]	ε [M-1cm-1]	$\lambda_{em\cdot max}$ [nm]
BODIPY-A	$CHCl_3$	499	52170	516
	MeCN	492	37520	508
H-BDP	$CHCl_3$	556	71120	565
	MeCN	546	97220	572
CN-BDP	$CHCl_3$	561	102540	578
	MeCN	552	69800	570
NO_2-BDP	$CHCl_3$	568	73250	590
	MeCN	558	41540	578
3,4 OMe-BDP	$CHCl_3$	570	89240	592
	MeCN	560	64660	591
OMe-BDP	$CHCl_3$	556	87660	586
	MeCN	558	60270	579
DMA-BDP	$CHCl_3$	596	55160	664
	MeCN	608	68480	n.d.
F-BDP	$CHCl_3$	556	90100	564
	MeCN	546	62830	574

* Photophysical properties of these BODIPYs in water were not recorded, since their low solubility and low quantum yield. Only H-BDP fluoresced strongly in water.).

Then, what about developing with the principle of changing e^- withdrawing ability of the functional group? Therefore, we designed pyridine modified styryl BODIPY, which was not reported before and this was utilized further for fluorescent probe

development by N-alkylation of the pyridine.

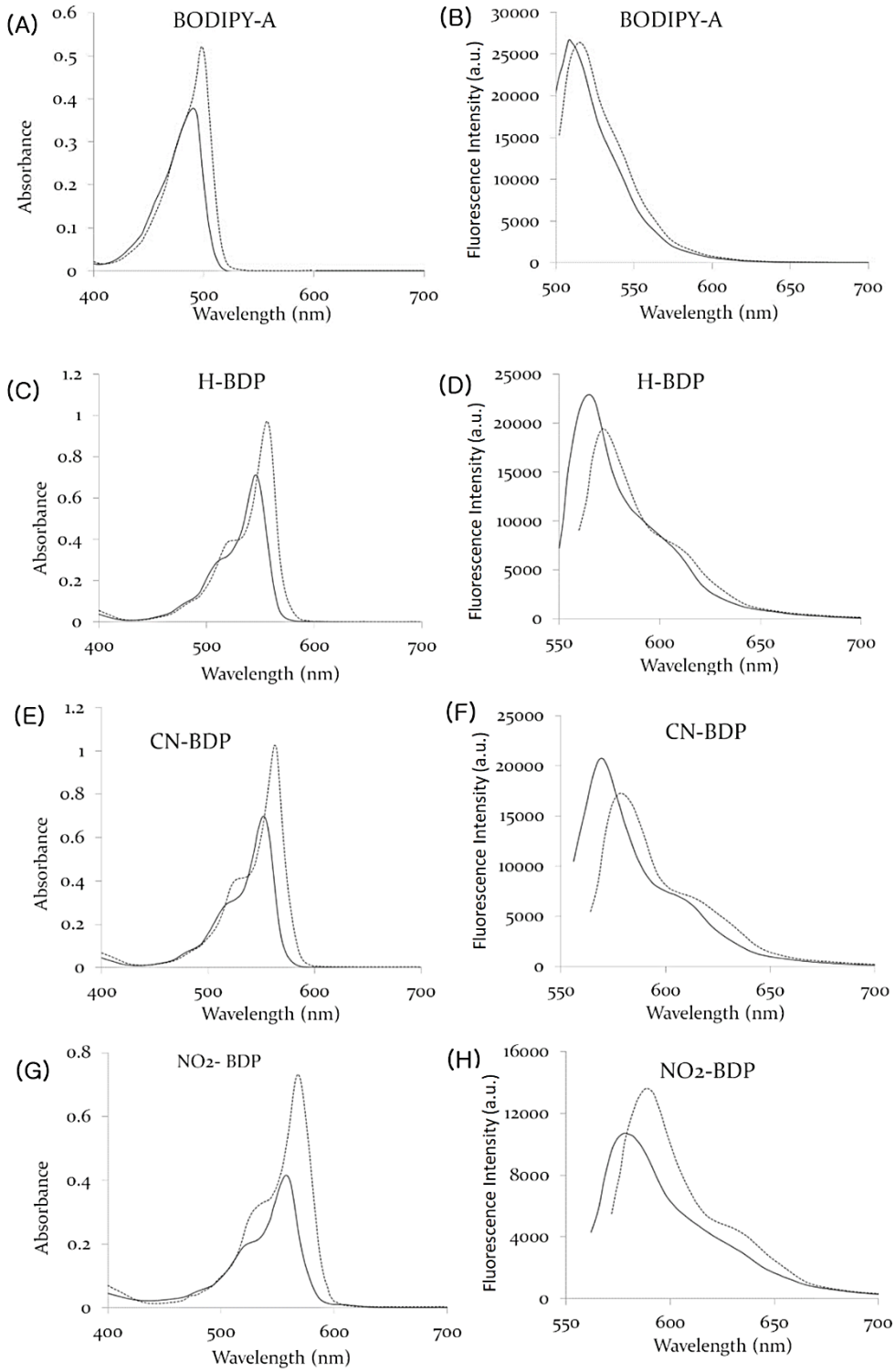

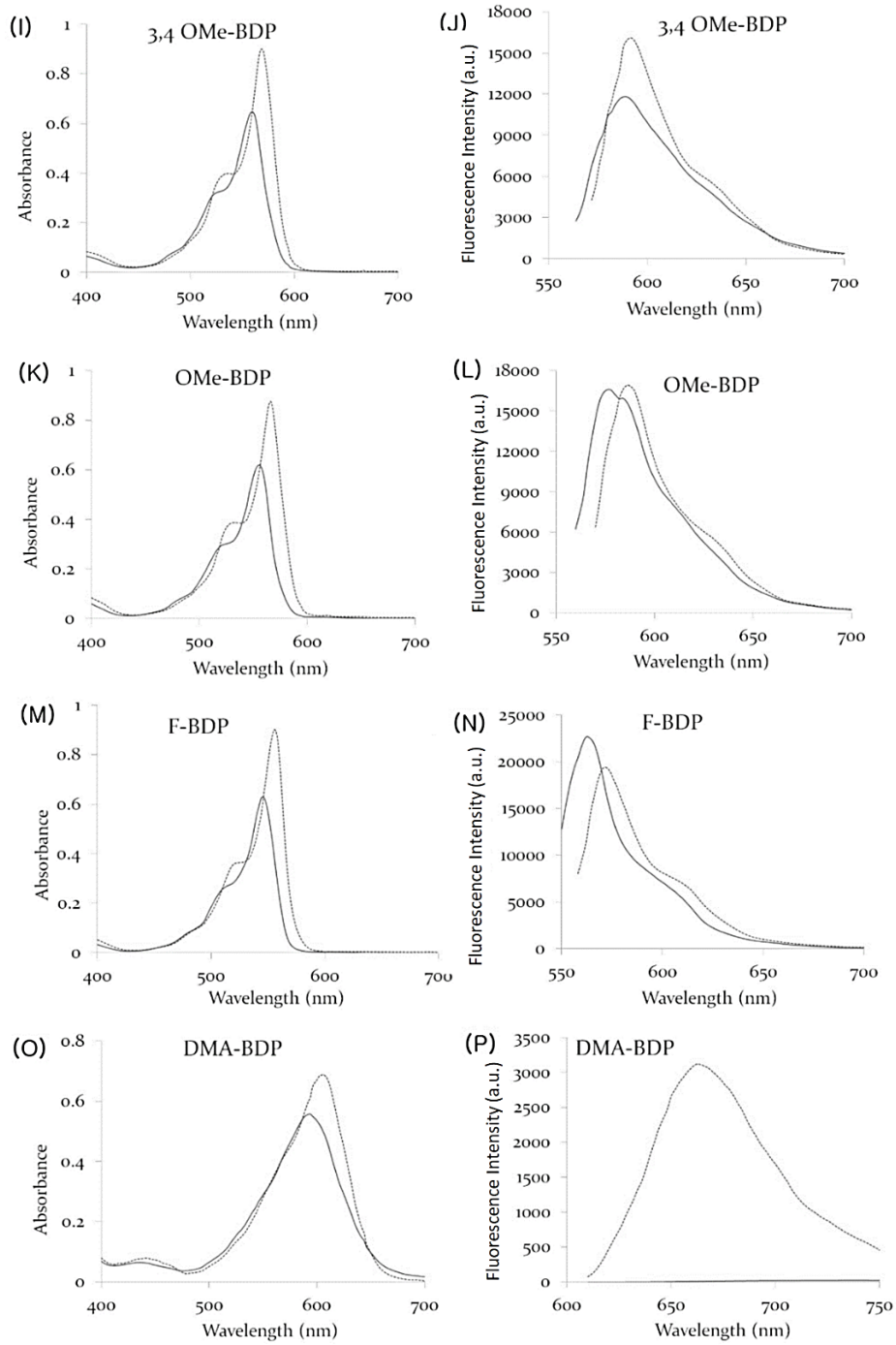

Figure 3.2.1. Absorption and fluorescence spectra of BODIPY-A (A), (B), H-BDP (C), (D), CN-BDP (E), (F), NO_2-BDP (G), (H), 3,4 OMe-BDP (I), (J), OMe-BDP (K), (L), F-BDP (M), (N), DMA-BDP (O), (P) in $CHCl_3$ (dotted line), MeCN (solid line) (contained 0.1% DMSO as co-solvent, 10 μM BODIPYs).

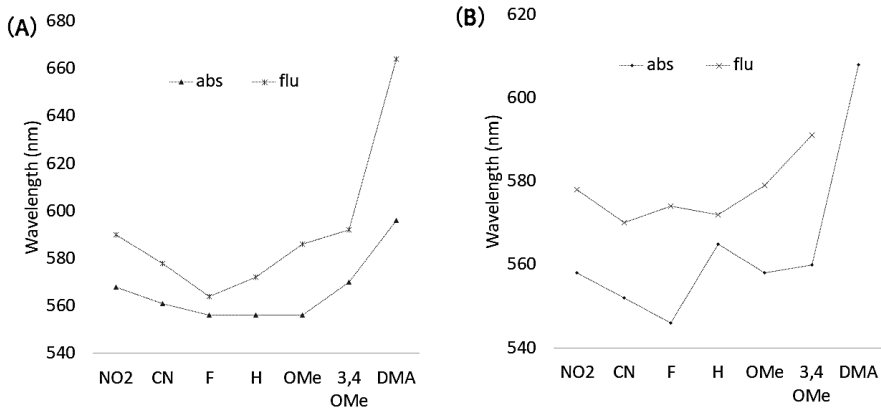

Figure 3.2.2. Plot of absorption and fluorescence wavelength maximum value of BODIPYs in chloroform (A) and acetonitrile (B).

Design fluorescent probes based on pyridine modified styryl BODIPY

Simple condensation with BODIPY-A and pyridine carboxaldehyde leaded to **py-BDP**. The **py-BDP** was alkylated further for analyte sensor development. Photophysical properties of **py-BDP** and its derivatives were listed in **Table 3.2.2** (see spectra in **Figure 3.2.3**).

Scheme 3.2.2. Synthesis of pyridine/picolinium styryl BODIPYs

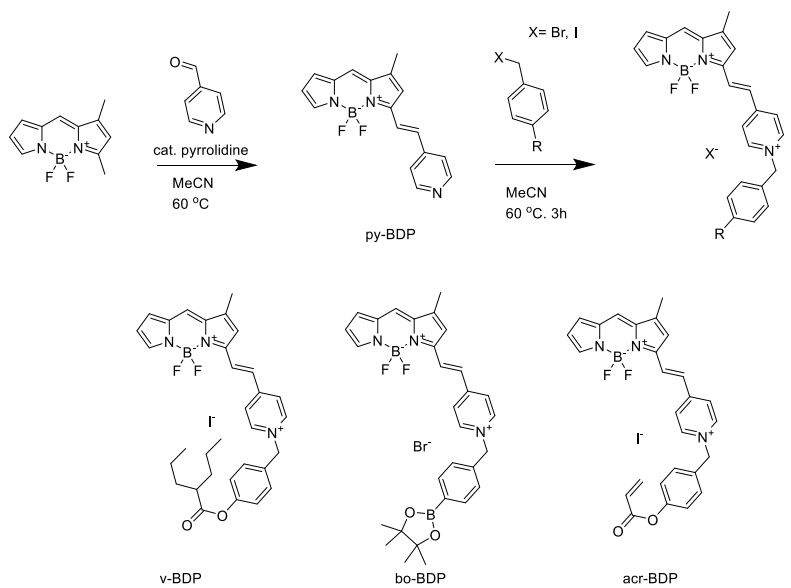

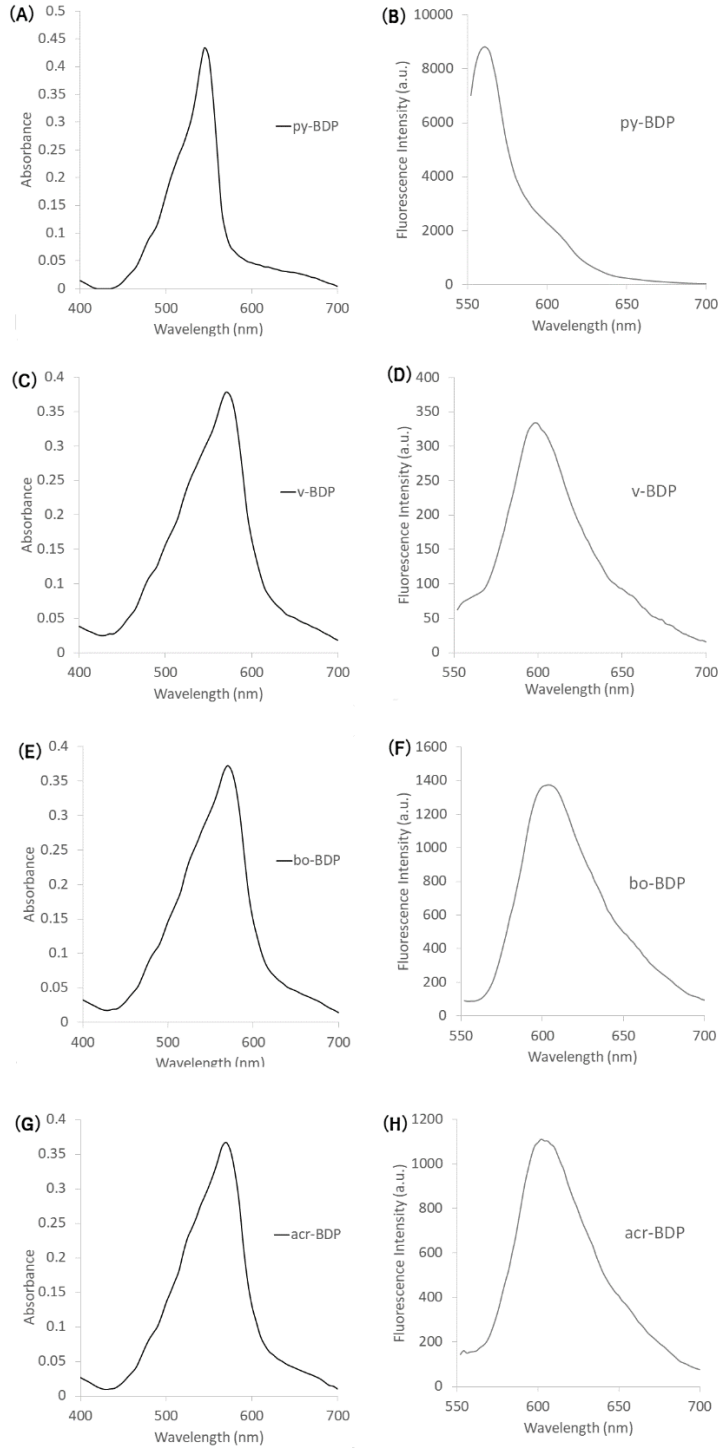

Figure 3.2.3. Absorption and fluorescence spectra of py-BDP (A), (B), v-BDP (C), (D), bo-BDP (E), (F), acr-BDP (pH 7.4, 10 mM phosphate buffer. 0.1 % DMSO, 10 μM BODIPYs).

Table 3.2.2. Photophysical properties of styryl BODIPYs in phosphate buffer (10 mM, pH 7.4. 1% DMSO as cosolvent)

BODIPY	λ_{abs}. max [nm]	ε [M-1cm-1]	λ_{em}. max [nm]
py-BDP	543	43440	564
v-BDP	575	37800	599
bo-BDP	575	37270	600
acr-BDP	576	36740	601

As our expectation, **py-BDP** showed red-shifted absorption and fluorescence wavelength. Moreover, **py-BDP** was well dissolved in buffer solution and showed intense fluorescence still. Also, the derivatives showed more red-shifted fluorescence and absorption wavelength. Probe **v-BDP**, which was designed for use in drug delivery experiments, showed dramatic fluorescence change in presence of esterase (see section 3.3). Experiments are related to this are discussed in the next section. However, **bo-BDP** (designed as a probe for H_2O_2)[5] and **acr-BDP** (designed as a probe for cysteine)[6] did not showed performance as probes, that did not react with the certain target.

Scheme 3.2.3. Picolinium styryl BODIPYs for analyte sensing

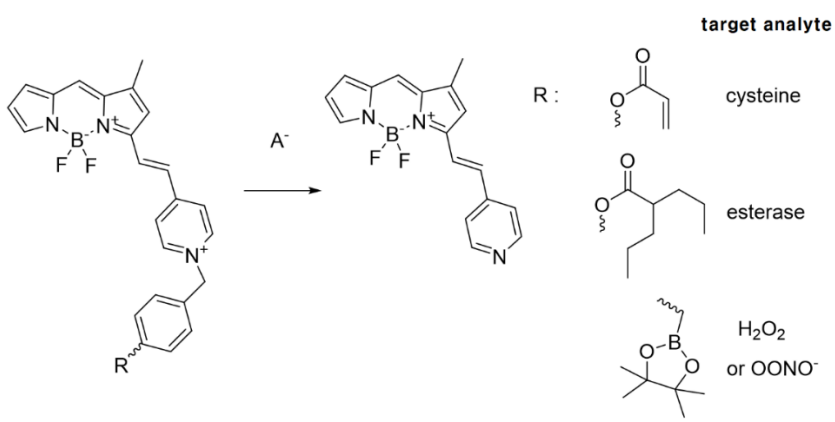

In summary, styryl BODIPYs were synthesized and we recorded photophysical properties of that. Effects of functional group on photophysical properties of styryl

BODIPY were analyzed. Based on the results, we designed and synthesized py-BDP and its derivatives for fluorescent probes. Although introduced known strategies for probe development, not every BODIPY derivatives could produce the desired result. In section 3.3, experiments of v-BDP are covered in detail.

3.2.3 Experimental Section

Materials and Reagent

Materials and solvents were obtained from commercial suppliers (Sigma-Aldrich, TCI, Acros, Samchun Chemical and Alfa Aesar) and were used without further purification. Photophysical properties were recorded by a microplate reader (cuvette, micro plate). The microplate reader was Spectra Max M2 from Molecular Device co. Synthesized compounds were characterized by ^{1}H-NMR, ^{13}C-NMR (Bruker 300 MHz NMR spectroscopy) and MALDI-TOF mass spectrometry.

General Procedure for Synthesis of styryl BODIPYs

To a 50 mL RBF, 110 mg of BODIPY-A (0.5 mmol) and 0.5 mmol of aldehyde derivative were added. Next, 30 mL of acetonitrile was charged to the RBF. A magnetic stirring bar was added to the RBF. With stirring, 2-3 drops of pyrrolidine is added to the RBF and the solution was warmed to ~60 ºC for 2h. Checked by TLC, when BODIPY-A was consumed, volatiles were removed by rotatory evaporator. After then, remained residue was purified by wet silica gel column chromatography. (Hex : EA = 20 : 1 → 5 : 1)

NMR, Mass Characteristics and NMR Spectra of styryl BODIPYs

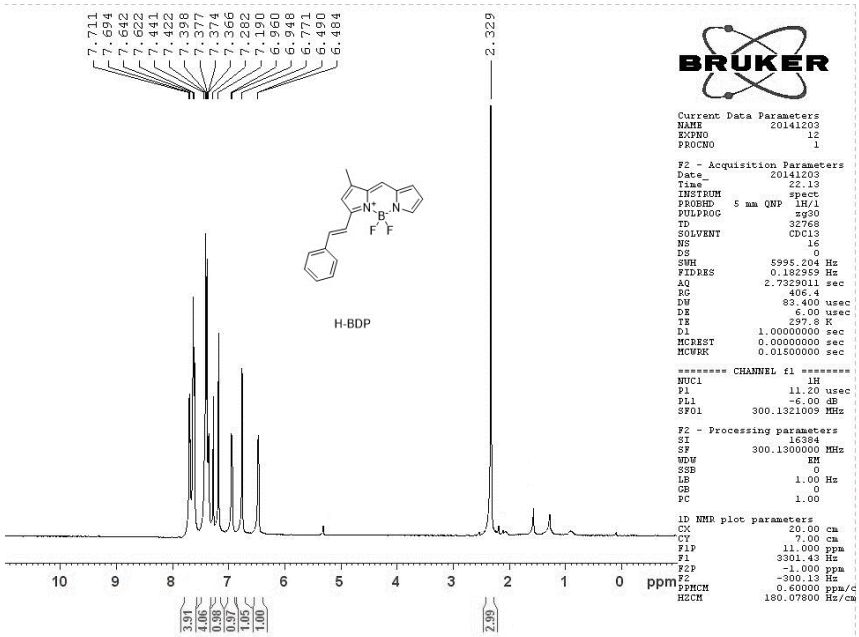

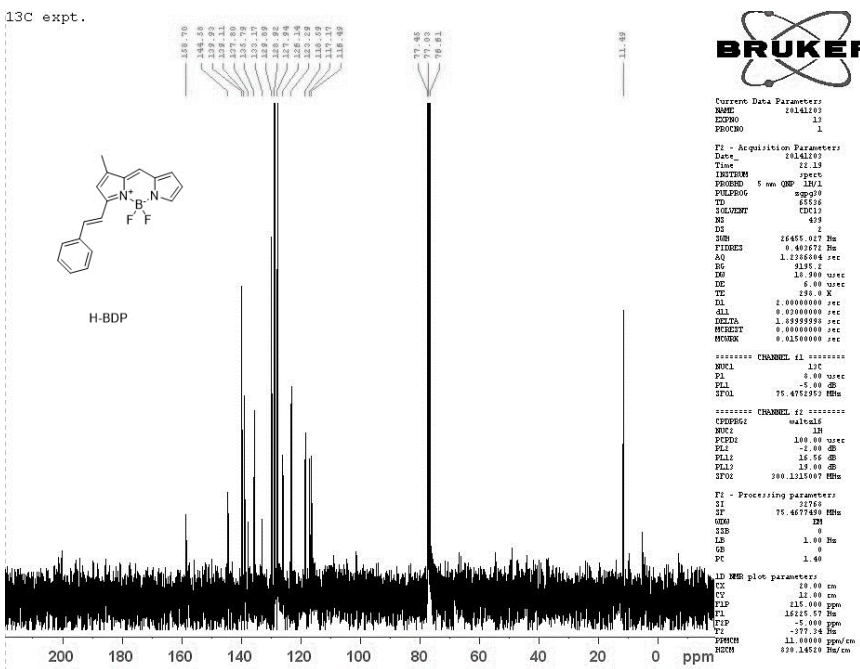

H-BDP ^{1}H NMR ($CDCl_3$, 300 MHz) 7.711-7.622 (m, 4H), 7.441-7.366 (m, 4H), 7.190 (s, 1H), 6.954 (d, J = 3.6 Hz, 1H), 6.771 (s, 1H), 6.487 (d, J = 1.8 Hz, 1H), 2.329 (s, 1H). ^{13}C NMR ($CDCl_3$, 75 MHz) 158.70, 144.58, 138.93, 139.11, 137.80, 135.79, 133.17, 129.89, 128.92, 127.94, 126.14, 123.29, 118.59, 117.17, 116.49, 11.49. MALDI-TOF: m/z. 308.241.

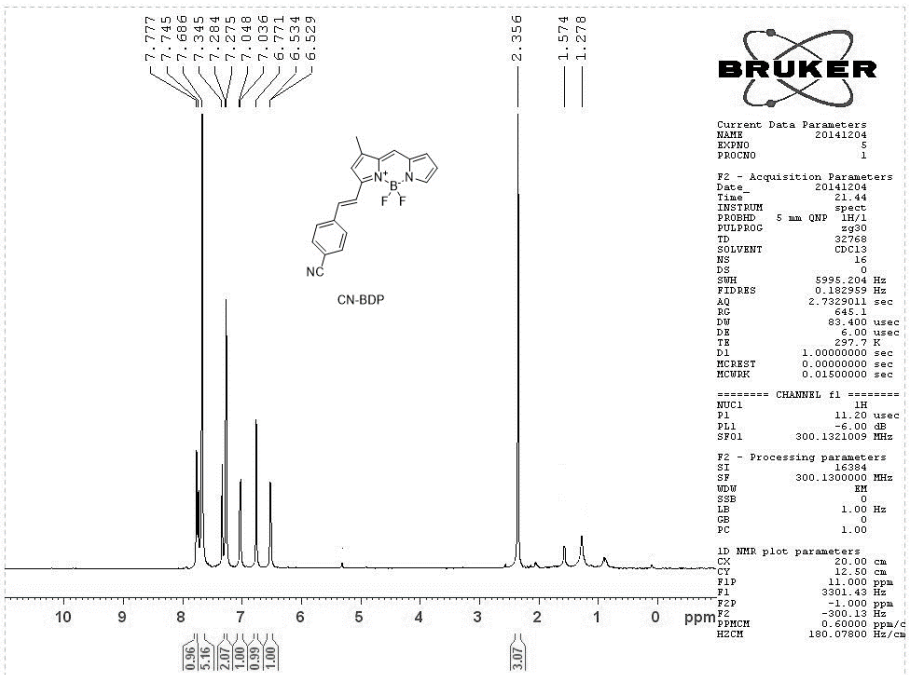

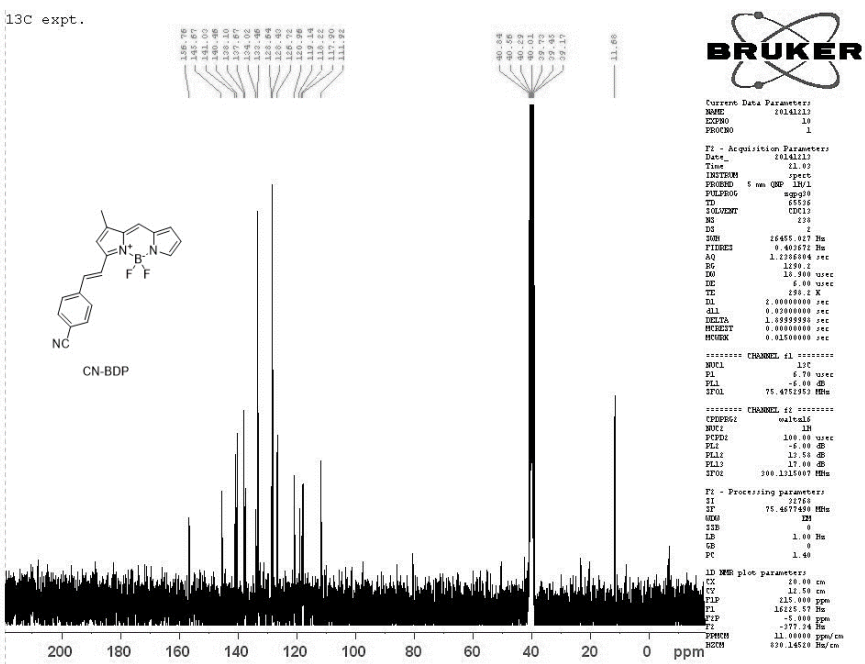

CN-BDP ^{1}H NMR (DMSO-d_6, 300 MHz) 7.777-7.686 (m, 6H), 7.345-7.275 (m,2H), 7.042 ((d, J = 3.6 Hz, 1H), 6.771 (s 1H), 6.532 (d, J = 1.5 Hz, 1H), 2.356 (s, 1H). ^{13}C NMR ($CDCl_3$, 75MHz) 156.75, 145.67, 141.03, 140.46, 138.10, 137.67, 134.02, 133.46, 128.64, 128.43, 125.72, 120.96, 119.14, 118.22, 117.90, 111.92, 11.68. MALDI-TOF: m/z. 333.344.

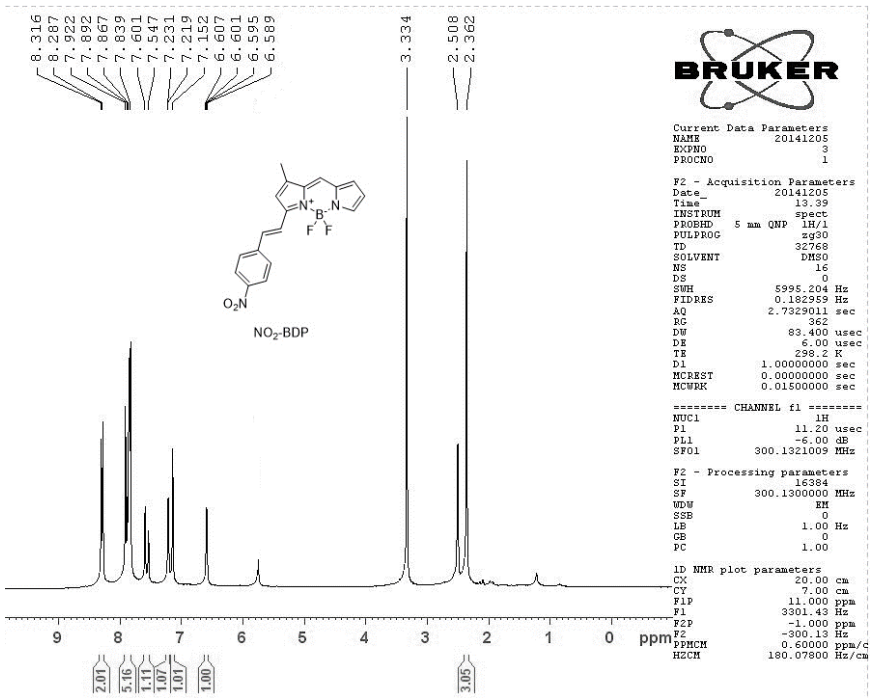

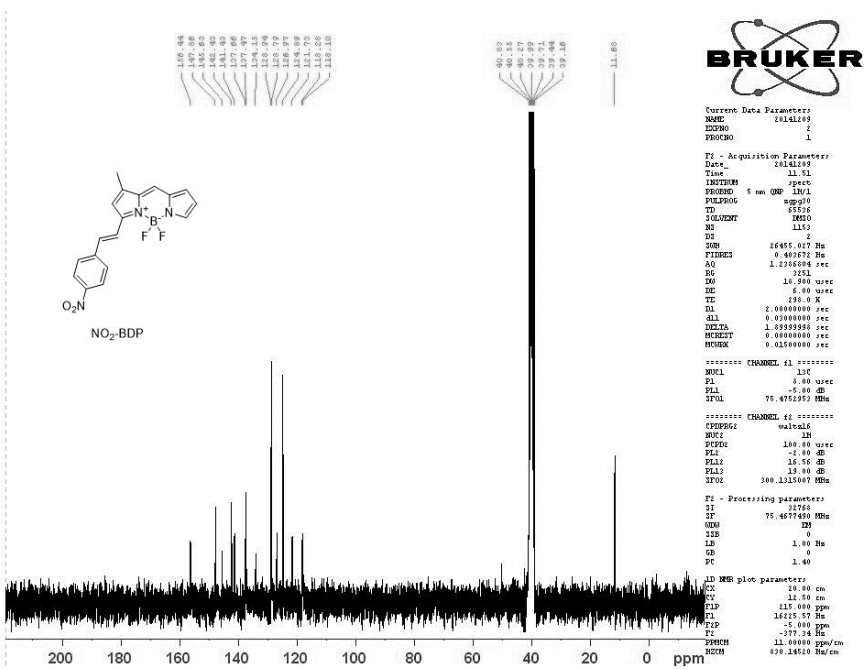

NO_2-BDP ^{1}H NMR (DMSO-d_6, 300 MHz) 8.316-8.287 (m, 2H), 7.922-7.839 (m, 5H), 7.574 (d, J=16.2 Hz, 1H), 7.231-7.152 (m, 2H), 6.607-6.589 (m, 1H), 2.362 (s, 1H). ^{13}C NMR (DMSO-d_6, 75MHz) 156.44, 147.86, 145.63, 142.43, 141.43, 137.66, 137.47, 134.15, 128.94, 128.79, 126.97, 124.89, 121.73, 118.28, 118.10, 11.68. MALDI-TOF: m/z. 353.328.

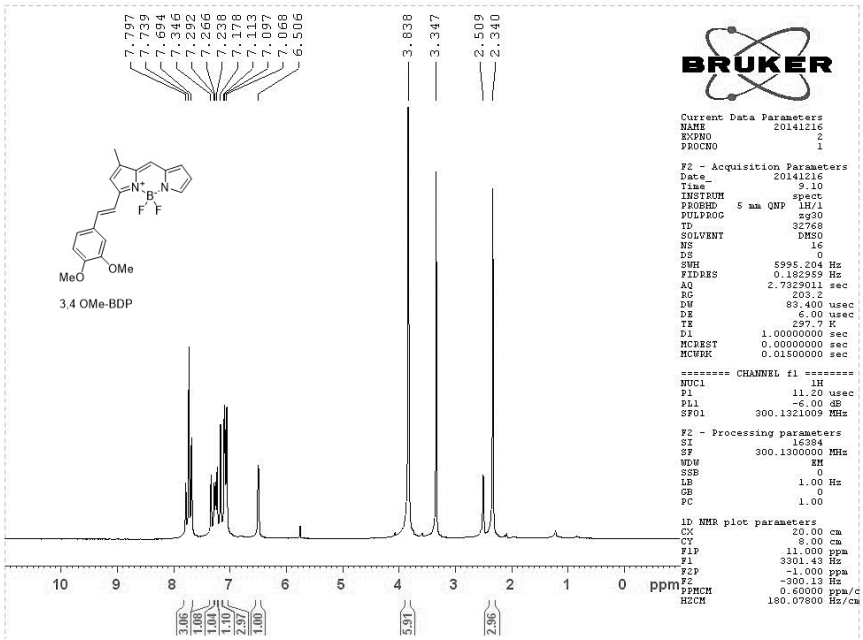

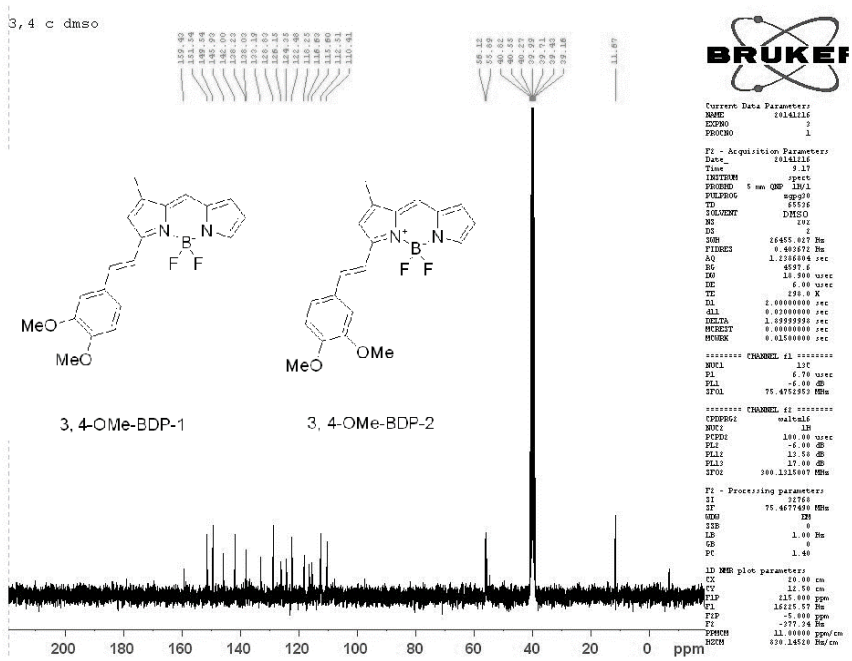

3,4 OMe-BDP ^{1}H NMR (DMSO-d_6, 300 MHz) 7.797-7.694 (m, 3H),), 7.346-7.238 (m,2H), 7.178 (s, 1H), 7.113-7.068 (m, 3H), 6.506 (s, 1H), 3.838 (s, 1H), 2.340 (s, 1H). ^{13}C NMR (DMSO-d_6, 75MHz) 159.45, 151.54, 149.54, 145.93, 142.00, 138.03, 133.19, 128.83, 126.15, 124.35, 122.48, 116.25, 116.63, 115.60, 112.51, 110.41, 11.67. MALDI-TOF: m/z. 368.434.

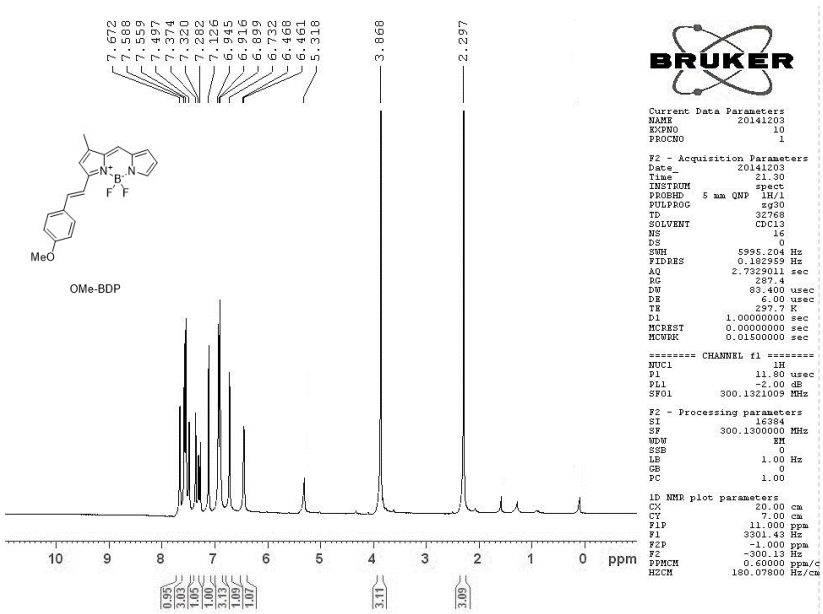

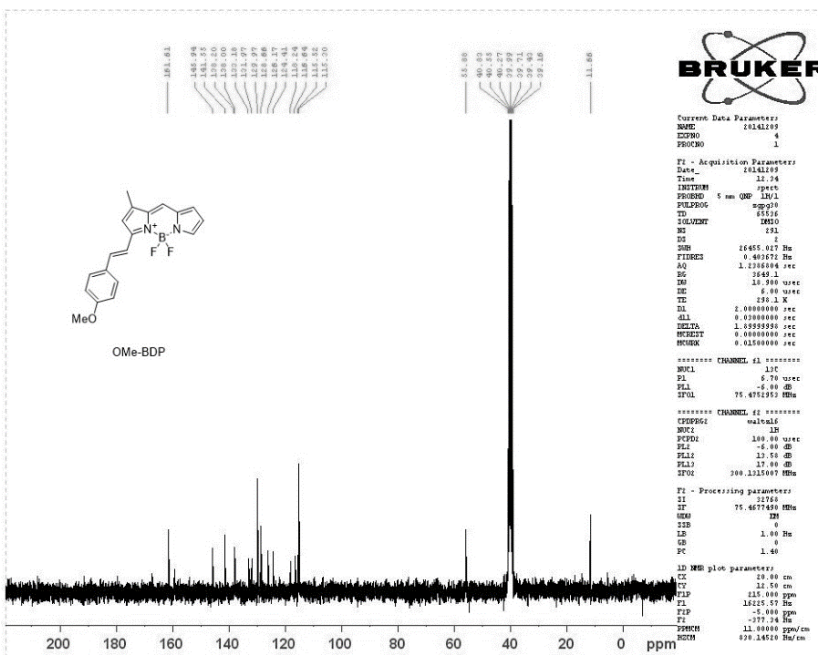

MeO-BDP ^{1}H NMR ($CDCl_3$, 300 MHz) 7.672 (s, 1H), 7.588-7.497 (m, 3H), 7.374 (s, 1H), 7.302-7.282 (d, J=6 Hz, 2H), 7.126 (s, 1H) 6.954-6.899 (m, 3H), 6.732 (s, 1H) 6.465 (d, J=2.1 Hz, 1H), 3.686 (s, 3H), 2.297 (s, 3H) ^{13}C NMR (DMSO-d_6, 75MHz) 161.61, 145.94, 141.55, 138.20, 138.00, 133.18, 131.97, 129.97, 128.66, 126.17, 124.41, 118.24, 116.64, 115.52, 115.30, 55.88, 11.66. MALDI-TOF: m/z. 338.377.

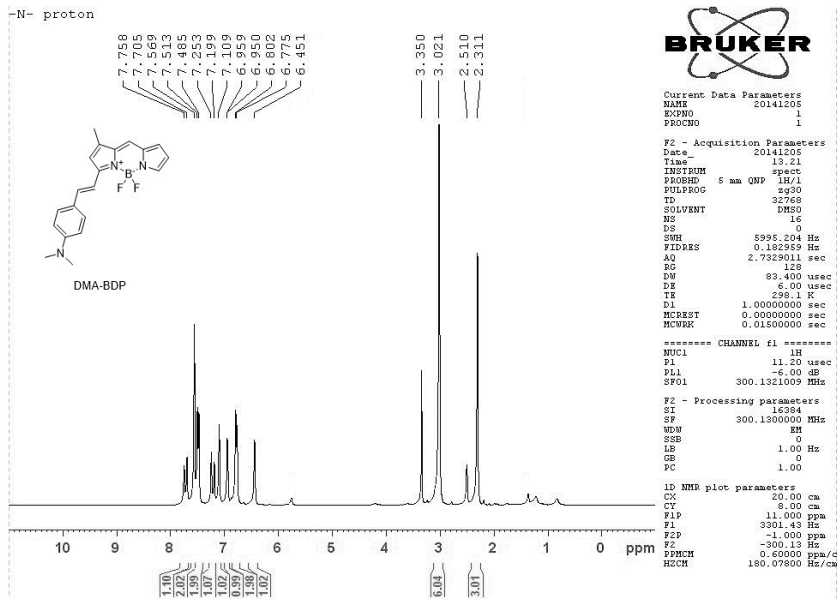

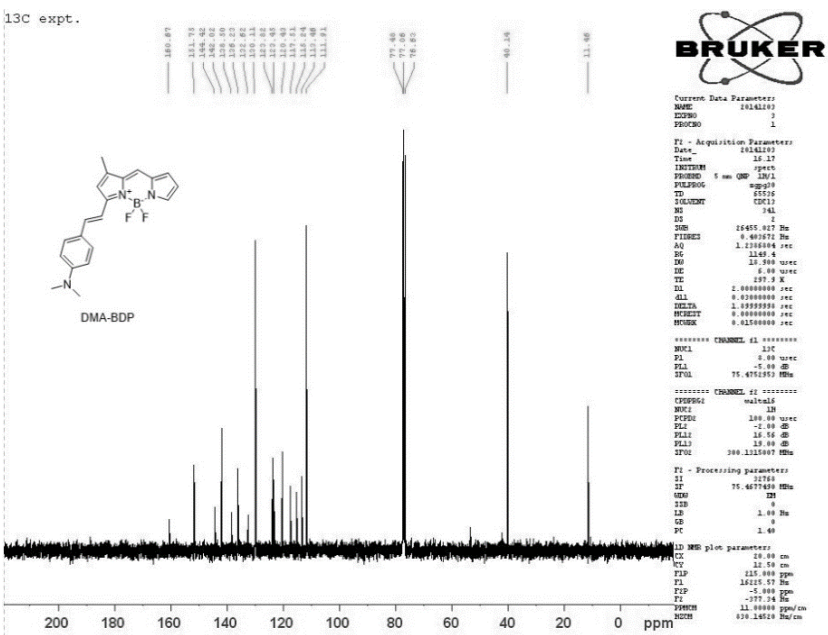

DMA-BDP ^{1}H NMR ((DMSO-d_6, 300 MHz) 7.732 (d, J=15.9, 1H), 7.569-7.485 (m, 3H), 7.266 (d, J=16.2, 1H), 7.109 (s, 2H), 6.955 (d, J=2.7, 1H) 6.788 (d, J=8.1 Hz, 2H), 6.451 (s, 1H) 6.465 (d, J=2.1 Hz, 1H), 3.021 (s, 6H), 2.311 (s, 3H). ^{13}C NMR ($CDCl_3$, 75MHz) 160.67, 151.75, 144.42, 142.02, 138.50, 136.23, 132.62, 130.11, 123.82, 123.45, 120.43, 117.51, 115.24, 113.46, 111.91, 40.14, 11.46. MALDI-TOF: m/z. 351.418.

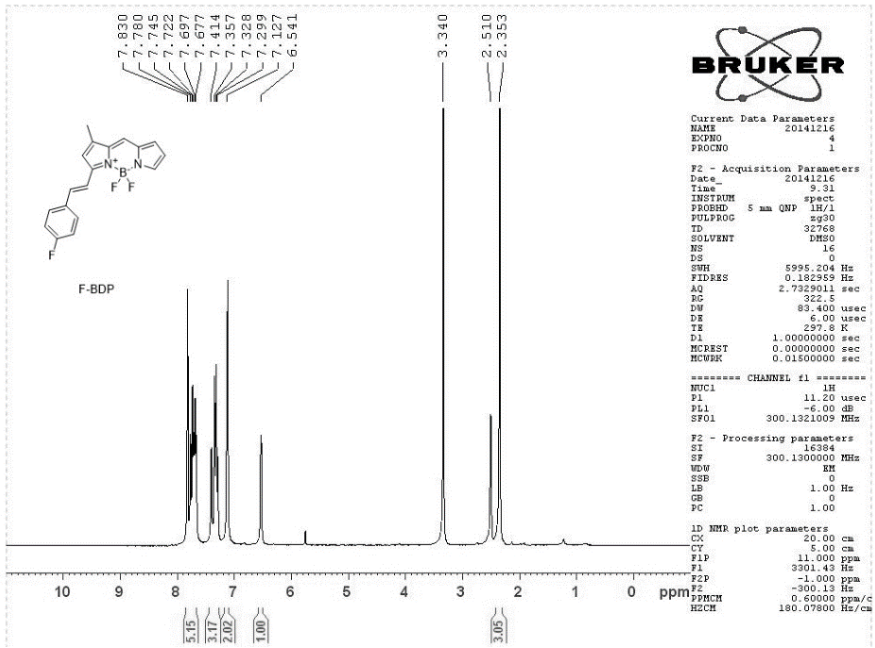

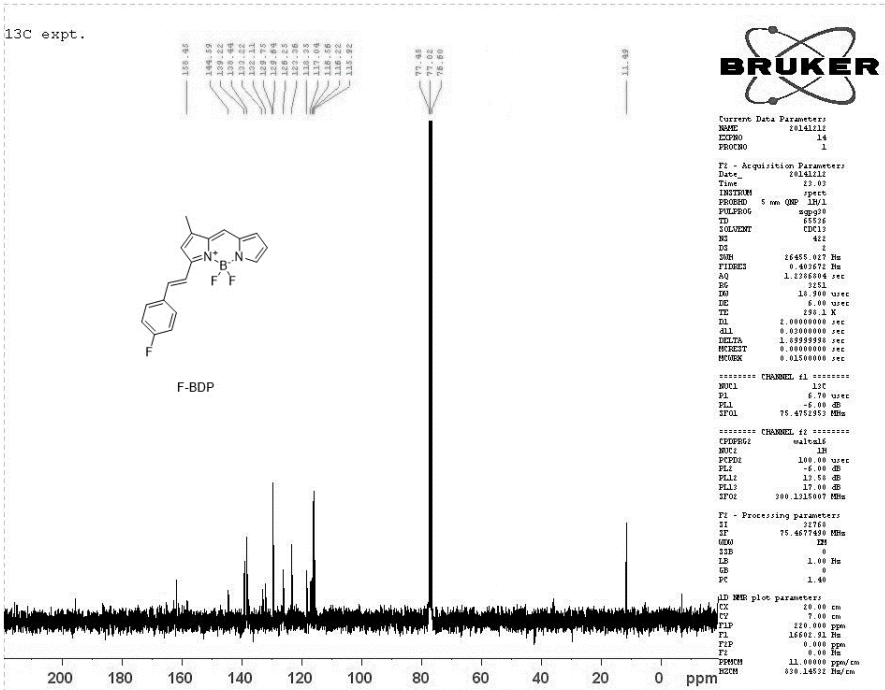

F-BDP ^{1}H NMR (DMSO-d_6, 300 MHz) 7.830-7.677 (m, 5H), 7.414-7.299 (m,3H), 7.127 (s, 1H), 6.541 (s 1H), 2.353 (s, 1H). ^{13}C NMR ($CDCl_3$, 75MHz) 158.45, 144.59, 139.22, 138.44, 133.22, 132.11, 129.75, 129.64, 123.35, 118.35, 117.04, 116.55, 116.22, 115.92, 117.92, 11.68. MALDI-TOF: m/z. 326.291.

General Procedure for Synthesis of picolinium styryl BODIPY

To a 50 mL RBF, 110 mg of py-BDP (0.5 mmol) and 1 mmol of halomethyl phenyl derivative were added. Next, to the RBF, a magnetic stirring bar was added and 30 mL of acetonitrile was charged. The solution was warmed to ~60 ºC for 3h. Checked by TLC, when py-BDP was consumed, volatiles were removed in low pressure by rotatory evaporator. After then, remained residue was purified by wet silica gel column chromatography. (Hex : EA = 1: 1 → MC : MeOH = 30 : 1). Fluffy dark purple powder.

Synthesis of py-BDP

To a 50 mL RBF, 110 mg of BODIPY-A (ref) (0.5 mmol) and 0.5 mmol of pyridine aldehyde were added. Next, 30 mL of acetonitrile was charged to the RBF. A magnetic stirring bar was added to the RBF. With stirring, 2-3 drops of pyrrolidine is added to the RBF and the solution was warmed to ~60 ºC for 4h. Checked by TLC, when BODIPY-A was consumed, volatiles were removed by rotatory evaporator. After then, remained residue was purified by wet silica gel column chromatography. (Hex : EA = 5 : 1 → 3 : 2). Gold green powder.

NMR, Mass Characteristics and NMR Spectra of picolinium styryl BODIPYs

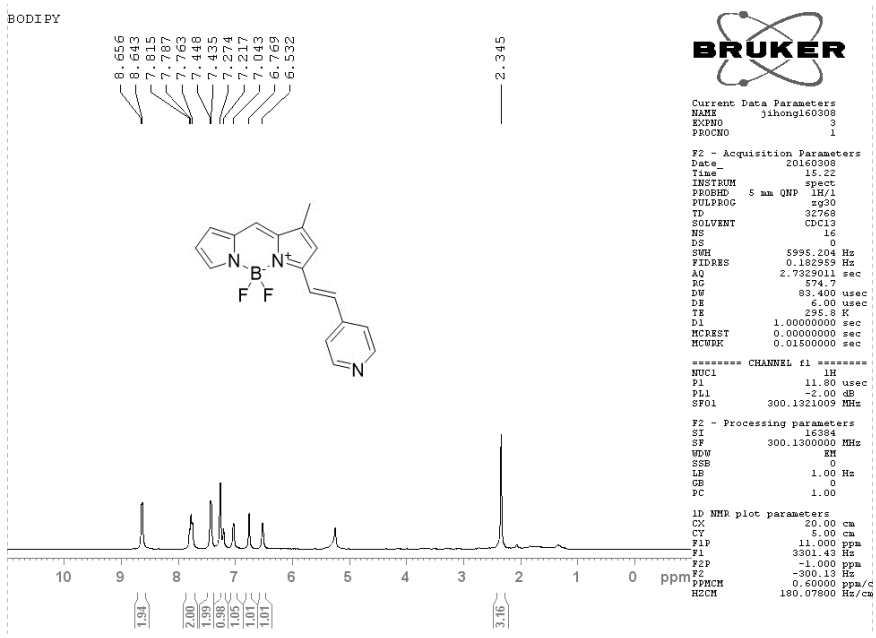

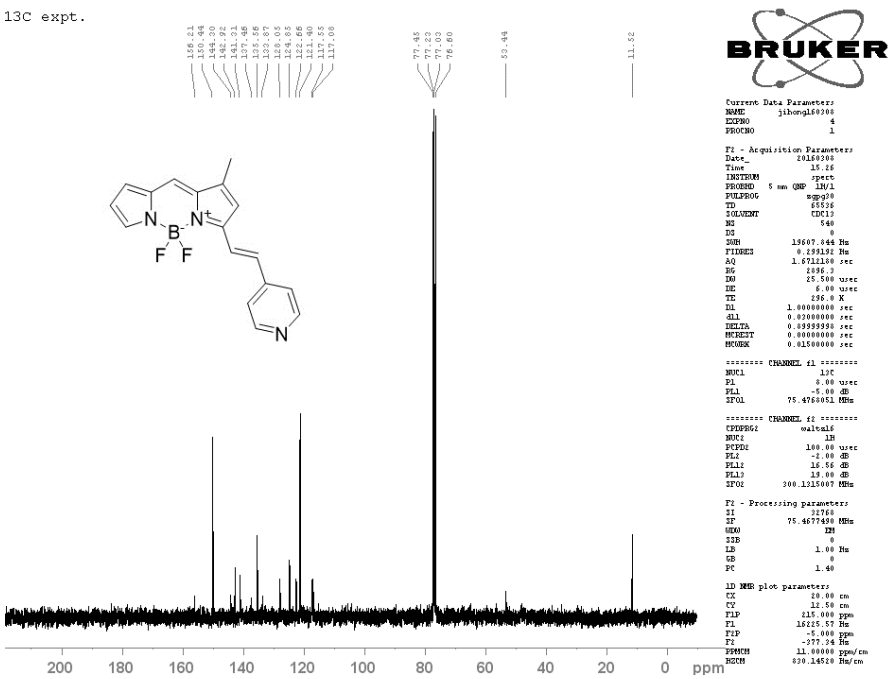

py-BDP ^{1}H NMR ((CDCl$_3$, 300 MHz) 8.649 (d, J=3.83 2H), 7.815-7.763 (m, 2H), 7.441 (d, J=3.84 Hz, 2H), 7.441 (d, J=16.84 Hz, 1H), 7.274-7.217 (m, 2H), 7.043 (s, 1H), 6.769 (s, 1H), 6.5312(s, 1H), 2.345 (s, 3H). ^{13}C NMR (CDCl$_3$, 75MHz) 156.21, 150.44, 144.30, 142.92, 141.31, 137.46, 135.56, 133.87, 128.05, 124.85, 122.66, 121.40, 117.55, 117.08, 11.52. MALDI-TOF m/z : 310.294.

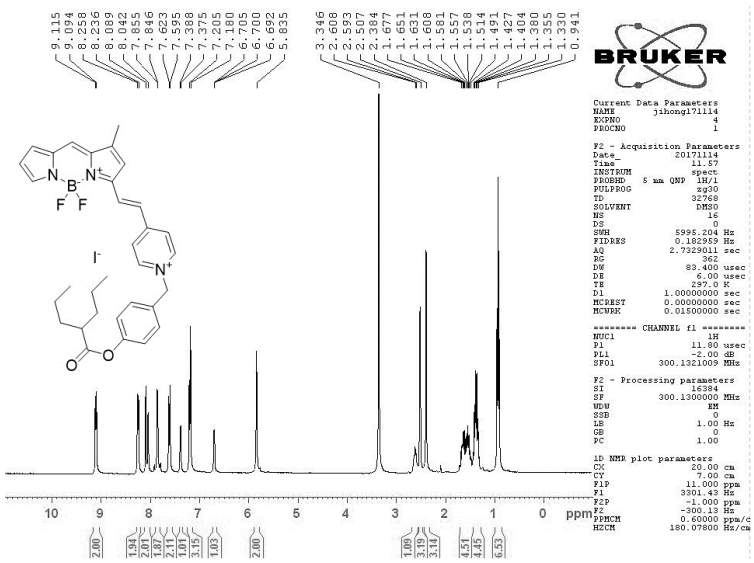

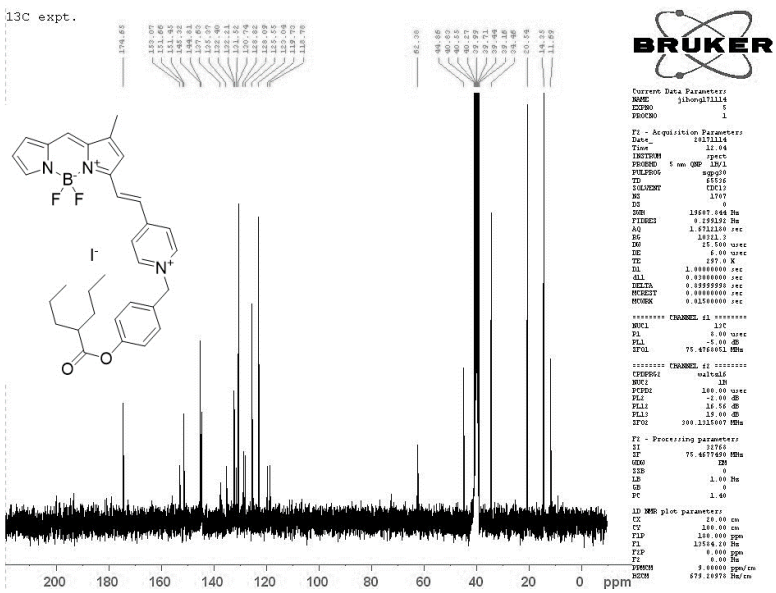

v-BDP ^{1}H NMR (DMSO-d$_6$, 300 MHz), 9.105 (d, J=6.3, 2H), 8.247 (d, J=6.6, 2H), 8.089-8.042 (m, 2H), 7.581 (d, J=2.7 Hz, 2H), 7.609 (d, J=2.7, 2H), 7.382 (d, J=3.9, 1H), 7.205-7.180 (m, 2H), 6.705-6.692 (m, 1H), 5.835, (S, 2H), 2.608 (m, 1H), 2.593 (water), 2.384 (s, 3H) 1.677-1.514 (m, 4H), 1.491-1.330 (m, 4H), 0.941 (m, J= 7.536, 6H) ^{13}C NMR (DMSO-d$_6$, 300 MHz) 174.65, 153.07, 151.66, 151.45, 145.32, 144.81, 137.64, 135.37, 132.40, 132.21, 131.52, 120.74, 128.82, 128.09, 125.55, 123.04, 119.73, 118.78, 62.38, 44.86, 34.46, 20.54, 14.35, 11.69. MALDI-TOF m/z : 542.760.

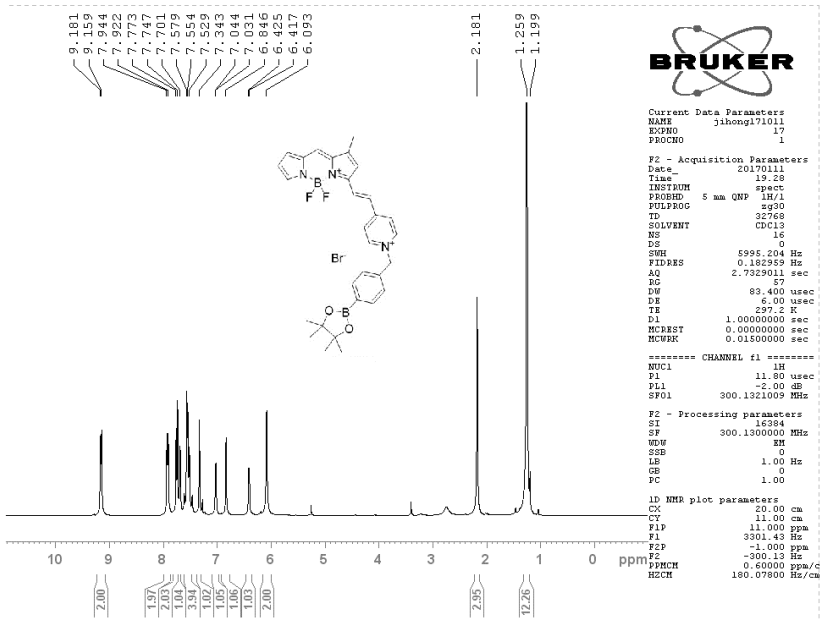

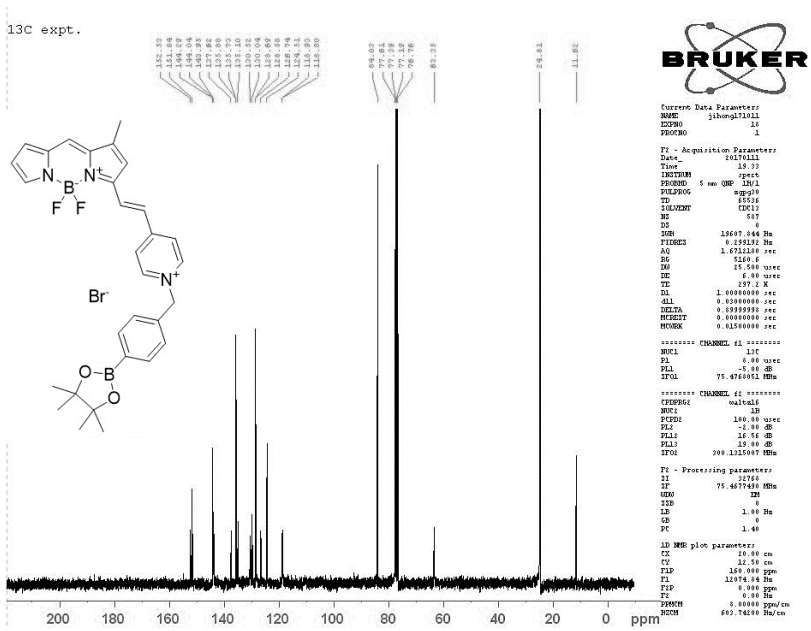

bo-BDP ^{1}H NMR ((CDCl$_3$, 300 MHz), 9.170 (d, J=6.426, 2H), 7.933 (d, J=6.435, 2H), 7.773-7.701 (m, 3H), 7.580-7.529 (m, 3H), 7.343 (s, 1H), 7.375 (d, J=3.80 Hz, 1H), 6.846 (s, 1H), 6.401 (d, J=2.35 Hz, 1H), 6.093 (s, 2H), 2.181 (s, 3H), 2.259 (s, 12H), ^{13}C NMR (CDCl$_3$, 75MHz) 152.53, 151.84, 144.29, 144.04, 143.95, 137.62, 135.73, 135.10, 130.52, 130.04, 128.69, 128.58, 126.74, 124.51, 118.93, 118.80, 84.03, 63.35, 24.81, 11.62. MALDI-TOF m/z : 526.571.

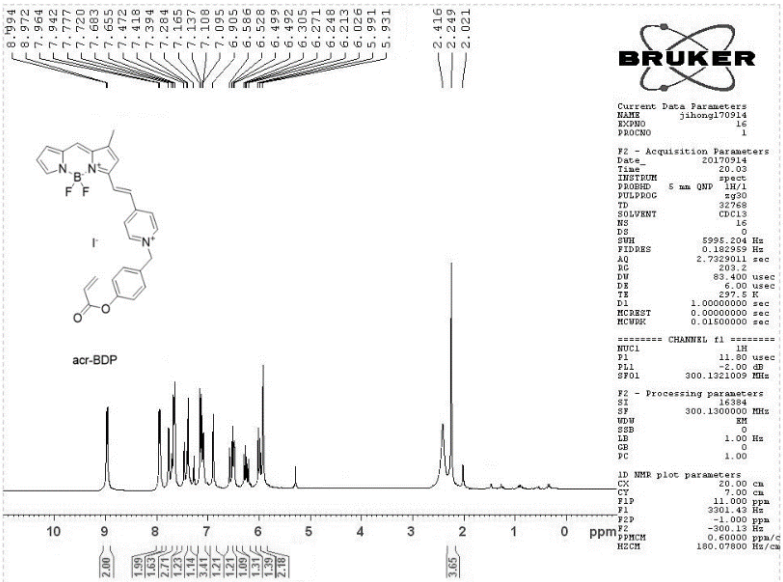

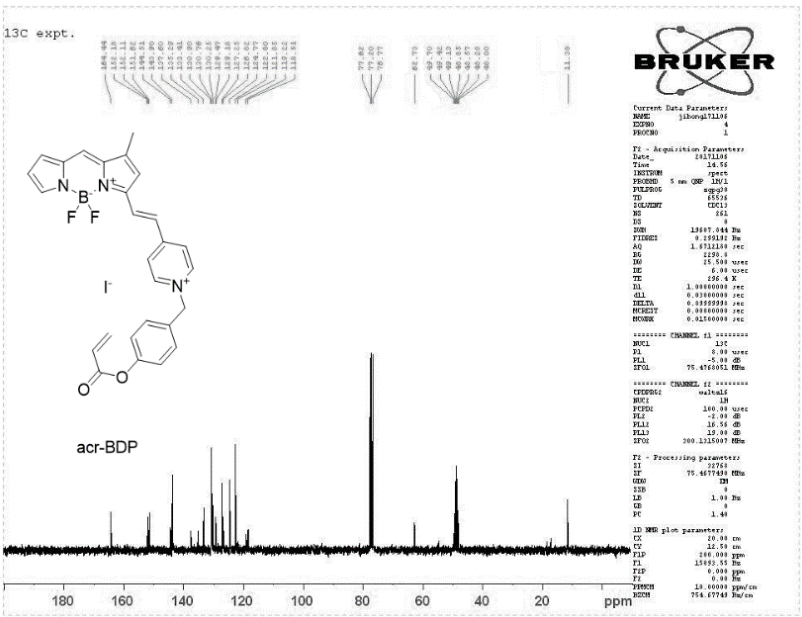

acr-BDP ^{1}H NMR ($CDCl_3$, 10% MeOD, 300 MHz) 8.983 (d, J= 6.6 Hz, 2H), 7.953 (d, J= 6.6 Hz, 2H), 7.777-7.655 (m, 4H), 7.427-7.394 (m, 2H), 7.165-7.095 (m, 3H), 6.905 (s, 1H) 6.586-6.492 (m, 2H), 6.271-6.213 (m, 2H), 5.991-5.931 (m, 3H), 2.249 (s, 3H). ^{13}C NMR ($CDCl_3$, 10% MeOD, 75MHz) 164.44, 152.18, 152.11, 151.62, 144.51, 143.90, 137.60, 135.29, 133.41, 130.90, 130.76, 130.25, 129.47, 129.18, 127.25, 126.82, 124.77, 122.80, 121.85, 119.22, 118.51, 62.73, 11.38. MALDI-TOF m/z : 470.18.

3.2.4 References

1. Lee, J.-S.; Kang, N.-y.; Kim, Y. K.; Samanta, A.; Feng, S.; Kim, H. K.; Vendrell, M.; Park, J. H.; Chang, Y.-T., Synthesis of a BODIPY Library and Its Application to the Development of Live Cell Glucagon Imaging Probe. *Journal of the American Chemical Society* **2009,** *131* (29), 10077-10082.

2. Zhai, D.; Lee, S.-C.; Vendrell, M.; Leong, L. P.; Chang, Y.-T., Synthesis of a Novel BODIPY Library and Its Application in the Discovery of a Fructose Sensor. *ACS Combinatorial Science* **2012,** *14* (2), 81-84.

3. Cheng, T.; Xu, Y.; Zhang, S.; Zhu, W.; Qian, X.; Duan, L., A Highly Sensitive and Selective OFF-ON Fluorescent Sensor for Cadmium in Aqueous Solution and Living Cell. *Journal of the American Chemical Society* **2008,** *130* (48), 16160-16161.

4. Xu, W.; Ren, C.; Teoh, C. L.; Peng, J.; Gadre, S. H.; Rhee, H.-W.; Lee, C.-L. K.; Chang, Y.-T., An Artificial Tongue Fluorescent Sensor Array for Identification and Quantitation of Various Heavy Metal Ions. *Analytical Chemistry* **2014,** *86* (17), 8763-8769.

5. Xu, J.; Zhang, Y.; Yu, H.; Gao, X.; Shao, S., Mitochondria-Targeted Fluorescent Probe for Imaging Hydrogen Peroxide in Living Cells. *Analytical Chemistry* **2016,** *88* (2), 1455-1461.

6. Han, C.; Yang, H.; Chen, M.; Su, Q.; Feng, W.; Li, F., Mitochondria-Targeted Near-Infrared Fluorescent Off–On Probe for Selective Detection of Cysteine in Living Cells and in Vivo. *ACS Applied Materials & Interfaces* **2015,** *7* (50), 27968-27975.

3.3 Mitochondria targeting cellular imaging probe based on picolinium styryl BODIPY for cancer treatment study

3.3.1 Introduction

The terms target and targeting are used very commonly. It may seem strange to question their meaning, but appropriate using the terms ‘targeting’ and ‘target’ is important. In fact, ‘targeting’ was a military term which is the process of selecting objects or installations to be attacked, or destroyed. While conducting the operation, civilians must not be harmed. From this point of view, targeting is the drug molecule's ability to track, interact and react only with the ‘target’ without side reaction.

Many recent reports divulge that mitochondrial bioenergetics and biosynthesis are required for tumorigenesis.[1-3] The major function of mitochondria cells is supplying adenosine triphosphate (ATP). In most of human cell, 80–90% of ATP is produced from the mitochondria. Mitochondria makes ATP by passing electrons generated from the oxidation of carbohydrate down the respiratory chain to react with oxygen, using the redox energy to translocate protons across the mitochondrial inner membrane.[4] This process results a proton electrochemical potential gradient across the inner membrane comprising a transmembrane electric potential of up to 200mV and an internal pH ~8. Consequently, the mitochondrial membrane potential is much higher than that of other cellular organelles and lipophilic cations can readily be accumulated in mitochondria through electrostatic interactions in the mitochondrial matrix by response to the negative membrane potential. This cation preference feature of mitochondria enables a prodrug, which have the lipophilic cation, to track the mitochondria selectively and treat the cancer cell.[5-7] Also, the mitochondrial targeting strategy based on the mitochondrial targeting signal peptides is available[8], but we will focus on the strategy which is based on lipophilic cation. Most common strategies to deliver molecular fluorophore to the mitochondria is the use of electronically delocalized cations including triphenylphosphonium (TPP) and

picolinium moiety, because of cation preference feature of mitochondria.[9-11] Fluorophores with these positive charge groups could go by plasma membranes and afterwards accumulate in mitochondria. Valproic acid is a fatty acid with anticonvulsant properties which is commonly used for the treatment of epilepsy. Histone deacetylase plays key role in the epigenetic regulation and the VPA is known for histone deacetylase inhibitor (HDAi).[12-13] Many recent reports demonstrated that the VPA is an anticancer therapeutic drug for the treatment of tumors. [14-16] Most researchers suggested anticancer mechanisms of VPA may contribute to VPA-induced inhibition of histone deacetylases which prevents tumorigenesis. Thus, real-time monitoring of cell morphology changes during the cell death that could provide information of VPA's the anticancer mechanism.

Herein, we synthesized mitochondria targetable **v-BDP** and the anticancer drug is conjugated via an ester bond to the **v-BDP**. It was designed to guide the drug to the mitochondria and to release VPA by mitochondrial esterase. This was developed to observe phenomena occurring in the cell while drug delivering.

Scheme 3.3.1. Mitochondria targeting esterase triggered drug releasing and fluorescing of v-BDP.

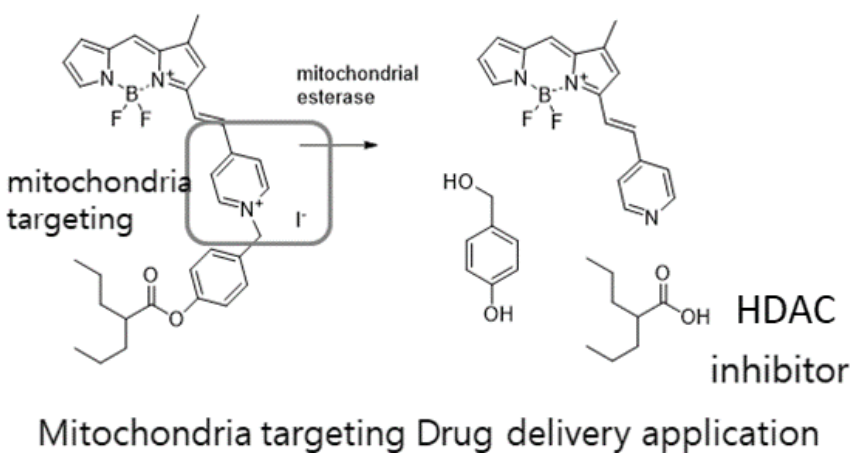

Mitochondria targeting Drug delivery application

3.3.2 Data & Results

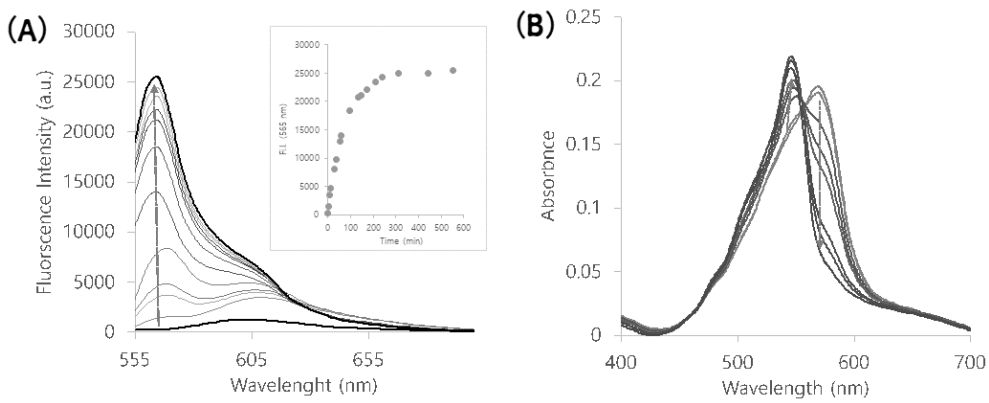

Figure 3.3.1. Time-dependent fluorescence emission (A) and absorption (B) spectra of v-BDP (5 μM) upon treatment with PLE (0.5 U/mL) in phosphate buffer solution (10 mm, pH 7.44) containing 1% DMSO as a cosolvent at 37 °C. Inset graph, x-axis: elapsed time from 0 to 550 min, y-axis: fluorescence intensity at 565 nm. λ_{ex} =540 nm.

The UV/Vis absorption and emission spectra of v-BDP were measured in phosphate buffer solution (**see Figure 3.3.1**). V-BDP displayed absorption maxima at approximately 575 nm and emission maxima at approximately 599 nm. To confirm the feasibility of v-BDP as fluorescent probe for esterase, v-BDP was treated with porcine liver esterase (PLE) in phosphate buffer solution (10 mM, pH 7.44, 1% DMSO) at 37 °C. The absorption and fluorescence spectra changes of v-BDP then monitored in the presence of esterase (**see Figure 3.3.1**). Also, v-BDP did not showed any significant fluorescent changes in acid/basic media (**Figure 3.3.2**).

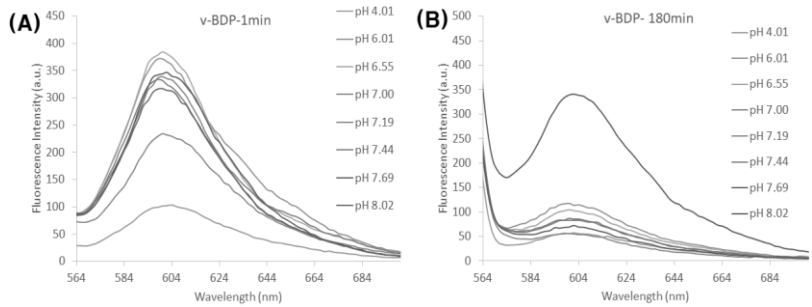

Figure 3.3.2. Fluorescence spectra of v-BDP (10 μM) in buffer solutions at various pH. (A) Fluorescence of v-BDP was incubated for 1 minute in buffer solutions. (B) Fluorescence of v-BDP was incubated for 180 minutes in buffer solutions. λ_{ex} =540 nm.

Kinetics studies

To determine the kinetic constants of probe **v-BDP**, the probe of the final concentrations was hydrolyzed by PLE (0.35 U/mL). The reaction was monitored by measuring fluorescence change at 565 nm for the probe at 37 ˚C. The initial velocity was calculated from the slope of each progress curve. The parameters such as K_m and k_{cat} with PLE for the probe was determined by Lineweaver-Burk plot.

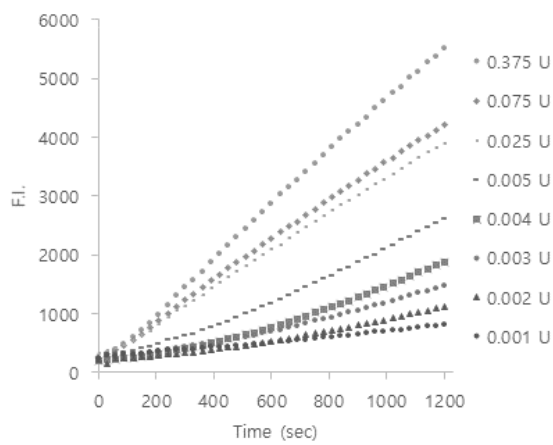

Figure 3.3.3. Progress curves of hydrolysis of **v-BDP (**2.5 μM) upon incubation with PLE at a series of concentrations (0.001-0.375 U/mL) in phosphate buffer solution (10 mM, pH 7.4, 37 ˚C) containing 1% DMSO as a cosolvent. Fluorescence intensity at 565 nm was measured. λexc = 540 nm.

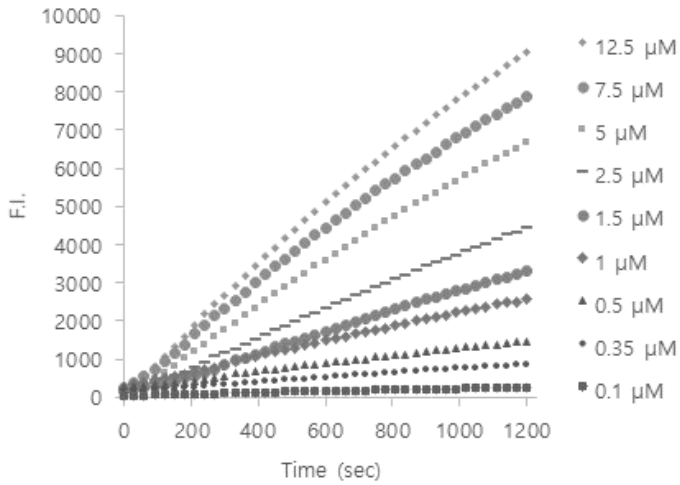

Figure 3.3.4. Progress curves of hydrolysis of probe **v-BDP** at a series of concentrations (0.1 – 12.5 μM) upon incubation with PLE (0.375 U/mL) in phosphate buffer solution (10 mM, pH 7.4, 37 ˚C) containing 1% DMSO as a cosolvent. Fluorescence intensity at 565 nm was measured. λ_{exc} = 540 nm.

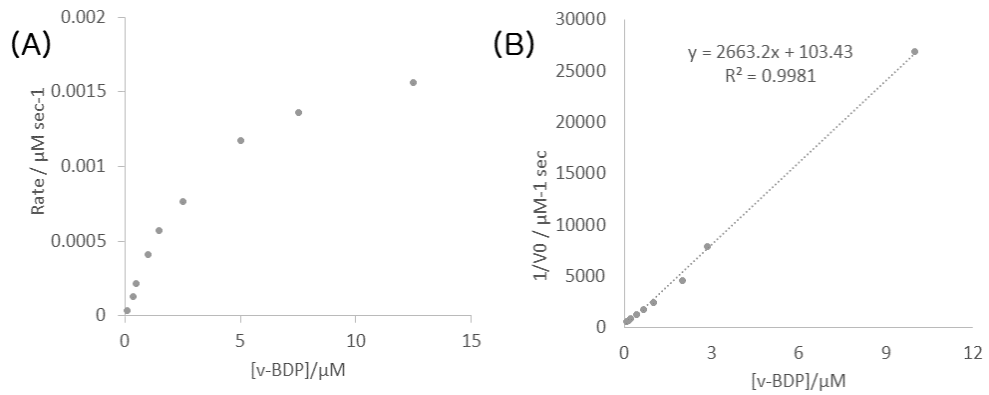

Figure 3.3.5. (A) A plot of the initial velocity v_0 of the hydrolysis of **v-BDP** by esterase versus concentration of **v-BDP**. (B) Lineweaver-Burk plot.

From Lineweaver-Burk plot we get: V_{max} : 0.0387 μM/sec K_M = 25.85 μM, k_{cat} = 0.260 (sec^{-1}) k_{cat}/k_m = 1.006 x 10^{-6} (esterase molecular weight: 168 kDa. [E_0] = 1.488 x 10^{-7} M (0.375 U/ml = 0.025 mg/ml))

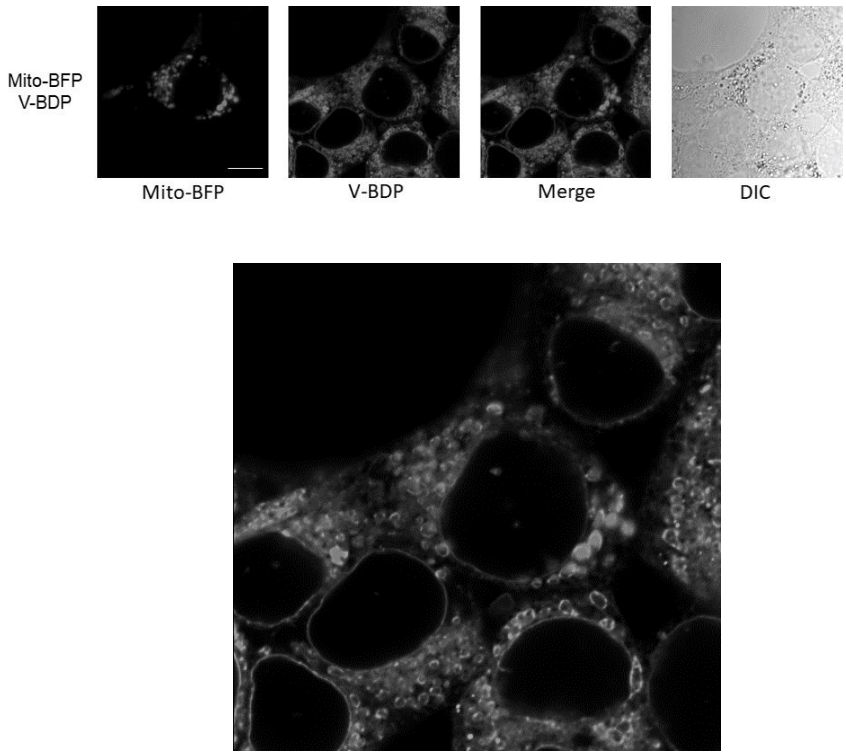

Figure 3.3.6. Representative confocal fluorescence images of washed HEK293T cells that were incubated with **v-BDP** (10 μM) for 30minutes at 37 °C in Dulbecco's modified Eagle's Medium. Mito-BFP: blue channel fluorescent imaging from blue fluorescent protein expressed in mitochondria matrix (λexc = 410 nm), v-BDP: orange channel fluorescent imaging (λexc = 567 nm). Merge images were enlarged to observe more closely.

Cellular imaging experiment

The potential utility of **v-BDP** for the imaging of mitochondria targeting drug release in living cells was evaluated by confocal fluorescence microscopy. Human embryonic kidney 293T (HEK293T) cells were used whose genes were modified for mitochondria specific imaging experiment (see detail in Experimental section). As seen in **Figure 3.3.6**, **v-BDP** was observed as accumulated on the outer walls of mitochondria. In other words, **v-BDP** cannot pass mitochondrial membrane by. Currently, we are investigating the cause of this phenomenon and are studying how to use it.

3.3.3 Experimental section

Cell culture, transfection and cell imaging

Human embryonic kidney 293T (HEK293T) cells were grown on the cell culture plate for 16 hours in the DMEM (Dulbecco's Modified Eagle's Medium, Gibco) supplemented with 10% FBS, 50 units/mL penicillin, and 50 μg/mL streptomycin at 37 °C under 5% CO_2. Especially, for imaging experiment, we used fibronectin-coated glass for cell culturing. Plasmids were transfected into grown cells with calcium phosphate transfection reagents. After 24hr transfection, 10μM v-BDP in DMEM was treated into cells for 30 min. After two times washing with DPBS, the cells were fixed by 4% paraformaldehyde for 15 min and then again washed with DPBS twice. Cell images were taken using a Carl Zeiss LSM780NLO confocal laser scanning microscope (Jena, Germany) and analyzed using the Carl Zeiss ZEN2012 software (UNIST Olympus Biomed Imaging Center, Ulsan, Republic of Korea).

Plasmids and Cloning

Genes were cloned into the specified vectors using standard enzymatic restriction digest and ligation with T4 DNA ligase. To generate constructs where short tags (e.g., V5 or Flag epitope tag) or signal sequences were appended to the protein, the tag was included in the primers used to PCR-amplify the gene. PCR products were digested with restriction enzymes and ligated into cut vectors (e.g., pcDNA3, and pDisplay). In all cases, the CMV promoter was used for expression in mammalian cells. The genetic constructs cloned and used for this study are summarized in **Table 3.3.1**.

Table 3.3.1. Construct Information

Name (expected size)	Features	Promotor/ Vector	Details

Mito-BFP (unprocessed: 29.4 kDa, processed: 26.4 kDa)	*NotI*-Mito-*BamHI*-BFP-Stop-*XhoI*	CMV/ pcDNA3	Mito-: MLATRVFSLVGKRAISTSVCVR AH (matrix targeting sequence, Fornuskova et al., 2010) BFP: Blue fluorescent protein
ss-APEX2-V5-KDEL* (unprocessed: 30.3 kDa, processed: 28 kDa)	*EcoRV-ss-HA-ApaI*-BFP-KDEL-Stop-*NotI*	CMV/ pDisplay	ss: METDTLLLWVLLLWVPGSTGD (IgK chain leader sequence for ER lumen) KDEL: ER retention motif BFP: Blue fluorescent protein

3.3.4 References

1. Tan, A. S.; Baty, J. W.; Berridge, M. V., The role of mitochondrial electron transport in tumorigenesis and metastasis. *Biochimica et Biophysica Acta (BBA) - General Subjects* **2014,** *1840* (4), 1454-1463.

2. Teoh, S. T.; Lunt, S. Y., Metabolism in cancer metastasis: bioenergetics, biosynthesis, and beyond. *Wiley Interdisciplinary Reviews: Systems Biology and Medicine*, e1406-n/a.

3. Weinberg, S. E.; Chandel, N. S., Targeting mitochondria metabolism for cancer therapy. *Nature Chemical Biology* **2014,** *11*, 9.

4. Chinnery, P. F.; Turnbull, D. M., Mitochondrial DNA mutations in the pathogenesis of human disease. *Molecular Medicine Today* **2000,** *6* (11), 425-432.

5. Murphy, M. P.; Smith, R. A. J., Targeting Antioxidants to Mitochondria by Conjugation to Lipophilic Cations. *Annual Review of Pharmacology and Toxicology* **2007,** *47* (1), 629-656.

6. Modica-Napolitano, J. S.; Aprille, J. R., Delocalized lipophilic cations selectively target the mitochondria of carcinoma cells. *Advanced Drug Delivery Reviews* **2001,** *49* (1),

63-70.

7. Murphy, M. P., Targeting lipophilic cations to mitochondria. *Biochimica et Biophysica Acta (BBA) - Bioenergetics* **2008,** *1777* (7), 1028-1031.

8. von Heijne, G.; Steppuhn, J.; Herrmann, R. G., Domain structure of mitochondrial and chloroplast targeting peptides. *European Journal of Biochemistry* **1989,** *180* (3), 535-545.

9. Xu, Z.; Xu, L., Fluorescent probes for the selective detection of chemical species inside mitochondria. *Chemical Communications* **2016,** *52* (6), 1094-1119.

10. Dickinson, B. C.; Srikun, D.; Chang, C. J., Mitochondrial-targeted fluorescent probes for reactive oxygen species. *Current Opinion in Chemical Biology* **2010,** *14* (1), 50-56.

11. Zhu, H.; Fan, J.; Du, J.; Peng, X., Fluorescent Probes for Sensing and Imaging within Specific Cellular Organelles. *Accounts of Chemical Research* **2016,** *49* (10), 2115-2126.

12. Göttlicher, M.; Minucci, S.; Zhu, P.; Krämer, O. H.; Schimpf, A.; Giavara, S.; Sleeman, J. P.; Lo Coco, F.; Nervi, C.; Pelicci, P. G.; Heinzel, T., Valproic acid defines a novel class of HDAC inhibitors inducing differentiation of transformed cells. *The EMBO Journal* **2001,** *20* (24), 6969-6978.

13. Krämer, O. H.; Zhu, P.; Ostendorff, H. P.; Golebiewski, M.; Tiefenbach, J.; Peters, M. A.; Brill, B.; Groner, B.; Bach, I.; Heinzel, T.; Göttlicher, M., The histone deacetylase inhibitor valproic acid selectively induces proteasomal degradation of HDAC2. *The EMBO Journal* **2003,** *22* (13), 3411-3420.

14. Bolden, J. E.; Peart, M. J.; Johnstone, R. W., Anticancer activities of histone deacetylase inhibitors. *Nat Rev Drug Discov* **2006,** *5* (9), 769-84.

15. Cornago, M.; Garcia-Alberich, C.; Blasco-Angulo, N.; Vall-llaura, N.; Nager, M.; Herreros, J.; Comella, J. X.; Sanchis, D.; Llovera, M., Histone deacetylase inhibitors promote glioma cell death by G2 checkpoint abrogation leading to mitotic catastrophe. *Cell Death &Amp; Disease* **2014,** *5*, e1435.

16. JASEK, E.; LIS, G. J.; JASIŃSKA, M.; JURKOWSKA, H.; LITWIN, J. A., Effect of Histone Deacetylase Inhibitors Trichostatin A and Valproic Acid on Etoposide-induced Apoptosis in Leukemia Cells. *Anticancer Research* **2012,** *32* (7), 2791-2799.

국문 초록

작은 분자에 기반한 형광 프로브는 높은 수준의 감도, 빠른 응답속도 및 단순함으로 인해 광학학적 이미징과 분석적 센싱에 유용한 도구로 이용된다. 또한 새로운 형광 프로브의 개발은 그 유용성만큼이나 중요하다. 수많은 학자들이 형광 프로브를 개발해왔지만, 새로운 형광 프로브의 개발을 위한 체계적인 접근법은 여전히 부족하다.

기존의 프로브를 개발하기 위한 전략은 목표 지향적 접근법이었다. 프로브는 개별 표적에 대한 분자 인식 메커니즘에 대한 경험적 지식을 바탕으로 설계되었다. 그러나 경험에 의존한 이 전략은 알려지지 않은 목표를 연구함에 있어서 한계를 보인다. 한편, 광범위한 화학적 다양성을 지닌 다양성 지향 프로브 라이브러리는 새로운 표적에 대한 프로브를 개발할 수 있는 대체 수단이 될 수 있다. 하지만, 이 전략은 막대한 노동력과 시간이 필요하며, 성공률도 매우 낮다.

우리는 두 전략에 대한 대안으로 집중된 형광 프로브 라이브러리를 고안하였다. 각각의 프로브는 표적과 표적 군에 대한 이해를 바탕으로 설계되었다.

이 논문은 스티릴 기반 형광 염료로 구성된 집중된 라이브러리를 통하여 다양한 목표 물질에 대해 선택적인 형광 프로브의 효율적인 개발에 관한 내용을 담고 있다. 첫째, 금속 양이온에 대한 형광 프로브 라이브러리를 고안하였으며, 각각의 프로브는 금속이온에 대한 양이온 리간드와 피콜리

늄/퀴놀리늄 이 스티릴 그룹으로 연결되었다. 이 라이브러리를 이용하여, 수은이온, 은이온, 아연이온에 대한 선택적인 프로브를 개발하였다. 둘째, 이전의 스티릴 다이-금속이온 복합체를 이용한 인산 생체분자에 대한 프로브 라이브러리를 고안하였고, 그 결과 dTTP에 대한 형광 프로브를 개발하였다. 셋째, 이전에 개발한 스티릴 염료 중 몇가지가 세포내에서 강한 형광을 보이는 것을 관찰하였다. 이를 통하여 핵산에 대한 형광 프로브를 개발하였으며, 핵산 분해 실험을 통하여 확인하였다. 넷째, 과산화수소에 대한 형광 프로브를 개발하였다. 이 프로브는 포도당 산화효소를 이용하여 포도당을 정량하였다. 또한 이 프로브는 다양한 생체 분자에 대한 산화 효소의 활성 및 생체 물질의 검출에 이용 할 수 있음을 보여주었다. 마지막으로, 미토콘드리아에 선택적으로 작용하는 암치료 연구에 이용될 스티릴 보디피 염료에 기반한 형광 이미징 프로브를 개발하였다. 이것은 세포 내 에스터레이즈에 의해 항암제를 미토콘드리아에 전달하도록 설계되었다.

키워드: 형광 프로브, 집중된 라이브러리, 스티릴 염료, 스티릴 보디피, 과산화수소, 티미딘 삼인산, 약물전달